12

RADC-TR-82-295, Vol II (of two)
Interim Report
November 1982

ACOSS-11 (ACTIVE CONTROL OF SPACE STRUCTURES)

The Charles Stark Draper Laboratory, Inc.

Sponsored by
Defense Advanced Research Projects Agency (DOD)
ARPA Order No. 3655

APPROVED FOR PUBLIC RELEASE; DISTRIBUTION UNLIMITED

ROME AIR DEVELOPMENT CENTER
Air Force Systems Command
Griffiss Air Force Base, NY 13441

This report has been reviewed by the RADC Public Affairs Office (PA) and is releasable to the National Technical Information Service (NTIS). At NTIS it will be releasable to the general public, including foreign nations.

RADC-TR-82-295, Volume II (of two) has been reviewed and is approved for publication.

APPROVED: Richard W Carman

RICHARD W. CARMAN
Project Engineer

APPROVED: Frank J Rehm

FRANK J. REHM
Technical Director
Surveillance Division

FOR THE COMMANDER: John P. Huss

JOHN P. HUSS
Acting Chief, Plans Office

If your address has changed or if you wish to be removed from the RADC mailing list, or if the addressee is no longer employed by your organization, please notify RADC (OCSE) Griffiss AFB NY 13441. This will assist us in maintaining a current mailing list.

Do not return copies of this report unless contractual obligations or notices on a specific document requires that it be returned.

Volume II

ACOSS-11 (ACTIVE CONTROL OF SPACE STRUCTURES)

R. R. Strunce
E. Fogel
D. R. Hegg
J. G. Lin
J. D. Turner
H. M. Chun

Contractor: The Charles Stark Draper Laboratory, Inc.
Contract Number: F30602-81-C-0180
Effective Date of Contract: 27 April 1981
Contract Expiration Date: 27 April 1984
Short Title of Work: Acoss-11 (Active Control of Space Structures)
Program Code Number: 1E20
Period of Work Covered: Nov 81 - Apr 82

Principal Investigator: Dr. Keto Soosaar
Phone: 617 258-2575

Project Engineer: Richard M. Carman
Phone: 315 330-3148

This research was supported by the Defense Advanced Research Projects Agency of the Department of Defense and was monitored by Richard M. Carman (RADC/OCSE), Griffiss AFB NY 13441 under Contract F30602-81-C-0180.

UNCLASSIFIED

SECURITY CLASSIFICATION OF THIS PAGE (When Data Entered)

REPORT DOCUMENTATION PAGE	READ INSTRUCTIONS BEFORE COMPLETING FORM
1. REPORT NUMBER: RADC-TR-82-295, Vol II (of two) 2. GOVT ACCESSION NO. AD-A124 746	3. RECIPIENT'S CATALOG NUMBER
4. TITLE (and Subtitle): ACOSS-11 (ACTIVE CONTROL OF SPACE STRUCTURES)	5. TYPE OF REPORT & PERIOD COVERED: Interim Report Nov 81 - Apr 82
	6. PERFORMING ORG. REPORT NUMBER: CSDL-R-1538
7. AUTHOR(s): R. R. Strunce, J. G. Lin, E. Fogel, J. D. Turner, D. R. Hegg, H. M. Chun	8. CONTRACT OR GRANT NUMBER(s): F30602-81-C-0180
9. PERFORMING ORGANIZATION NAME AND ADDRESS: The Charles Stark Draper Laboratory, Inc. 555 Technology Square Cambridge MA 02139	10. PROGRAM ELEMENT, PROJECT, TASK AREA & WORK UNIT NUMBERS: 62301E C6550116
11. CONTROLLING OFFICE NAME AND ADDRESS: Defense Advanced Research Projects Agency 1400 Wilson Blvd Arlington VA 22209	12. REPORT DATE: November 1982
	13. NUMBER OF PAGES: 162
14. MONITORING AGENCY NAME & ADDRESS(if different from Controlling Office): Rome Air Development Center (OCSE) Griffiss AFB NY 13441	15. SECURITY CLASS. (of this report): UNCLASSIFIED
	15a. DECLASSIFICATION/DOWNGRADING SCHEDULE: N/A

16. DISTRIBUTION STATEMENT (of this Report)

Approved for public release; distribution unlimited.

17. DISTRIBUTION STATEMENT (of the abstract entered in Block 20, if different from Report)

Same

18. SUPPLEMENTARY NOTES

RADC Project Engineer: Richard M. Carman (OCSE)

19. KEY WORDS (Continue on reverse side if necessary and identify by block number)

Broad-band Disturbance
Power Spectral Density
Sensor/Actuator Selection
Node Shape Matching
Least Squares Approximation
QR Factorization
Disturbance-Rejection Control
Kalman Filter

(see reverse)

20. ABSTRACT (Continue on reverse side if necessary and identify by block number)

Volume 2 of this report describes progress in the application of active controller design methods to the ACOSS Model No. 2 structure. Attention is focused on attenuation of the effects of a broad-band disturbance input upon line-of-sight rotation error, and upon the generation of smooth large-angle slew maneuvers. A ten-mode design model is used. For disturbance attenuation, a new method for sensor/actuator selection based directly on line-of-sight considerations is proposed. Three disturbance-

DD FORM 1 JAN 73 1473 EDITION OF 1 NOV 65 IS OBSOLETE

UNCLASSIFIED

SECURITY CLASSIFICATION OF THIS PAGE (When Data Entered)

attenuation designs are described. The first assumes a complete knowledge of the disturbance statistics, while the others assume no such explicit knowledge. All three designs indicate convincingly that damping augmentation alone is not sufficient to attenuate effects of the disturbance; augmentation of stiffness is also required. Extensions of large-angle slew control to incorporate feedback are also presented.

Item 19 (continued)

Separation Principle
Modal Parameter Objectives
Active Stiffness/Damping Augmentation
Augmented-state Regulator
Spillover Reduction
Actuator Synthesizers
Large-Angle Slew
Degree-of-Controllability
Residual Energy
Integral Precompensation
Riccati Differential Equation

ACKNOWLEDGEMENT

This report was prepared by the Charles Stark Draper Laboratory, Inc., under Contract F30602-81-C-0180. This research was supported by the Advanced Research Projects Agency of the Department of Defense and monitored by the Rome Air Development Center.

The program manager is Dr. Keto Soosaar and the project leader for Active Control of Space Structures (ACOSS) is Mr. Robert R. Strunce. The technical director for the ACOSS work presented in this report is Dr. Jiguan G. Lin. The authors of Volume 2 of this report are: Dr. Eliezer Fogel (Sections 3, 4), Dr. Daniel R. Hegg (Sections 1, 5), Dr. Jiguan G. Lin (Sections 5, 6), Mr. Robert R. Strunce (Sections 2, 4), and Dr. James D. Turner and Mr. Hon M. Chun (Section 7). Assistance from Mr. Timothy C. Henderson (Sections 2, 3), Mr. Warren J. Jasper (Sections 5, 6), Mr. J. G. Herther (Section 5), Mr. Robert R. Strunce (Sections 5, 6), Mr. Glen J. Kissel (Section 6), Dr. Daniel R. Hegg (Section 6), and Mr. David P. Latimer (Active Control Technology Software) is gratefully acknowledged.

Publication of this report does not constitute approval by the Defense Advanced Research Projects Agency or the United States Government of the findings or conclusions contained herein. It is published for the exchange and stimulation of ideas.

VOLUME 2

TABLE OF CONTENTS

Section			Page
1	INTRODUCTION		1-1
	1.1	Scope	1-1
	1.1.1	Vibration Control	1-1
	1.1.2	Large-Angle Slew Control	1-3
	1.2	Limitations	1-4
2	VCOSS EXAMPLE PROBLEM		2-1
	2.1	Introduction	2-1
	2.2	Broad-Band Disturbance	2-1
	2.3	Input Disturbance Implementation	2-3
	2.4	Response to Input Disturbance	2-5
3	SENSOR/ACTUATOR SELECTION		3-1
	3.1	Introduction	3-1
	3.2	The Node Shape Matching Concept	3-2
	3.2.1	Preliminaries	3-2
	3.2.2	Selection of Node Shapes	3-5
	3.2.3	Least Squares Formulation	3-8
	3.2.4	The QR Factorization	3-9
	3.3	Preliminary Selection and Refinement	3-11
	3.4	Results	3-11
		List of References	3-12

Section			Page
4	DISTURBANCE REJECTION CONTROL DESIGN		4-1
	4.1	Introduction	4-1
	4.2	Disturbance Rejection Control	4-2
	4.2.1	The Model	4-2
	4.2.2	Optimal Control Design	4-5
	4.3	Application to ACOSS Model No. 2.	4-9
		List of References	4-11
5	LINEAR-QUADRATIC OPTIMAL CONTROL DESIGN		5-1
	5.1	The Design Problem	5-1
	5.2	Description of Design Philosophy	5-1
	5.2.1	Generation of Desired Closed Loop Characteristics	5-2
	5.3	Generation of Weighting Matrices for Linear-Quadratic Design	5-9
	5.3.1	Relationships Between Closed-Loop Modal Parameters and Weighting Matrices	5-9
	5.3.2	Application In Design	5-13
	5.4	Design Results	5-14
	5.5	Numerical Experience in the Design Process	5-15
	5.5.1	Optimal vs. Nonoptimal Design	5-15
	5.5.2	Conditioning of the Control Weighting Matrix	5-15
	5.5.3	State vs. Augmented-State Weighting	5-16
	5.5.4	Active Damping vs. Active Stiffness-Damping Augmentation	5-16
	5.6	Work in Progress	5-17
		List of References	5-17
6	LINEAR-QUADRATIC OPTIMAL CONTROL DESIGN WITH SPILLOVER REDUCTION		6-1
	6.1	Introduction	6-1
	6.2	A Design of Actuator Synthesizers	6-1
	6.2.1	Synthesis for Prevention of Control Spillover	6-2

Section			Page
	6.2.2	Synthesis for Correction of Modal Control Authority	6-3
	6.3	Optimal Control Design with Spillover Reduction	6-5
	6.3.1	A Linear-Quadratic Optimal Control Design	6-6
	6.3.2	Design Results	6-6
		List of References	6-7
7		LARGE-ANGLE SPACECRAFT SLEWING MANEUVERS	7-1
	7.1	Introduction	7-1
	7.2	Reduced-Order Model Selection	7-2
	7.3	Retargeting Maneuvers For Flexible Spacecraft	7-4
	7.3.1	Optimal Control Problem	7-5
	7.4	Optimal Integral Pre-Compensation LQ Regulator Design	7-10
	7.4.1	Optimal Control Problem	7-11
	7.4.2	The Integral Pre-Compensation Regulator Design	7-12
	7.4.3	Some Frequency Domain Features of the Integral Pre-Compensation LQ Regulator Design	7-15
	7.4.4	Observer-Based Compensation Design	7-15
	7.4.5	Closed-Loop System Stability	7-17
	7.5	A Closed-Form Solution for the Differential Matrix Riccati Equation for Fixed Time Slewing Maneuvers	7-19
	7.5.1	Change of Variables for the Matrix Riccati Differential Equation	7-20
		List of References	7-24

SECTION 1

INTRODUCTION

1.1 Scope

Volume 2 of the present report gives an account of the progress made during the reporting period in implementing various strategies for active control on ACOSS Model No. 2. The design objective for the several vibration control strategies employed is to attenuate the line-of-sight (LOS) rotation error and defocus of the optical system induced by a broad-band disturbance. A slewing controller for implementing large changes in the rigid-body attitude of the structure with minimal associated line-of-sight error is also studied.

1.1.1 Vibration Control

A general form of disturbance containing both broad-band and discrete-frequency components has been communicated by Riverside Research Institute to assist in comparing competing designs of vibration controllers. Several modifications of this disturbance specification are made for the purpose of the present study in order to reduce computation costs. First, the bandwidth of the broad-band portion is 5 Hz., extending from 0 Hz. to 5 Hz. The reduction of the upper boundary from 15 Hz. to 5 Hz. is dictated by the reduced-order model (20 modes) being studied. The extension of the lower boundary to 0 Hz. enables the use of a simpler model of the disturbance without sacrifice of fidelity since rigid-body modes are not studied in the disturbance-rejection problem. Second, the disturbance is assumed to be fixed in direction at each specified point of application to the structure, varying

stochastically only in magnitude. In addition, the one-sided spectral density amplitude in the specification is retained for two-sided use. Details are presented in Section 2. These modifications do not alter the qualitative objective of the study; namely, to examine the fundamental difficulties associated with designing vibration controllers to stringent LOS-error tolerances in the presence of a broad-band disturbance.

A selection of structural vibration modes to be considered in the various designs, and a corresponding selection to be used in evaluating the designs, is determined by ranking each of the 156 structural modes in the NASTRAN finite element model with respect to the root-mean-square (RMS) error in LOS-rotation that results from the disturbance acting on that mode (viewed as a single channel). The highest ranking ten modes according to this criterion are chosen to constitute the model for the control designs, and the highest ranking twenty modes constitute the evaluation model. The upper limit on the number of modes to be included is chosen with consideration of the computation cost. The modes selected and their ranking are also given in Section 2.

A choice of location for sensors and actuators for the controller design is determined using an original approach particularly suited to the stringent performance requirements in the present design problem. Locations are chosen using algebraic methods which make explicit the contributions to the LOS-error associated with particular sensors or actuators. Details are given in Section 3.

Three different approaches to the design of a vibration controller are presented. The first approach, disturbance-rejection control, assumes that complete information on the statistical properties of the disturbance is available. Using this information, a stochastic dynamic model of the disturbance is concatenated with the open-loop design model of the structure. A linear-quadratic-Gaussian (LQG) controller for the enlarged system is designed. The design process involves a few

iterations in which weighting matrices are adjusted to achieve the desired performance. Details are given in Section 4. Satisfactory attenuation of the disturbance effects upon LOS-rotation error is achieved. It is important to note that this attenuation is achieved by moving the characteristic frequencies of the closed-loop system outside the bandwidth of the disturbance, as well as by adding damping to the different modes.

In the second approach, linear-quadratic (LQ) optimal control, more realistic assumptions with regard to the knowledge of the disturbance characteristics are made. The disturbance statistics are not assumed to be known. Instead, the effect of the disturbance, as reflected in the RMS values of the LOS-rotation error, is used to select desired values for closed-loop modal characteristic frequencies and damping ratios. Well-known relationships connecting closed-loop modal parameter values and weighting matrices for LQ design are exploited, thus generating a systematic analytical approach to the selection of weighting matrices. Details are given in Section 5. As in the first design approach, results show that LOS-error reduction is obtained principally by the augmentation of stiffness rather than of damping.

The third design approach is an extension of the second approach; actuator synthesizers are incorporated into the design to alleviate the problem of control spillover to certain modeled modes not in the controller design model. Details are given in Section 6.

1.1.2 Large-Angle Slew Control

A large-angle slew maneuver involves an input of energy to the vehicle which, in turn, induces vibration in the optical support structure. The control problem is to apply the energy to the structure in such a way that the desired attitude maneuver is accomplished and that the optical system supported by the structure returns rapidly to acceptable levels of performance following the maneuver. Several significant extensions to previous work are reported here. One is to solve the problem of slew to a moving, rather than a fixed, target. The

other is the development of a closed-loop control strategy using integral compensation based on measurements which include control and control rate signals, rather than a strategy based only on open-loop considerations. Details are given in Section 7.

1.2 Limitations

The present report gives an account of work in progress, rather than of completed work. The quantitative results in particular should be viewed in that light.

With respect to the vibration control designs, the present report does not include an account of an evaluation of the ten-mode controller designs against the twenty-mode evaluation model, or the effects of the use of an observer in the deterministic LQ controller designs. Investigations on these matters are in progress and will be reported on subsequently.

Substantial work has also been done in other related areas, such as suboptimal output feedback, modal-spring-plus-modal-dashpot output feedback, and system identification, in relation to ACOSS Model No. 2. In addition, fundamental investigations have been launched into problems associated with the explicit incorporation of the dynamics of actuators and of data-sampling devices into the mathematical model for the structure and controller. Accounts of this work will be reported in the future.

SECTION 2

VCOSS EXAMPLE PROBLEM

2.1 Introduction

The problem posed for the vibration control designs discussed in this report is based on the use of Revision 3 (VCOSS FLEX Model No. 2) of ACOSS Model No. 2, more lightweight and flexible than the original Model No. 2. The example problem is to design a control law for a 10-mode design model which is driven by a broad-band disturbance with a power spectral density (PSD) of 40 $N^2 \cdot sec$ over a 5 Hz. bandwidth and to evaluate the resulting controller with a 20-mode evaluation model. Table 2-1 presents the 10-mode and 20-mode models and their respective contribution to the line-of-sight (LOS) error resulting from the broad-band disturbance. The design objective is:

$$\begin{aligned} \text{LOS-X error} &\leq 0.05\ \mu\text{-radians} \\ \text{LOS-Y error} &\leq 0.05\ \mu\text{-radians} \\ \text{LOS-Z error} &\leq 25\ \mu\text{-meters} \end{aligned}$$

2.2 Broad-Band Disturbance

The analytical two-sided broad-band disturbance is characterized by a PSD which has a second-order rolloff ($1/s^2$) at 5 Hz. This is modeled as

$$S_{xx}(s) = \frac{G\omega_c^2}{\omega_c^2 - s^2} \qquad (2\text{-}1)$$

where

$$G = 40\ N^2 \cdot sec$$

$$\omega_c = 2\pi f_c$$

$$f_c = 5\ Hz.$$

Eq. (2-1) may be written as

$$S_{xx}(s) = F(s)\ F(-s) \qquad (2\text{-}2)$$

where

$$F(s) = \frac{\sqrt{G}\ \omega_c}{s + \omega_c}$$

A plot of the PSD for the input disturbance is shown in Figure 2-1. The mean square value of this disturbance is

$$\psi^2 = \frac{G\ \omega_c}{2} = \frac{40(2\pi 5)}{2} = 628.32\ N^2$$

This disturbance is consistent with the general disturbance specification that has been communicated by Riverside Research Institute for comparison of controller design strategies.

2.3 Input Disturbance Implementation

The disturbance sources are located at node no. 37 and node no. 46 of the VCOSS FLEX Model No. 2. This is true for all modified versions of the ACOSS Model No. 2 (stiff and flexible models). The direction of this disturbance makes an equal angle with all three axes (x, y, z) at each location. Figure 2-2 shows the geometrical relationship. For convenience, it is assumed that the input disturbance is fixed in direction along the unit vector

$$\bar{U} = (\cos \alpha)\, i + (\cos \alpha)\, j + (\cos \alpha)\, k \qquad (2\text{-}3)$$

where $\alpha = 54.74°$

The "projection" of the input disturbance on each axis is the disturbance given in Section 2.2.

With the projected density S_{xx} equal in each direction, the number of performance evaluations can be reduced by a factor of three. The actuator influence matrix

$$\text{n modes} \left\{ \begin{bmatrix} \overbrace{b_{x1} \quad b_{y1} \quad b_{z1}}^{\text{node no. 37}} & \overbrace{b_{x1} \quad b_{y1} \quad b_{z1}}^{\text{node no. 46}} \\ \vdots \quad \vdots \quad \vdots & \vdots \quad \vdots \quad \vdots \\ b_{xn} \quad b_{yn} \quad b_{zn} & b_{xn} \quad b_{yn} \quad b_{zn} \end{bmatrix} \right. \qquad (2\text{-}4)$$

is multiplied by the matrix

$$
\begin{array}{l}
\\
\text{node no. 37} \\
\\
\\
\text{node no. 46} \\
\\
\\
\end{array}
\overbrace{\begin{bmatrix} 1 & 0 \\ 1 & 0 \\ 1 & 0 \\ 0 & 1 \\ 0 & 1 \\ 0 & 1 \end{bmatrix}}^{\text{2 inputs}}
\tag{2-5}
$$

to yield the reduced actuator influence matrix

$$
\begin{array}{l}
\\
\text{n modes}
\end{array}
\overbrace{\begin{bmatrix} (b_{x1} + b_{y1} + b_{z1}) & (b_{x1} + b_{y1} + b_{z1}) \\ \vdots & \vdots \\ (b_{xn} + b_{yn} + b_{zn}) & (b_{xn} + b_{yn} + b_{zn}) \end{bmatrix}}^{\text{2 inputs}}
\tag{2-6}
$$

Eq. (2-6) is essentially the sum of the actuator influences in the x, y, and z directions for each disturbance location. This results in only having to evaluate two inputs with respect to the line-of-sight performance requirements instead of six inputs.

2.4 Response to Input Disturbance

The output response is

$$P_{out,j}(s) = \left|H_{i,j}(s)\right|^2 P_{in}(s); \quad i=1,2 \ , \ j=1,2,3$$

where $P_{in}(s)$ is the PSD of the input disturbance described in Section 2.2 and $H_{i,j}(s)$ is the transfer function from the i-th component of the disturbance location (node no. 37 or no. 46) to the j-th LOS error function. Figures 2-3a through 2-3f present the PSD of the output for the open-loop 10-mode design model. Figures 2-4a through 2-4f present the PSD of the output for the open-loop 20-mode evaluation model.

Table 2-1. VCOSS example model.

		#	MODE	FREQUENCY (Hertz)	RMS LOS ERROR (micro-radian)
10-MODE DESIGN MODEL	20-MODE EVALUATION MODEL	1	23	1.55	1746.2
		2	22	1.15	513.5
		3	7	0.11	403.3
		4	12	0.55	202.1
		5	13	0.59	108.9
		6	14	0.61	83.2
		7	15	0.63	76.5
		8	9	0.14	50.9
		9	33	6.56	30.6
		10	34	8.06	25.8
		11	45	11.84	24.9
		12	40	11.55	19.4
		13	37	9.00	17.9
		14	16	0.64	13.4
		15	24	1.77	12.8
		16	10	0.17	9.1
		17	47	14.19	7.7
		18	48	15.02	7.1
		19	62	24.66	7.0
		20	56	21.31	7.0

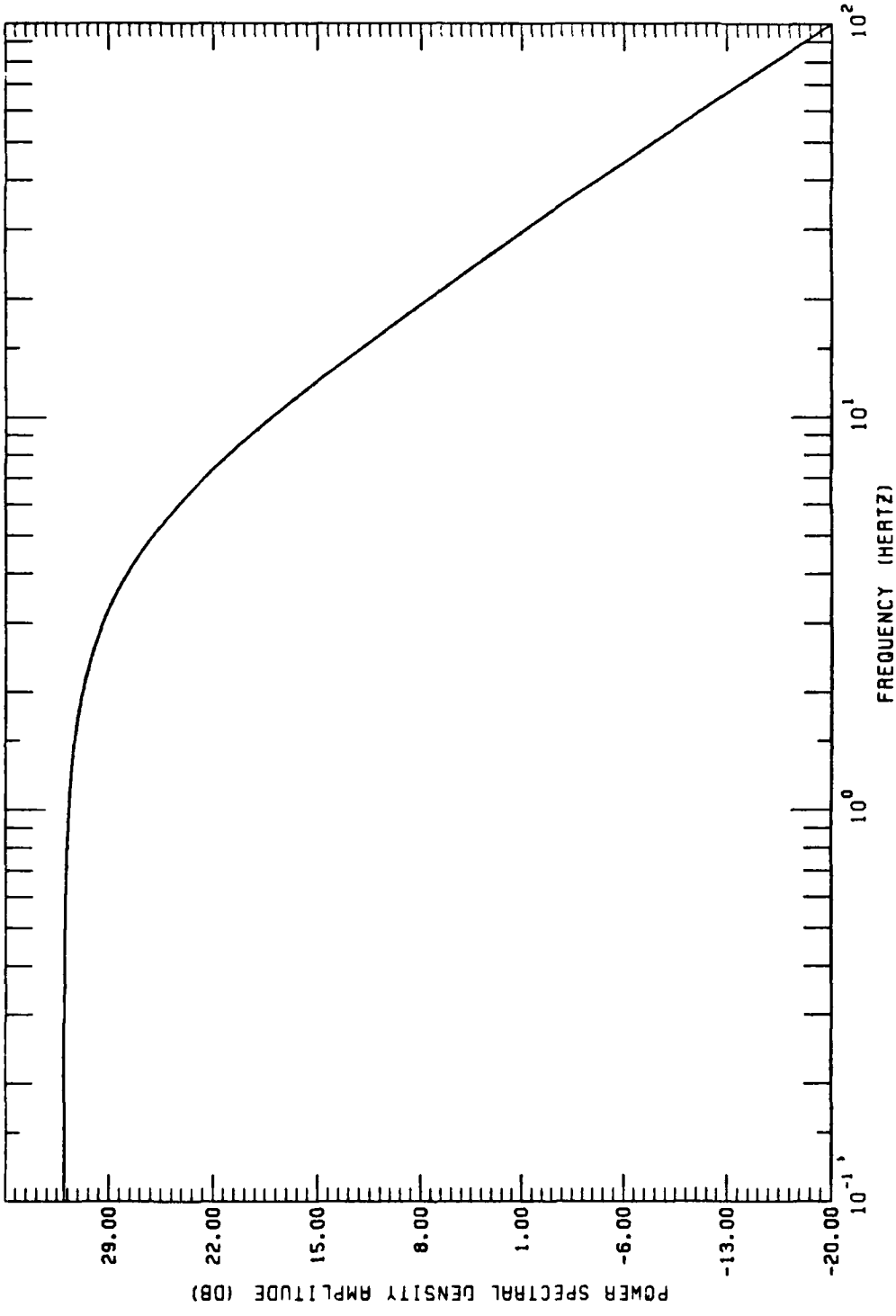

Figure 2-1. Power spectral density at input disturbance.

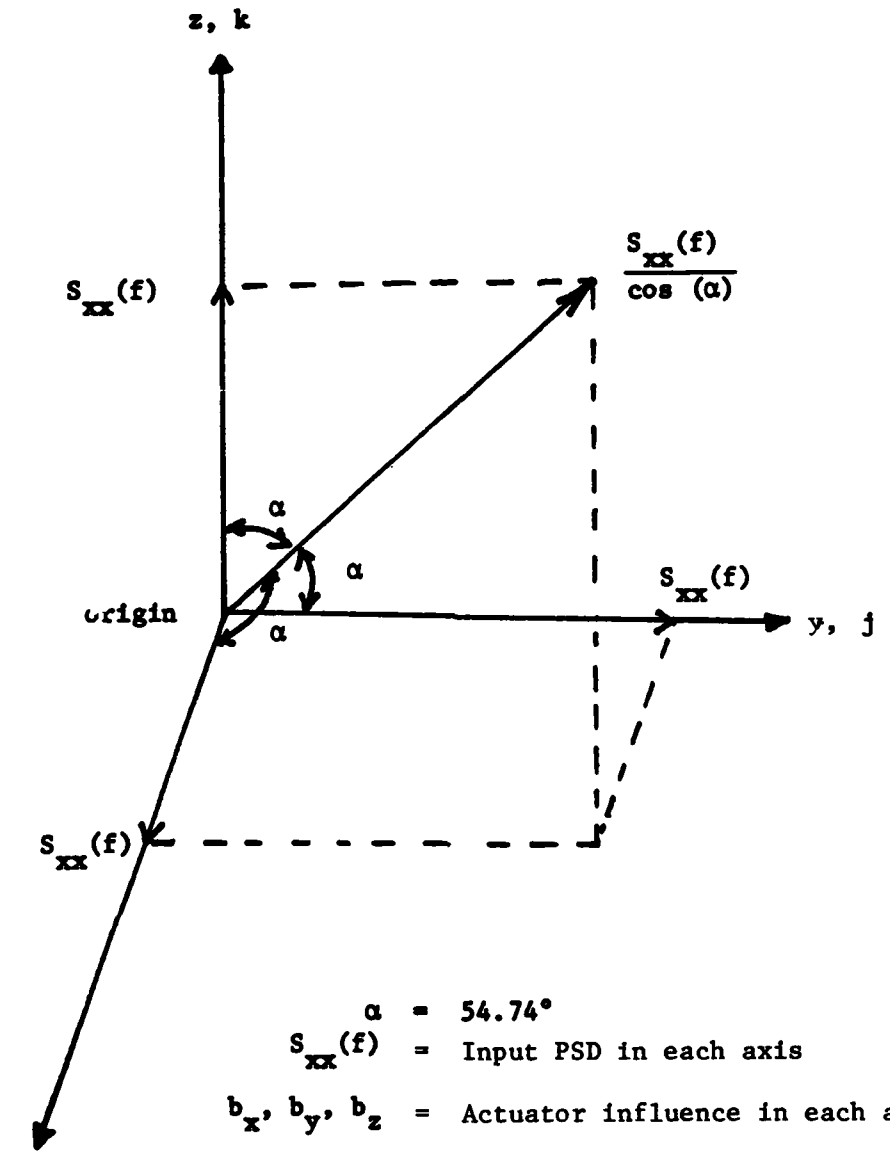

α = 54.74°

$S_{xx}(f)$ = Input PSD in each axis

b_x, b_y, b_z = Actuator influence in each axis

origin = Node no. 37 or no. 46

Note: $S_{xx}(f)\, b_x + S_{xx}(f)\, b_y + S_{xx}(f)\, b_z = S_{xx}(f)\, (b_x + b_y + b_z)$

Figure 2-2. Input disturbance geometrical relationship at node no. 37 and node no. 46.

Figures 2-3. Open-loop output power spectral density for 10-mode design model due to broad-band disturbance.

(On following pages)

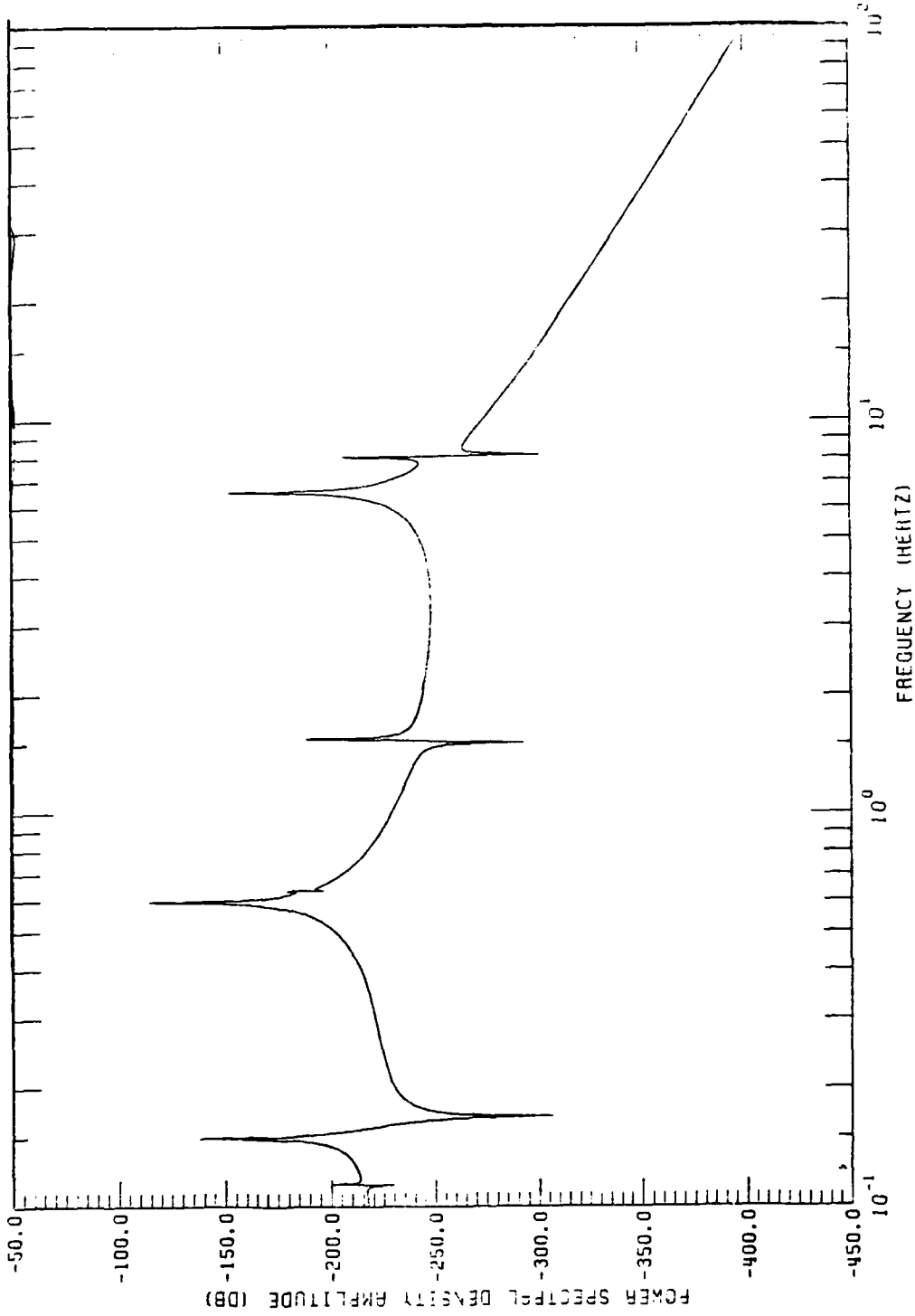

Figure 2-3a. Disturbance at node 37, output LOS-X.

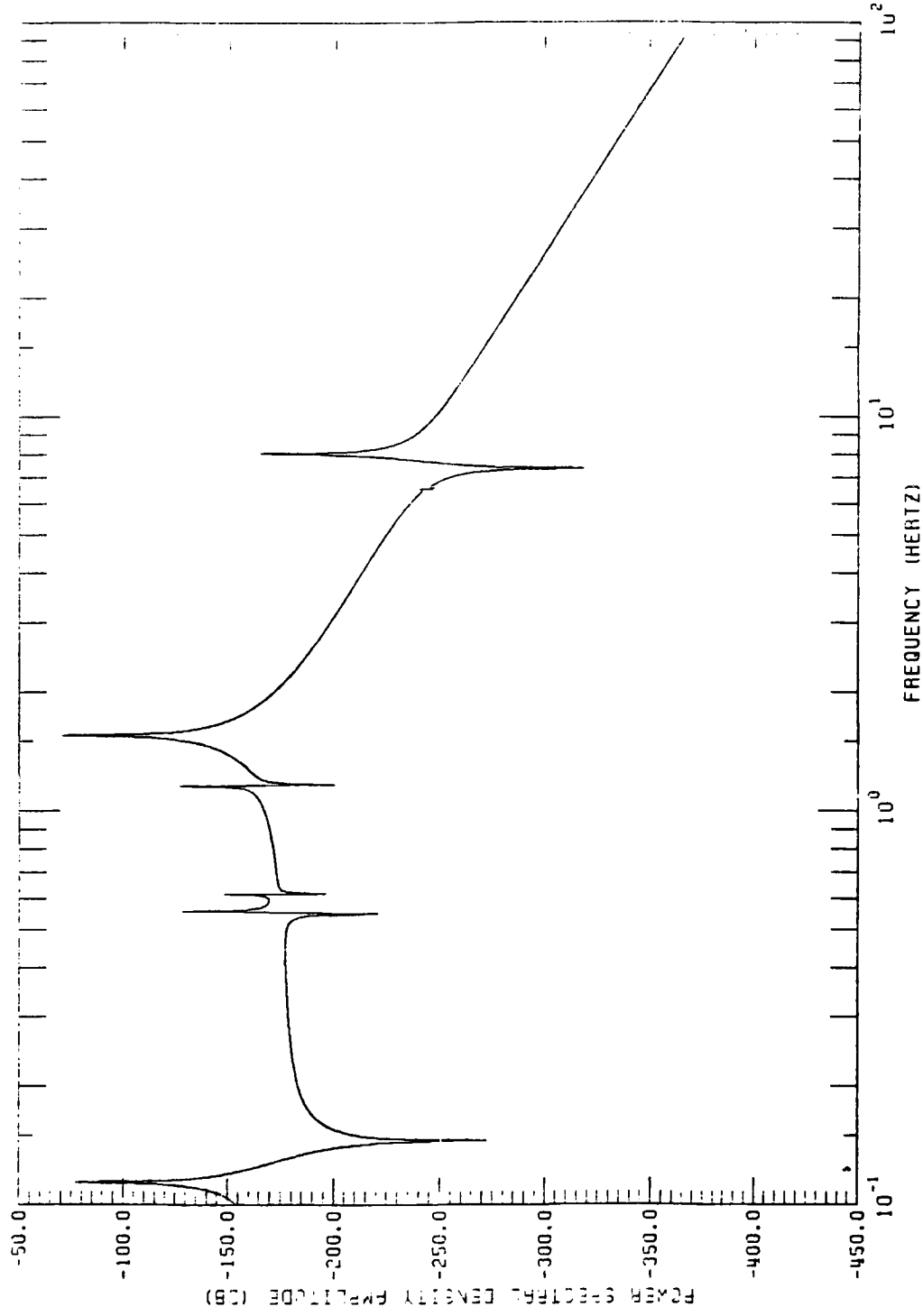

Figure 2-3b. Disturbance at node 37, output LOS-Y.

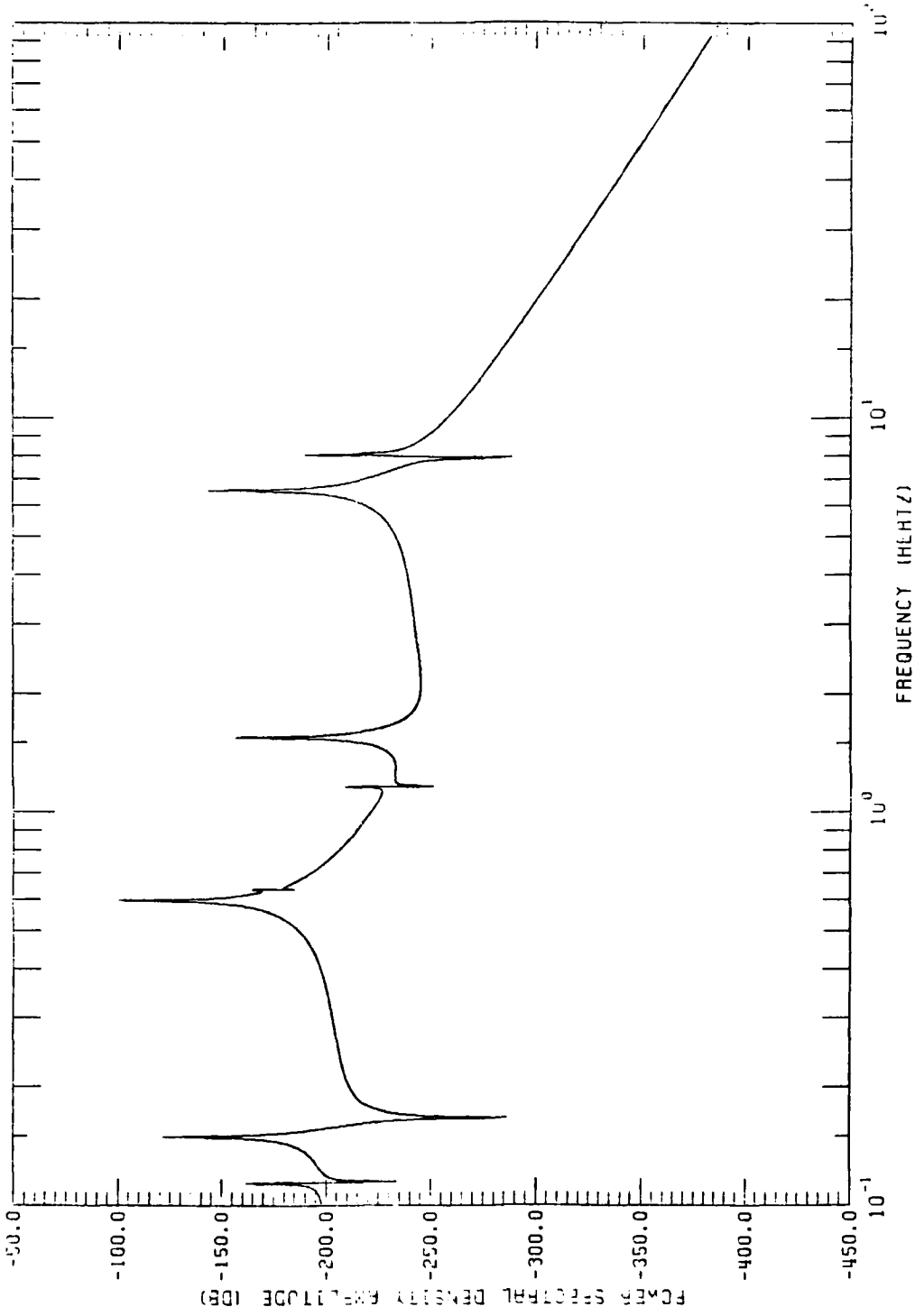

Figure 2-3c. Disturbance at node 37, output LOS-Z.

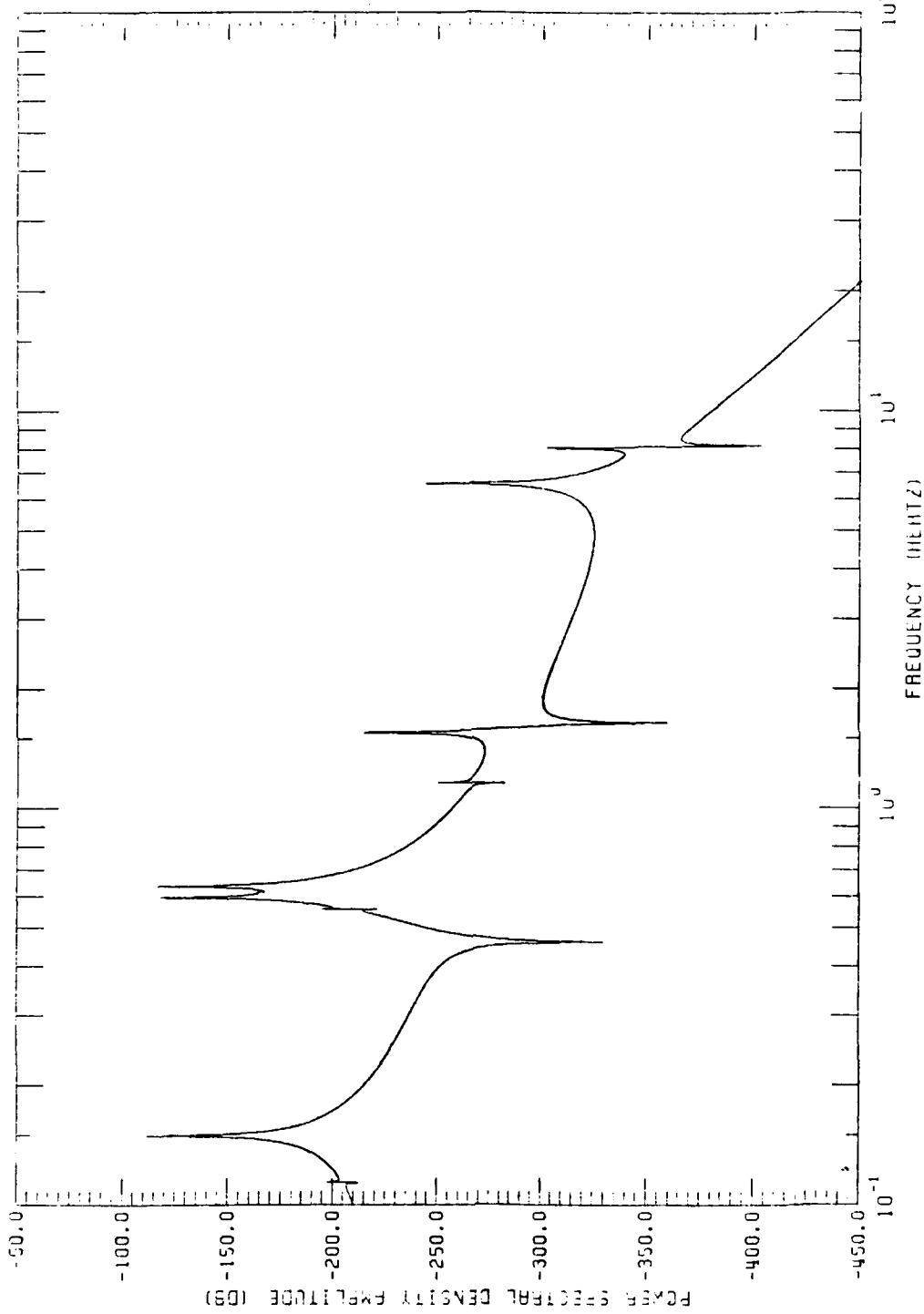

Figure 2-3d. Disturbance at node 46, output LOS-X.

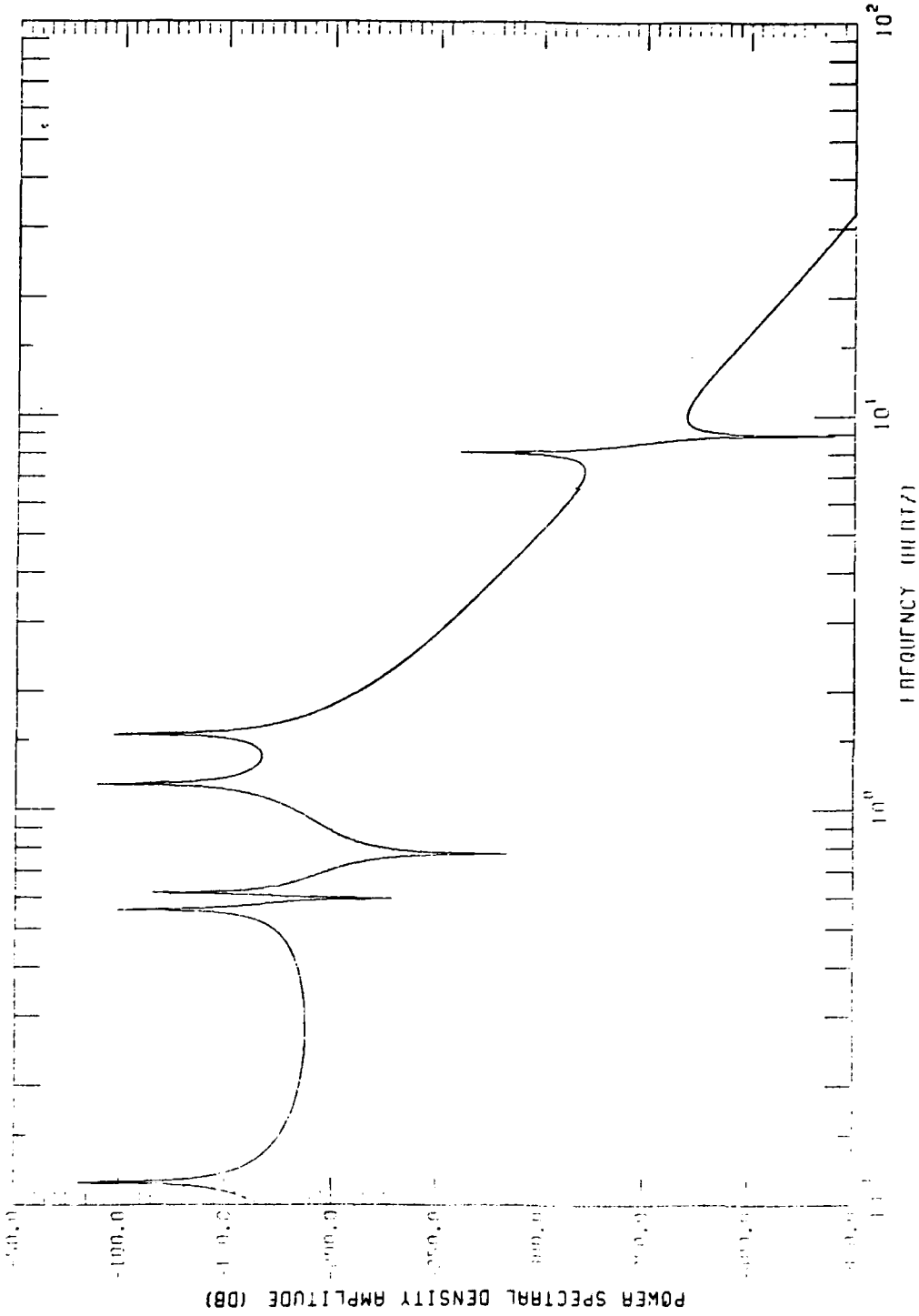

Figure 2-3e. Disturbance at node 46, output LOS-Y.

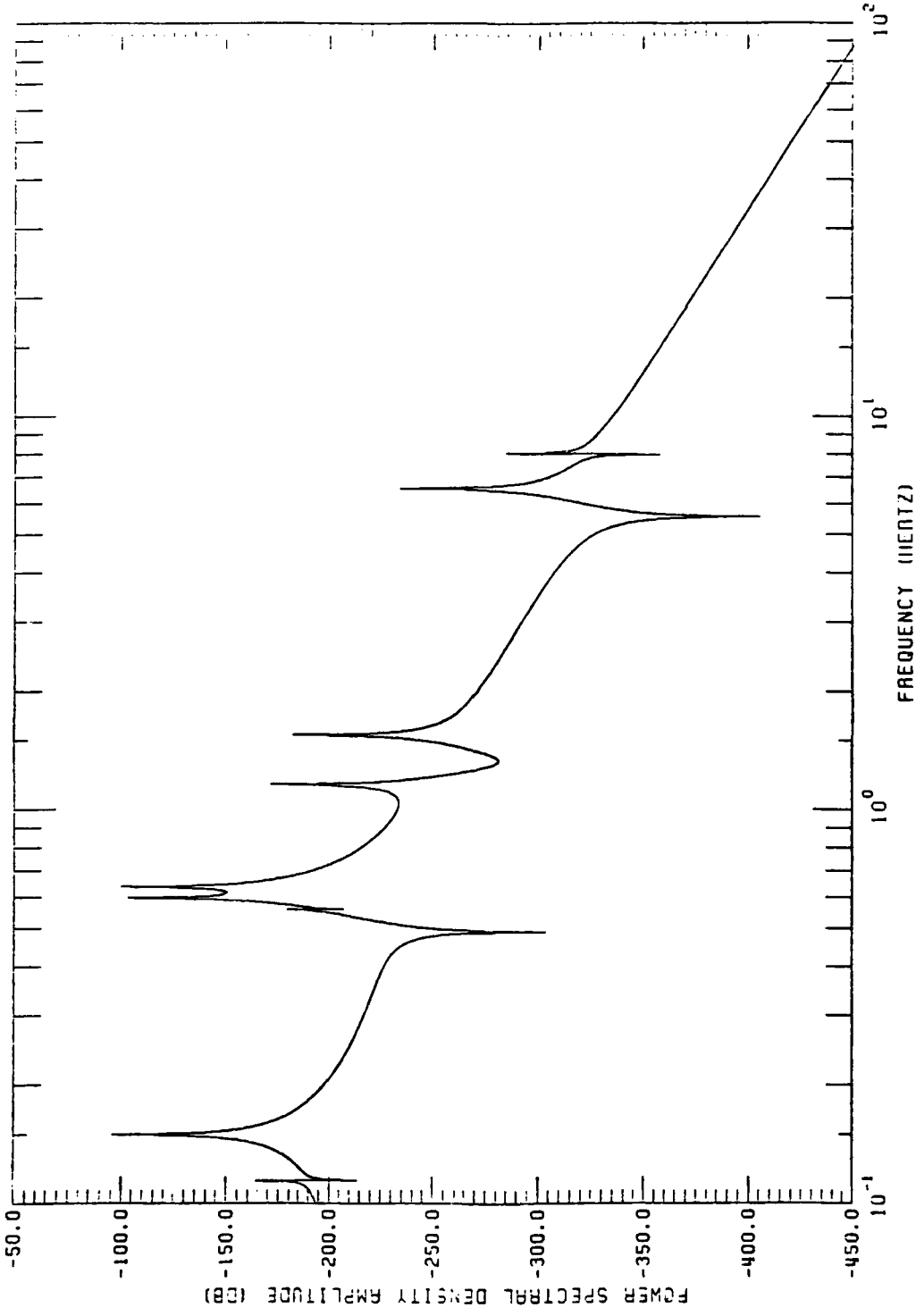

Figure 2-3f. Disturbance at node 46, output LOS-Z.

Figures 2-4. Open-loop output power spectral density for 20-mode evaluation model due to broad-band disturbance.

(On following pages)

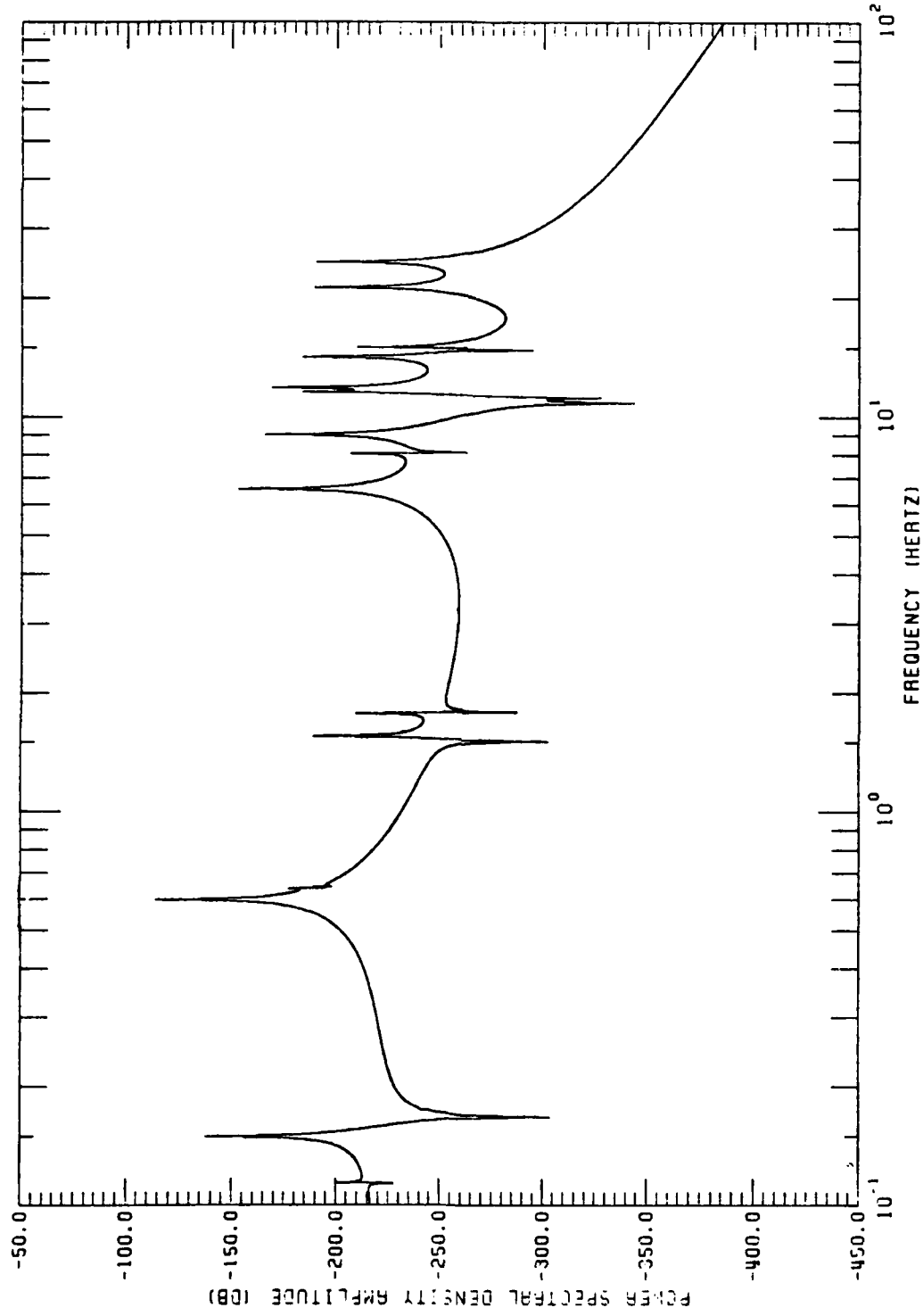

Figure 2-4a. Disturbance at node 37, output LOS-X.

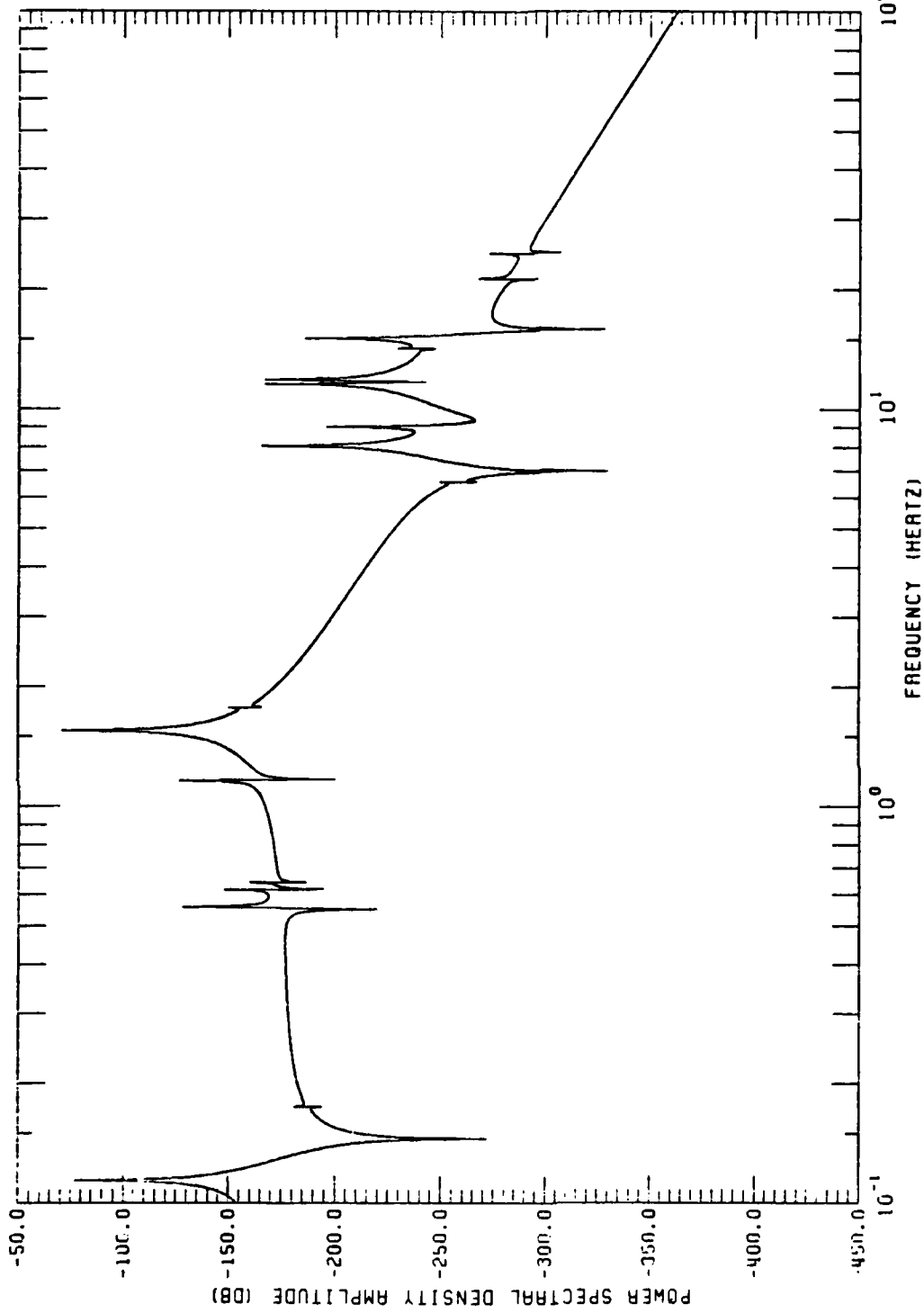

Figure 2-4b. Disturbance at node 37, output LOS-Y.

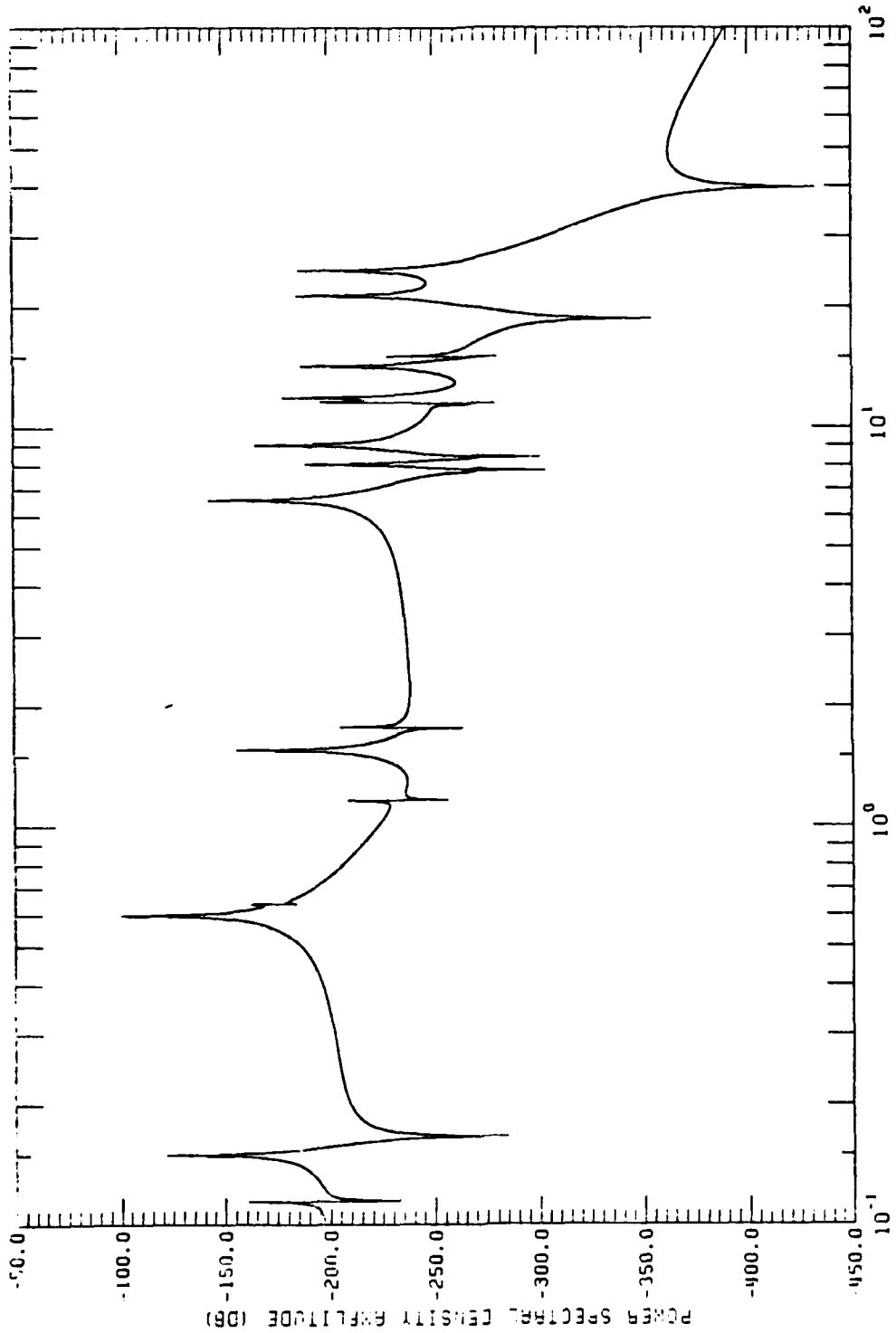

Figure 2-4c. Disturbance at node 37, output LOS-Z.

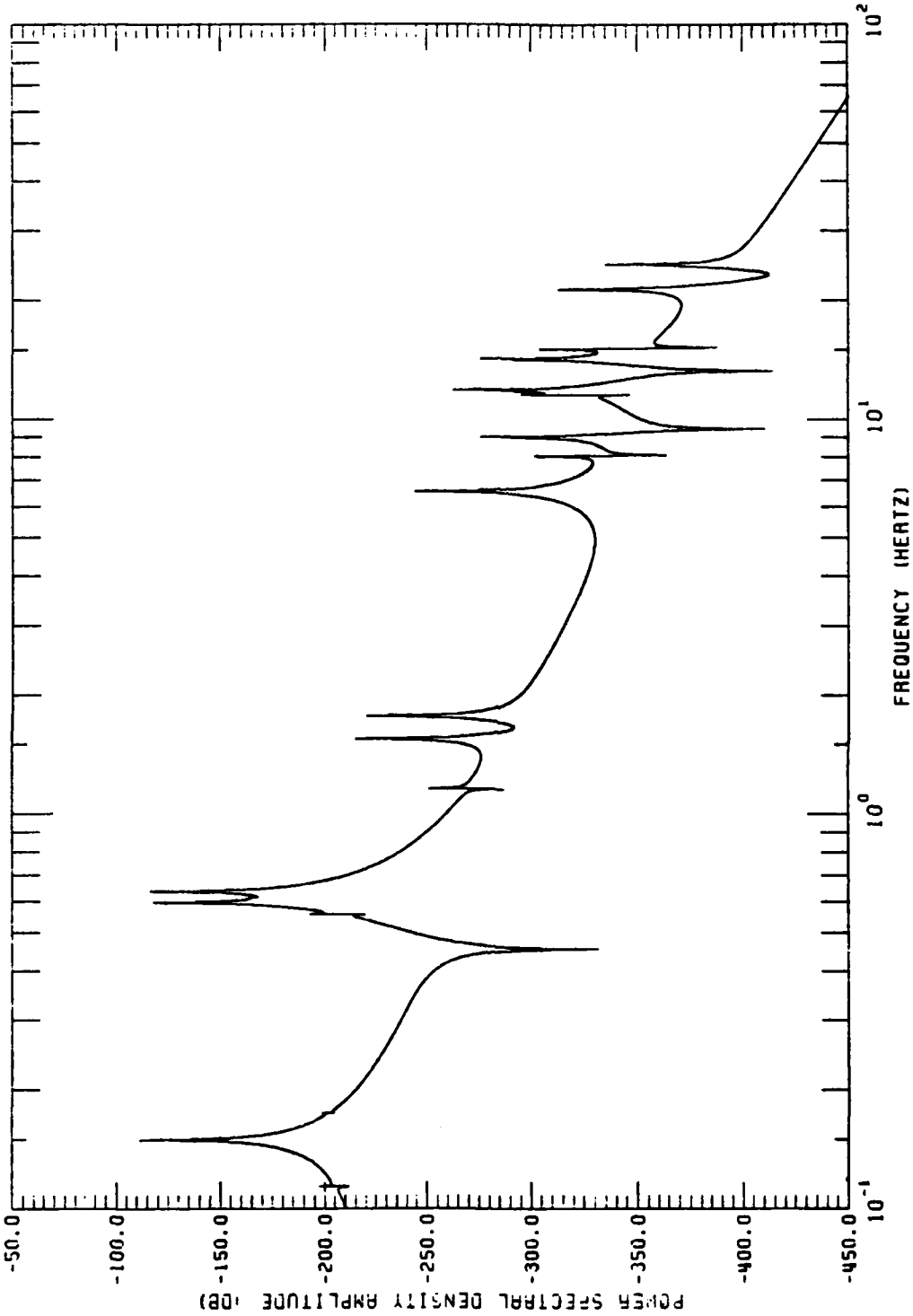

Figure 2-4d. Disturbance at node 46, output LOS-x.

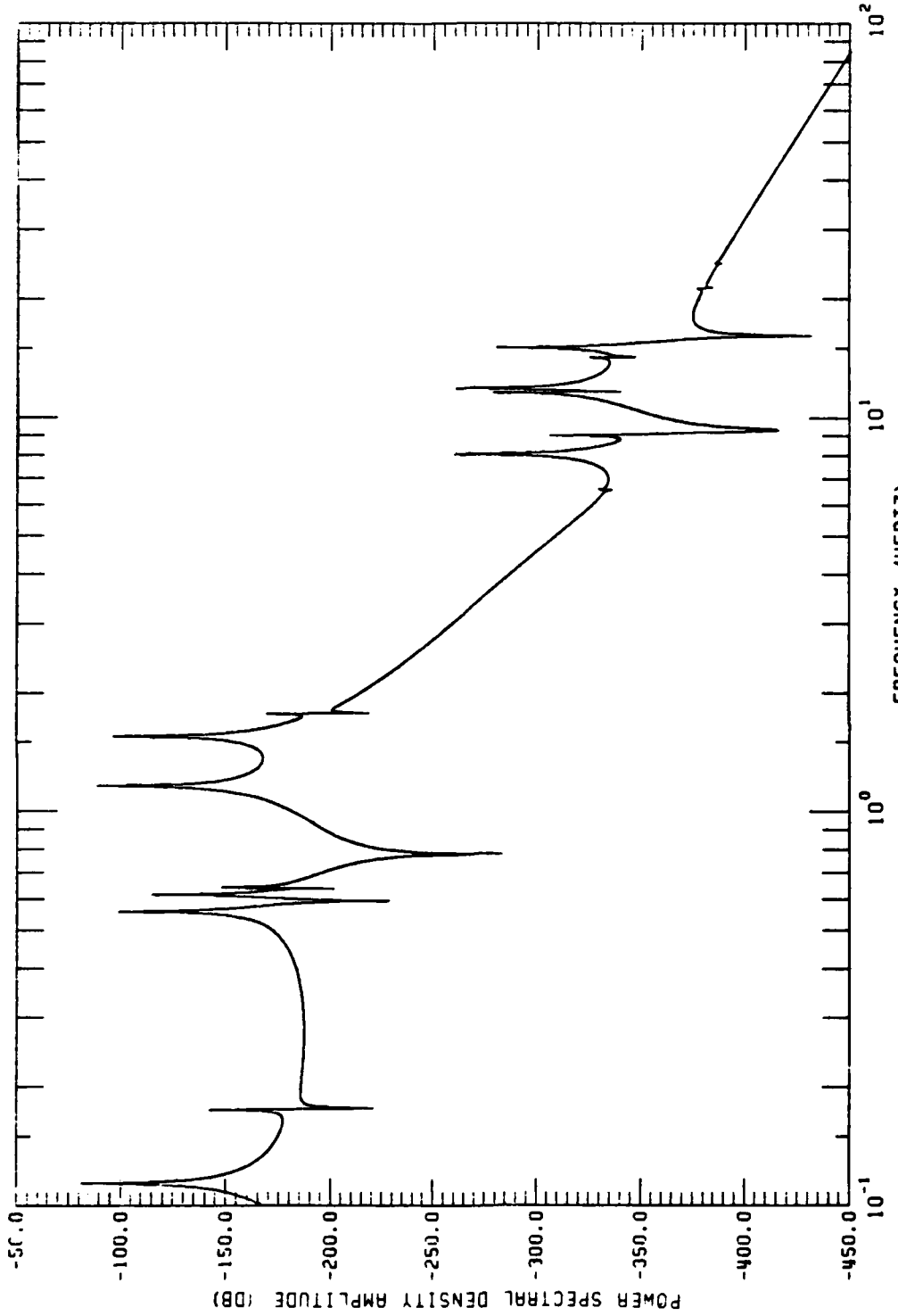

Figure 2-4e. Disturbance at node 46, output LOS-Y.

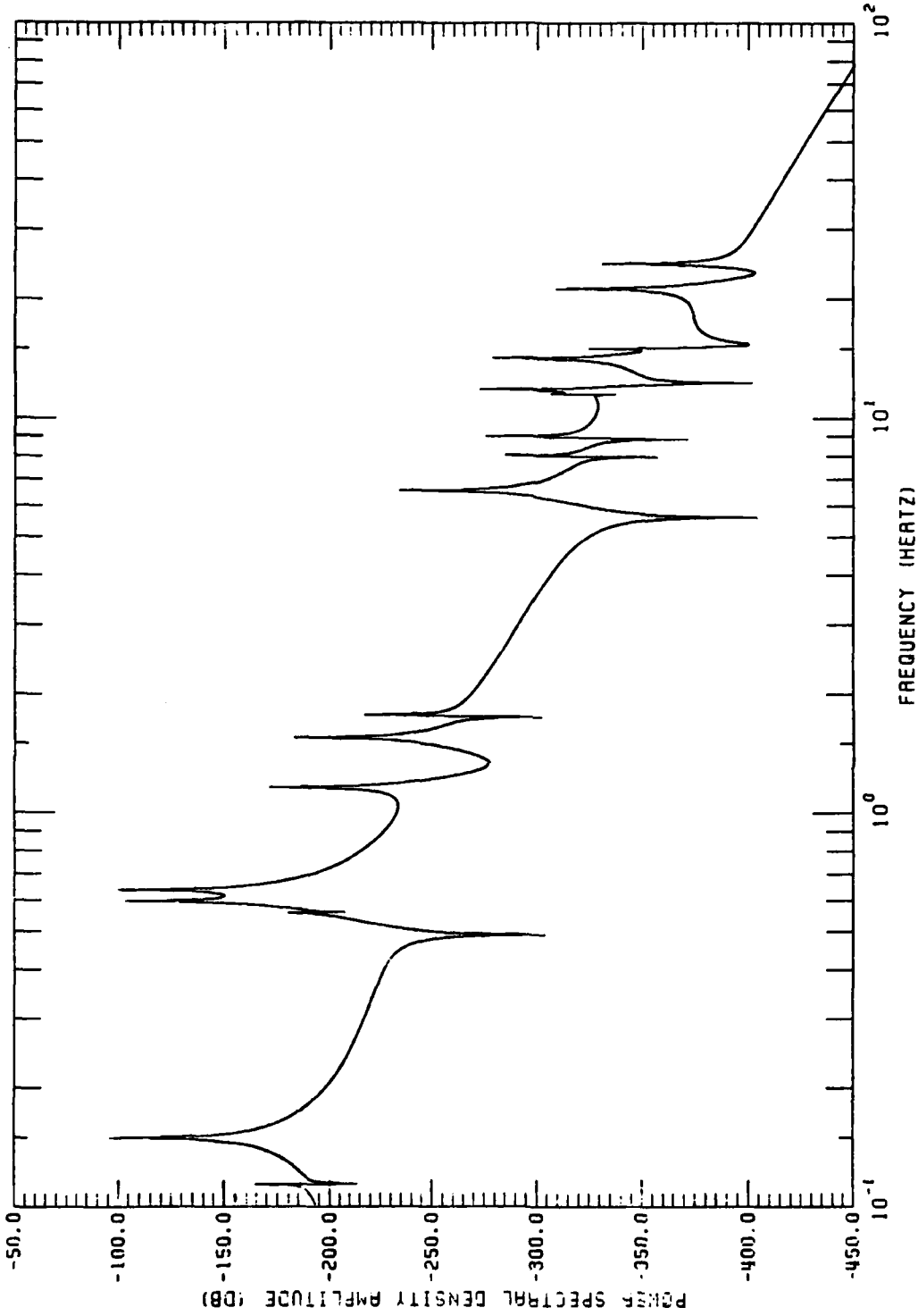

Figure 2-4f. Disturbance at node 46, output LOS-Z.

SECTION 3

SENSOR/ACTUATOR SELECTION

3.1 Introduction

The problem of selecting the location and type of sensors and actuators for the active control of large scale structures has not received enough attention by the community. Whereas such a selection is fairly straightforward for well understood structures (e.g., beam, plate) it is extremely difficult when one considers complex truss structures like the ACOSS Model No. 2. To demonstrate this difficulty consider the utilization of member dampers. Among the advantages of such actuators are their low price, ease of installation, availability, and the fact that they do not affect the rigid body motion. However, the number of members in ACOSS Model No. 2 (Revision 3) is 137, and thus the selection of location for such actuators is formidable. (Note that member actuators can also be placed between nodes which are actually not connected by members in the original structure design, making the problem even more prohibitive.)

In this section we address the selection of sensor/actuator location and derive a procedure which we believe should provide a meaningful selection. Our approach to the problem is demonstrated via application to ACOSS Model No. 2. The selection provided here has been used in the control designs discussed in the other sections of this report.

A flow chart of the selection procedure is given in Figure 3-1. The preliminary selection step and the "structural insights" are discussed in Section 3.3. Our main contribution, the LOS matching concept, is the subject of Section 3.2.

3.2 The Node Shape Matching Concept

3.2.1 Preliminaries

To establish convenient notations and terminology, a few definitions are called for at this point.

The vibration model of a structure can be specified via the triplet (S, Z, Φ) where

$S = [\omega_1, \omega_2, \cdots]$ denotes the structural frequencies

$Z = [\zeta_1, \zeta_2, \cdots]$ denotes the associated damping ratios

$\Phi = [\underline{\phi}_1, \underline{\phi}_2, \cdots]$ denotes the matrix of mode shapes

(Note: Φ is the modal matrix associated with $Z \equiv 0$.) Each of the vectors $\underline{\phi}_i$ is a 6N vector which describes the i-th mode shape at the N structural nodes in 6 degrees of freedom. Denote the rows of Φ by $\underline{f}_1, \underline{f}_2, \cdots$, i.e.,

$$\Phi^T = [\underline{f}_1, \underline{f}_2, \cdots, \underline{f}_{6N}] \tag{3-1}$$

where Φ^T denotes the transpose of Φ. Assume without loss of generality that the $\underline{f}_i$ are organized such that if

$$(i)_{\text{mod } 6} = j-1, \quad (i-j+1)/6 = \ell-1 \tag{3-2}$$

then $\underline{f}_i$ corresponds the ℓ-th mode in the j-th degree of freedom.

By analogy to the concept of mode shape, we define node shape as follows:

Definition. Let $\underline{x}$ be any vector of dimension 6N. Then $\phi^T\underline{x}$ is called a node shape associated with $\underline{x}$.

To illustrate the usefulness of the node shape concept, some examples are given:

(a) The Standard Node Shape

The vector $\underline{f}_i$ corresponds to the node shape at the ℓ-th node in the j-th degree-of-freedom using the relations (3-2). Thus choosing the vector $\underline{x}$ to have the entries $\underline{x}_i$, i=1, •••, N, satisfying

$$\underline{x}_i = \begin{cases} \alpha, & i = 6\ell + 1 \\ \beta, & i = 6\ell + 2 \\ \gamma, & i = 6\ell + 3 \\ 0, & \text{otherwise} \end{cases}$$

with $\alpha^2 + \beta^2 + \gamma^2 = 1$ gives the normalized translation node shape in the direction $\begin{bmatrix} \alpha \\ \beta \\ \gamma \end{bmatrix}$ at node ℓ.

(b) LOS Node Shape (See Ref. 3-1 for details)

The line-of-sight (LOS) error about the x and y axes is a linear combination of the displacement of the mirror support-points expressed as

$$\text{LOS} = \sum_{i=1}^{NS} \alpha_i u_i ,$$

where NS = number of mirror support degrees-of-freedom.

Since $u_i = \underline{\phi}_i^T \underline{\eta}$, the above can be expressed as

$$LOS = \sum_{i=1}^{NS} \alpha_i \underline{\phi}_i^T \underline{\eta}$$

$$= \left[\Phi^T a\right]^T \underline{\eta}$$

where

$$\mathscr{A}^T = \begin{bmatrix} \alpha_{LOSX,1} & \cdots & \alpha_{LOSX,NS} \\ \alpha_{LOSY,1} & \cdots & \alpha_{LOSY,NS} \\ \alpha_{DEFOCUS,1} & \cdots & \alpha_{DEFOCUS,NS} \end{bmatrix} = \begin{bmatrix} \underline{\alpha}_{LOSX}^T \\ \underline{\alpha}_{LOSY}^T \\ \underline{\alpha}_{DEFOCUS}^T \end{bmatrix}$$

to give $\underline{f}_{LOSX} = \Phi^T \underline{\alpha}_{LOSX}$, $\underline{f}_{LOSY} = \Phi^T \underline{\alpha}_{LOSY}$, $\underline{f}_{DEFOCUS} = \Phi^T \underline{\alpha}_{DEFOCUS}$, the three LOS errors.

(c) Axial Node Shape

The axial displacement of a member connecting nodes 1 and 2 is given by

$$A_{12} = \underline{b}_1^T \underline{u}_1 - \underline{b}_2^T \underline{u}_2$$

where

A_{12} = axial displacement between nodes 1 and 2,

$\underline{u}_1$, $\underline{u}_2$ = the displacement vectors at nodes 1 and 2, respectively, of the connecting element (1,2)

$\underline{b}_1$, $\underline{b}_2$ = coordinate transformation for element (1,2).

Expanding this equation to include all elements of interest, we get A=BU, where B is the matrix of element coordinate transforms. Transforming the displacement vector $\underline{u}$ into modal coordinates gives

$$A = (\Phi^T B^T)^T \underline{\eta}$$

and thus $\Phi^T B^T$ gives the node shape matrix for axial displacements. Each column of the matrix represents the axial displacement of one element for a unit amplitude of each mode.

In light of the above definition and examples we note that selecting the location and type of actuators (e.g. member damper, momentum wheel) and sensors is equivalent to choosing a set of node shapes in the sense of the above definition. We propose the following philosophy for the selection of a set of node shapes.

3.2.2 Selection of Node Shapes

The actuators/sensors location selection can be formulated using the following dynamic representation of the structure

$$\ddot{\underline{\eta}} + \mathscr{L}\dot{\underline{\eta}} + \Omega\,\underline{\eta} = (\Phi^T X_u)\,\underline{u} + (\Phi^T X_d)\underline{d} \qquad (3\text{-}3)$$

$$\underline{p} = (\Phi^T X_p)^T \underline{\eta} \quad , \qquad \underline{v} = (\Phi^T X_v)^T \dot{\underline{\eta}} \tag{3-4}$$

where

$$\mathscr{L} = \text{diag } (2\zeta_1\omega_1,\ 2\zeta_2\omega_2,\ \cdots\ 2\zeta_n\omega_n)$$

$$\Omega = \text{diag } (\omega_1^2,\ \omega_2^2,\ \cdots\ \omega_n^2)$$

$\underline{u}$ is the input (actuation) vector of dimension m_u

$\underline{p}$ is a position output (sensing) vector of dimension m_p

$\underline{v}$ is a velocity output (sensing) vector of dimension m_v

$\underline{d}$ is a disturbance input to the structure.

The matrices $X_u(n \times m_u)$, $X_p(m_p \times n)$, and $X_v(m_v \times n)$ generate the node shapes associated with the corresponding actuators/sensors location. For example, if $\underline{x}_u(1)$ is the first column of X_u, then $\Phi^T\underline{x}_u(1)$ is the node shape associated with u_1--the first actuator in the vector $\underline{u}$. Similarly, the node shape associated with p_1, the first position sensor, is $\Phi^T\underline{x}_p(1)$, where $\underline{x}_p(1)$ is the first column of X_p.

Noting that LOS = $\underline{f}_\star{}^T\underline{\eta}$, we can formulate the selection problem as follows:

> Find X_u, X_p, X_v to enable the best control of the LOS. Namely, if a certain mode does not affect the LOS significantly (corresponding to a relatively small entry in $\underline{f}_\star$) one does not have to control it or observe it.

This idea can be expressed mathematically in view of Eqs. (3-1) and (3-2) as follows.

Select X_p (and X_u and X_v) such that

$$\underline{f}_* \doteq \Phi^T X_p \cdot \underline{\alpha}$$

where $\underline{\alpha}$ is some arbitrary vector of appropriate dimension and $\doteq$ means "approximately equal".

The above formulation can be somewhat simplified, assuming an initial (large) set of locations has already been selected (see next section for this step). Let the corresponding node shapes be $\{\underline{f}_1, \cdots, \underline{f}_1\}$. The problem thus reduces to a selection of a subset of L node shapes out of the N which provides a good approximation of $\underline{f}_*$.

Criteria for selection

Choose nodes $\{i_1, i_2, \cdots i_L\}$ from $\{1, \cdots N\}$ such that

(1) $$\sum_{j=1}^{L} \alpha_j \underline{f}_{i_j} \doteq \underline{f}_* \text{ , and}$$

(2) All the α_j's are of comparable/acceptable order of magnitude.

Definition A selection of node shapes satisfying the criteria (1) and (2) is called a balanced selection.

Remarks

(i) The objective is to achieve a balanced selection with L as small as possible. A balanced set of sensors (actuators) means that similar sensors, i.e., with the same sensitivity, can be used at all locations (the same power is required of all the actuators).

(ii) It is obvious that a set of independent nodes are sought, barring redundancy (fault tolerance) considerations.

We propose as a mathematical criterion for "approximately equal" the quadratic cost function. Thus the selection problem can be formulated as follows.

3.2.3 Least Squares Formulation

Solve

$$\min_{\underline{\alpha}} \left[\underline{f}_* - \sum_{i=1}^{N} \alpha_i \underline{f}_i\right]^T D \left[\underline{f}_* - \sum_{i=1}^{N} \alpha_i \underline{f}_i\right] \qquad (3\text{-}5)$$

where $D = \text{diag}\left[d_1, d_2, \cdots d_N\right]$, subject to the constraints:

(a) N-L of the α_i's are zero, and

(b) The L nonzero α_i's form a balanced set.

To the best of our knowledge, the above problem has not been solved. Thus, we propose an iterative procedure to obtain an acceptable (suboptimal) approximation to the selection problem which is based on the QR factorization.

The purpose of the D matrix in Eq. (3-5) is to weight the different modes according to their relative contribution to the LOS performance. For example, in ACOSS Model No. 2, with the disturbance discussed in Section 2, a reasonable way to weight the modes is in proportion to the root-mean-square (RMS) LOS amplitude associated with the given disturbance.

3.2.4 The QR Factorization

Consolidating the set of node shapes $\underline{f}_1, \cdots, \underline{f}_N$ into a matrix F,

$$F = [\underline{f}_1 \quad \cdots \quad \underline{f}_N], \qquad n \times N$$

we can write Eq. (3-5) as

$$F\,\underline{\alpha} \overset{L.S.}{=} \underline{f}_* \tag{3-6}$$

where "$\overset{L.S.}{=}$" means equality in the Least Squares sense. Note that for the time being we ignore constraint (a). Using the QR factorization (a standard program available in LINPACK) we get

$$F = QR \tag{3-7}$$

where

$$Q = [\underline{q}_1 \quad \cdots \quad \underline{q}_N]\ ;\ \underline{q}_i^T \underline{q}_j = \delta_{ij};\quad \underline{q}_i \in R^n$$

$$R = \begin{bmatrix} r_{11} & x & x & \cdots & x \\ & r_{22} & x & & x \\ & & r_{33} & & \\ & & & \ddots & \\ & 0 & & & r_{NN} \\ \hline & & 0 & & \end{bmatrix} = \begin{bmatrix} & R_u & \\ \hline & 0 & \end{bmatrix}$$

and each x denotes an arbitrary value. Using the QR factorization, we also have the additional property

$$r_{ii} \geq r_{i+1,\ i+1} \geq \cdots \geq r_{NN} \geq 0$$

and each r_{ii} is larger than any other entry in its row. Using the QR factorization, Eq. (3-6) can be written as

$$R\ \underline{\alpha} \overset{\text{L.S.}}{=} Q^T \underline{f}_* \ , \quad B = R_u \underline{\alpha} = [\underline{q}_1 \cdots \underline{q}_N]^T \underline{f}_* \ , \tag{3-8}$$

$$\underline{\alpha} = R_u^{-1} [\underline{q}_1 \cdots \underline{q}_N]^T \underline{f}_*$$

Note that $\underline{q}_i (\underline{q}_i^T \underline{f}_*)$ is the projection of $\underline{f}_*$ on $\underline{q}_i$ and that $r_{ii}\underline{q}_i$ is the length of the component of $\underline{f}_i$, orthogonal to the span of $\{\underline{f}_1, \cdots, \underline{f}_{i-1}\}$. Thus the pair (r_{ii}, b_i) gives an indication of the contribution of $\underline{f}_i$ to the L.S. approximation of $\underline{f}_*$. Thus, elimination of $\underline{f}_i$'s with relatively small r_{ii} or b_i or $r_{ii} \cdot b_i$ will not result in a significant increase in the error of the L.S. approximation, i.e., in the norm of the residual vector R

$$\underline{R} = \underline{f}_* - [\underline{q}_1, \cdots \underline{q}_N]\ \underline{\alpha} \tag{3-9}$$

3.3 Preliminary Selection and Refinement

As discussed in the previous section, the selection procedure is simplified by starting with an initial set of locations, say $\underline{f}_1, \cdots, \underline{f}_N$.

The preliminary N actuators/sensors have been selected as member actuators (sensors). This selection is based on the ranking of the members according to their elongation for each mode. The members undergoing the most elongation (stress) for those modes which have most effect on the LOS are selected as the initial set.

Application of the selection procedure of the previous section leads to a reduced set of members with LOS node shape matching which does not differ considerably from the match obtained with the preliminary selection. If the matching is not satisfactory, additional actuators have to be added. Inspection of the mismatch in the residuals as defined in Eq. (3-9) indicates the modes which are not well-matched (i.e., controlled or observed from the selected set.) The actuators (sensors) to be added should compensate for this deficiency. As discussed in the next section, it is possible that there exists no member capable of controlling certain modes which do have significant influence on the LOS. In such an event, a different type of actuator (force or torque generating actuators) must be utilized. The selection of the locations for such actuators can be aided by visual inspection of the vibrating structure simulation and/or the analysis of the mode shape.

3.4 Results

The selection procedure described above has been applied to ACOSS Model No. 2.

Test 1. A 50 mode model has been used. The initial set of actuators included all mirror mounts as well as some members. The selection procedure has been applied to yield a perfect match of the LOS where the

locations selected were the mirror mounts. This academic test verifies the basic philosophy.

Test 2. For the purpose of the control design demonstration, the 20-mode model has been selected. The weighting matrix D of Eq. (3-5) has been selected so that each mode is weighted by its expected RMS error due to the prescribed disturbance. An initial set of member actuators has been selected using the elongation concept. Iterating the selection procedure resulted in unsatisfactory residuals. Examination of the problematic modes revealed that the uncontrolled modes were solar panel modes which have strong coupling to the LOS. Moreover, it was observed that there exists no member capable of providing good control/observation authority on these modes. Adding force actuators proved to be satisfactory. The final selection is given in Figure 3-2. Note that the selection is not obvious intuitively, but can (after the fact) be given acceptable structural justification. Moreover, it is conceivable that by changing the properties of the selected members, the structure will be less sensitive (in terms of LOS performance) to the given disturbances.

References

3-1 Henderson, T., "Active Control of Space Structures (ACOSS) Model 2", Charles Stark Draper Laboratory, Cambridge, MA, Report C-5437, Sept. 1981.

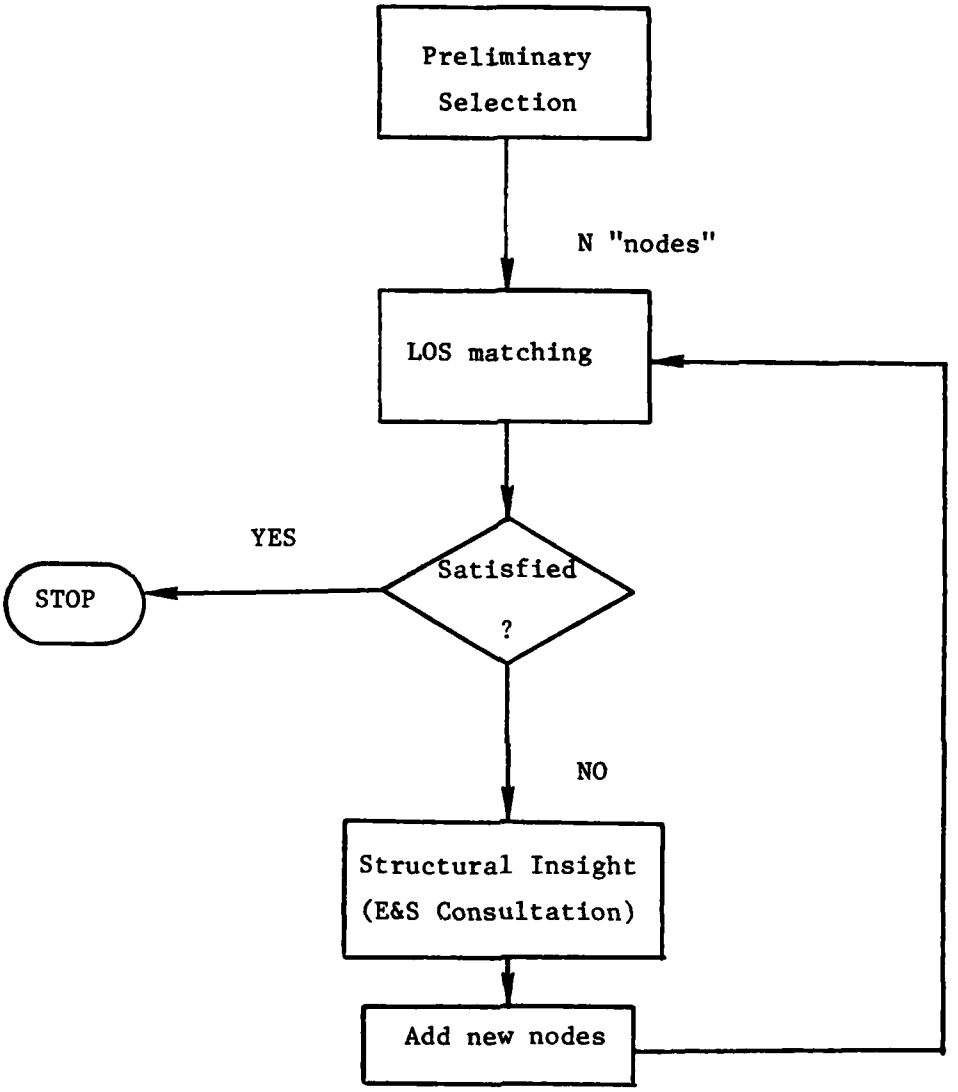

Figure 3-1. Procedure.

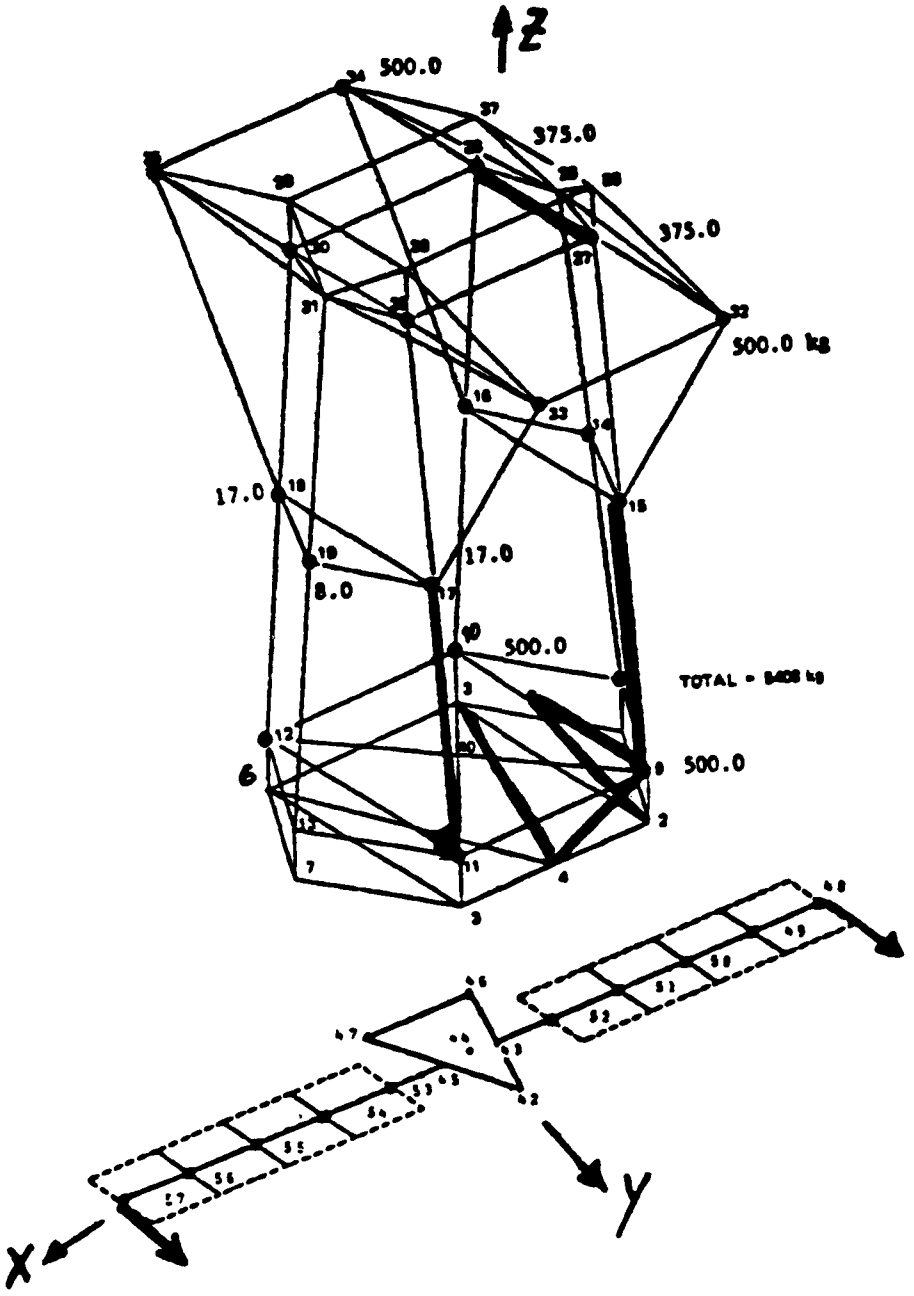

Figure 3-2. Final selection of sensors (actuators).

SECTION 4

DISTURBANCE REJECTION CONTROL DESIGN

4.1 Introduction

The broad-band disturbance described in Section 2 poses a difficult control problem. Specifically, the RMS value of the line-of-sight (LOS) due to the disturbance is, in the open loop, of the order of 100 μ-radians (μrad) in LOS-X and over 1000 μrad in LOS-Y (see Table 4-1), whereas the desired RMS of the LOS error should not exceed 0.05 μrad. Namely, the control objective is to reduce the effect of the disturbance by four orders of magnitude!!!

To assess our ability to achieve this design objective, an optimal disturbance rejection controller is presented in this section. The goal here is to assess the following issues: (a) Can the control objective be achieved under optimal (unrealistic) conditions? (b) If the answer to (a) is affirmative, what insight into the design of a realistic control might be gained from the characteristics of the optimal control?

It is demonstrated in this section that the control objective can be achieved under optimal conditions, and conclusions are drawn with regard to the type of control that should be designed to reject the given level of disturbance.

In Section 4.2, the control design philosophy is outlined. Section 4.3 is devoted to a detailed description of the designed controller. The frequency response of the controlled structure, the

feedback gains, and the pole distribution of the closed loop system are presented. We also make an effort to extrapolate from this design to the desired features of a realistic design.

4.2 Disturbance Rejection Control

4.2.1 The Model

The theory of optimal disturbance rejection is most conveniently studied via the state-space representation of the system dynamics (structure and disturbance model) [Ref. 4-1]. Thus, we use the following representation for the N-mode structure

$$\dot{x} = Ax + B_u u + B_d d \,, \qquad x \in R^{2N};\ u \in R^m,\ d \in R^P \tag{4-1}$$

$$y = Cx \,, \qquad y \in R^{\ell} \tag{4-2}$$

$$LOS = C_L x \,, \qquad LOS \in R^3 \tag{4-3}$$

where, as is common in the context of structures, A is given by:

$$A = \left[\begin{array}{ccc:ccc} & & & 1 & & \\ & 0 & & & \ddots & 0 \\ & & & 0 & & \ddots \\ \hdashline & & & & & 1 \\ -\omega_1^2 & & 0 & -2\zeta_1\omega_1 & & 0 \\ & \ddots & & & \ddots & \\ & & \ddots & & & \\ 0 & & -\omega_N^2 & 0 & & -2\zeta_N\omega_N \end{array}\right] \tag{4-4}$$

B_u = actuators influence matrix of dimension $2N \times m$,
m = number of actuators

C = sensors observation-matrix of dimension $\ell \times 2N$,
ℓ = number of sensors.

Here we consider colocated sensors/actuators, thus $\ell = m$. The disturbance influence-matrix is B_d, where in our analysis it is of dimension $2N \times 2$. (See Section 2.)

Finally, since the objective is to control the structure subject to the disturbance, as specified via its power spectral density (PSD) in Section 2, it is convenient to consider the disturbance as a stochastic process represented by the state equation

$$\dot{d} = A_d d + B_\omega \omega \tag{4-5}$$

where

$$A_d = \begin{bmatrix} \lambda_1 & 0 \\ 0 & \lambda_2 \end{bmatrix} \qquad B_\omega = \begin{bmatrix} b_{\omega 1} & 0 \\ 0 & b_{\omega 2} \end{bmatrix} \tag{4-6}$$

and $\omega = \begin{bmatrix} \omega_1 \\ \omega_2 \end{bmatrix}$ is a (vector) white noise with $E\left(\begin{bmatrix} \omega_1 \\ \omega_2 \end{bmatrix} \begin{bmatrix} \omega_1 & \omega_2 \end{bmatrix}\right) = I$.

Here, λ_1 and λ_2 reflect the bandwidth of the disturbances and $b_{\omega 1}$, $b_{\omega 2}$ their amplitudes.

Combining the structure representation of Eqs. (4-1)-(4-4) with the disturbance model of Eqs. (4-5)-(4-6) yields the augmented system equations

$$\frac{d}{dt} \begin{bmatrix} x \\ d \end{bmatrix} = \begin{bmatrix} A & B_d \\ 0 & A_d \end{bmatrix} \begin{bmatrix} x \\ d \end{bmatrix} + \begin{bmatrix} 0 \\ B_\omega \end{bmatrix} \omega + \begin{bmatrix} B_u \\ 0 \end{bmatrix} u \tag{4-7a}$$

$$y = \begin{bmatrix} C & 0 \end{bmatrix} \begin{bmatrix} x \\ d \end{bmatrix} \tag{4-7b}$$

$$LOS = \begin{bmatrix} C_L & 0 \end{bmatrix} \begin{bmatrix} x \\ d \end{bmatrix} \tag{4-7c}$$

or, equivalently, with proper definitions of the augmented terms in Eq. (4-7), the augmented system dynamic equations can be written as

$$\dot{x}_a = A_a x_a + B_{a\omega} \omega + B_{au} u \tag{4-8a}$$

$$y = C_a x_a \tag{4-8b}$$

$$LOS = C_{aL} x_a \tag{4-8c}$$

The model of the system in Eq. (4-8) is the basis for the control design below. It is thus appropriate at this junction to question the availability of such a model for a control design. Specifically, one should question the validity of the disturbance model. The assumption that the spectral content of the disturbance is available is a reasonable one, as the disturbance source is often understood or can be measured. Hence, assuming knowledge of the terms defined in Eq. (4-6) is reasonable. The difficult assumption is that made with regard to the knowledge of the matrix B_d. Although certain noise sources (e.g., imbalance of a rotating wheel) have well-defined points of contact with the structure (i.e., well-defined B_d), other noise sources may have more distributed effect on the structure, such that knowledge of B_d is

less likely. The principal value of the control design study to be described below is in the exposition of the characteristics and limitations of a disturbance rejection controller which is based on the assumed knowledge with regard to the disturbance.

4.2.2 Optimal Control Design

Given the augmented dynamic equation Eq. (4-8), we design the optimal disturbance rejection controller using the separation principle [Ref. 4-1]:

(a) We assume that the augmented state is available, and design an optimal regulator.

(b) Using the available measurement y, we construct a Kalman type filter to estimate the state. It should be noted that, in our problem formulation, there is no measurement noise. We use the noise variance as a design parameter which helps in the loop shaping and circumvents the problem of designing a "singular Kalman filter" or an arbitrary observer.

(c) We cascade the state estimator by the optimal state feedback gain.

The design of the optimal regulator involves the following procedure.

(a.1) Define the cost functional

$$J = \lim_{T\to\infty} \frac{1}{T} \int_0^T \left[(LOS)^T Q (LOS) + \rho\, U^T R U \right] dt \qquad (4\text{-}9)$$

Free design parameters in Eq. (4-9) are the matrix

$$Q = \begin{bmatrix} q_1 & 0 & 0 \\ 0 & q_2 & 0 \\ 0 & 0 & q_3 \end{bmatrix}$$

and the scalar ρ.

We have arbitrarily fixed R to be the identity matrix, since we assume that all actuators are of the same type; i.e., their power consumption and influence are the same, such that they should be penalized equally. Obviously, if some actuators are more expensive to use in some sense (e.g., a propellant actuator), this should be reflected in the corresponding entry of the matrix R. The cost functional depends on the line-of-sight output variable "LOS" and not explicitly on the state, since we are interested only in line-of-sight performance. The free parameters q_i, i=1,2,3, are chosen to reflect the contribution of the i-th degree of freedom to the line-of-sight error. The scalar ρ is an adjustable parameter to be tuned to achieve the design objectives.

(a.2) The regulator gain G is calculated via the equations:

$$G = -(\rho R)^{-1} B_a^T P \qquad (4\text{-}10a)$$

$$A_a^T P + P A_a + (C_{aL})^T Q (C_{aL}) + P B_{au} (\rho R)^{-1} B_{au}^T P = 0 \qquad (4\text{-}10b)$$

The regulated system (with state feedback) is given by

$$\dot{x}_a = (A_a + B_{au} G)\, x_a + B_{a\omega}\, \omega \tag{4-11a}$$

$$LOS = C_{aL} x_a \tag{4-11b}$$

(b) The optimal state estimator is calculated using the relations dual to those used in the optimal regulator design. The estimator equation is

$$\frac{d}{dt}\hat{x}_a = A_a \hat{x}_a + B_{au}\, u + K[y - C_a \hat{x}_a] \tag{4-12}$$

where the optimal estimator gain K is calculated via

$$K = L\, C_a^T\, (\rho_o I)^{-1} \tag{4-13a}$$

$$A_a L + L\, A_a^T + B_{a\omega}\, B_{a\omega}^T - L\, C_a^T (\rho_o I)^{-1}\, C_a L = 0 \tag{4-13b}$$

The gain calculated in Eq. (4-13) is optimal with respect to the cost functional

$$J = E[(\hat{x}_a - x_a)^T\, (\hat{x}_a - x_a)] \tag{4-14}$$

where E denotes the expectation operator. The scalar ρ_o is a design parameter in this section.

In optimal estimation theory, $\rho_o I$ is replaced by the measurement noise covariance matrix.

Note: The Riccati equation Eq. (4-10b) is of order 2N+p. Since the disturbance state d is uncontrollable, the Riccati equation can be partitioned, to yield

$$A^T P_{11} + P_{11} A + Q - P_{11} B_u R^{-1} B_u^T P_{11} = 0 \qquad (4\text{-}15a)$$

$$(A - B_u R^{-1} B_u P_{11})^T P_{12} + P_{12} A_d + P_{11} B_d = 0 \qquad (4\text{-}15b)$$

where Eq. (4-15a) is a Riccati equation of order 2N (quadratic equation in P_{11}) and Eq. (4-15b) is known as a Sylvester equation [Ref. 4-2]. The optimal gain is given by

$$K = - (\rho R)^{-1} \left[B_u^T P_{11} \quad B_u^T P_{12} \right] \qquad (4\text{-}15c)$$

For a large number of disturbances (p large; see Eq. (4-1)), solving Eq. (4-15) rather than Eq. (4-10) has definite numerical advantages. However, in our case, $p << 2N$ which reduces the benefit in solving Eq. (4-15), especially when we note the additional software needed to solve the Sylvester equation. Nevertheless, it is important to note the relations in Eq. (4-15), since it clearly shows that the stability of the state feedback does not depend on the disturbance model. The latter enters into the plant only in the feed-forward term

$$- (\rho R)^{-1} B_u^T P_{12} \, d$$

Although partitioning of Eq. (4-13) does not yield the same benefit as in the optimal state feedback, it should be noted that the stability of the disturbance rejection scheme still does not depend on the accuracy of the disturbance model. This follows from the separation theorem [Ref. 4-1] which implies separate pole assignment for the regulator and the estimator. Namely, N of the poles are assigned by the matrix K, as if the filter were not in the loop, and N poles are the filter poles. Thus, from the stability point of view, the questions raised above concerning the disturbance model are of no consequence. Inaccuracy of the disturbance models, as discussed above, will only affect the RMS value.

4.3 Application to ACOSS Model No. 2

The disturbance rejection control scheme outlined above has been applied to ACOSS Model No. 2. The design involved few iterations in which the various design parameters mentioned earlier have been adjusted and the corresponding performance (RMS values and frequency response) assessed. It was found that the control penalty has to be of the order 10^{-17} to achieve the design objectives. Namely, to achieve four orders of magnitude reduction in the RMS value requires substantial control effort which translates into low control penalty in the quadratic cost function Eq. (4-9). Furthermore, best results have been obtained when LOS-Y was weighted 10 times more than LOS-X, whereas LOS-Z (defocus) can be lightly weighted in the cost penalty. A sample of the RMS LOS-error for different design parameters is given in Table 4-1. For each design, values are given both for the case that state feedback is applied directly to the state (LQR) and to the estimated state (OBS/LQR). In Figures 4-1a through 4-1f, the closed-loop frequency response with optimal state feedback, and the open loop response from u_i, i=1,2, ($u_1 \equiv$ disturbance at node 37; $u_2 \equiv$ disturbance at node 46) to y_j, j=1,2,3, (LOS-X, LOS-Y, LOS-Z) are plotted. Figures 4-2a through 4-2f give the corresponding closed-loop responses with observer in the loop, and give a comparison with the responses for the closed-loop sy tem without an observer. All figures are for Case 5 of Table 4-1.

Examination of Table 4-1 and Figures 4-1a through 4-2f reveals the following features of the disturbance rejection controller.

There is a reduction of the gain over the 0-5 Hz range of 150 db to 200 db. There is some difficulty in controlling the three closely-spaced modes 13, 14, 15 (0.59 Hz, 0.61 Hz, 0.63 Hz respectively), a phenomenon which exhibits itself in the "glitch" at about 0.6 Hz in Figures 4-1a, 4-1c, 4-1d, 4-1e and 4-1f. (See explanation in Ref. 4-3.) However this is a local phenomenon which does not affect the RMS value significantly. Figures 4-2a through 4-2f are the corresponding frequency responses when a Kalman filter is introduced into the loop. There is good correspondence of the frequency response in each case between the optimal closed loop with and without the filter in the low frequencies (less than 5 Hz). For higher frequencies the optimal control with filter has higher gain to yield a broader bandwidth transfer function. Note in particular the deterioration in performance for the channel u_1 to y_2 where the transfer function is almost flat with the filter in place, resulting in increase of the RMS LOS value from 0.002 μrad to 0.130 μrad. A possible explanation of this severe deterioration in performance is the difficulty in estimating the state of the disturbance at node 37. This difficulty might stem from the sensors location, since only one sensor is located on the upper support truss compared to six on the lower support truss and two on the solar panels (see Section 3). Node 37 is on the upper support truss. Thus, changing the sensor configuration might rectify this difficulty.

Further insight to the behavior of the optimal control can be gained by examining the shift in the pole positions due to the feedback (Table 4-2). It is observed that although some damping is added to the various modes, significant effort is made in shifting the modes to higher frequencies, i.e., out of the disturbance range. This observation is supported also by observing that the regulator gains (Table 4-3) are of the order 10^6 for position feedback (columns 1-10) and only of the order 10^3 for the velocity feedback (column 11-20). Note that relatively low gains are applied to the disturbance states.

We conclude from the above observations that achieving the design objectives under realistic conditions requires sophisticated control design. Specifically, it was observed that damping augmentation will not suffice even if a high level of damping were possible. The difficulty in controlling closely-spaced modes also indicates the possible collapse of control schemes (ours or others) if some weakly excited modes are ignored in the proximity of controlled modes.

References

4-1 Kwakernaak, H. and R. Sivan, 1972. Linear Optimal Control Systems, Wiley-Interscience, New York.

4-2 Klema, V. C. and A. J. Laub, 1980, "The Singular Value Decomposition: Its Computation and Some Applications," IEEE Trans. Automatic Control, Vol. AC-25, April 1980.

4-3 Ginter, S. D., 1982. "Limitations on Active Control of Vibrations in Systems with Clustered Natural Frequencies," Ph.D. Thesis, Dept. of Aeronautics and Astronautics, Massachusetts Institute of Technology, Cambridge, MA (also Report CSDL-T-787, Charles Stark Draper Laboratory).

Table 4-1. Performance of disturbance rejection control design.

Description		Weights			RMS LOS-Error (μ radians)					
Case	Design - 10 modes	q_1	q_2	q_3	U1-Y1	U1-Y2	U1-Y3	U2-Y1	U2-Y2	U2-Y3
1a	Open Loop				90.55	1732.00	202.50	114.00	717.60	282.10
1b	Design Objective				0.05	0.05	25.	0.05	0.05	25.
2a	LQR	1	1	7	0.05	0.025	0.028	0.012	0.003	0.006
2b	OBS/LQR				0.06	0.130	0.035	0.012	0.049	0.006
3a	LQR	1	1	10^{-4}	0.003	0.019	7.000	0.002	0.003	6.164
3b	OBS/LQR				0.006	0.130	7.000	0.002	0.049	6.164
4a	LQR	1	1	10^{-3}	0.007	0.019	3.464	0.004	0.003	1.673
4b	OBS/LQR				0.009	0.130	3.464	0.004	0.049	1.673
5a	LQR	1	10	10^{-3}	0.007	0.002	3.464	0.004	0.003	1.673
5b	OBS/LQR				0.009	0.127	3.493	0.004	0.049	1.673

Parameters: $\rho_R = \rho_0 = 10^{-17}$

$$Q = \begin{bmatrix} q_1 & 0 & 0 \\ 0 & q_2 & 0 \\ 0 & 0 & q_3 \end{bmatrix}$$

Nomenclature: U1 - disturbance at node 37
U2 - disturbance at node 46
Y1 - LOSX Y2 - LOSY Y3 - LOSZ

Table 4-2. Effect of disturbance rejection control on poles distribution.

Open Loop Poles		Closed Loop Poles	
Damping	Frequency (Rad/Sec)	Damping	Frequency (Rad/Sec)
1.000000000E-03	7.160763140E-01	8.372573140E-02	9.940162706E-01
1.000000000E-03	9.399396780E-01	4.139322023E-03	3.390439591E+00
1.000000000E-03	3.501929280E+00	1.134785571E-03	3.947093264E+00
1.000000000E-03	3.745931630E+00	3.662730703E-01	6.418666406E+00
1.000000000E-03	3.862723350E+00	7.708973906E-02	6.680841689E+00
1.000000000E-03	3.998178408E+00	8.298167313E-03	7.360250222E+00
1.000000000E-03	7.280605320E+00	7.552205241E-01	1.290327148E+01
1.000000000E-03	9.745694160E+00	6.425144177E-01	2.639987792E+01
1.000000000E-03	4.123443600E+01	6.990949448E-01	2.745457654E+02
1.000000000E-03	5.067395020E+01	7.020272817E-01	4.200244983E+02

Table 4-3. Regulator gain of disturbance rejection control.

	1	2	3	4	5	6	7
1)	1.181E+06	-1.668E+05	1.297E+04	4.502E+04	1.122E+03	-3.255E+04	4.686E+02
2)	-2.208E+06	3.127E+05	-2.431E+04	-8.438E+04	-4.351E+03	6.100E+04	-1.507E+03
3)	-7.919E+06	1.113E+06	-8.657E+04	-3.006E+05	-2.409E+04	2.172E+05	-7.259E+03
4)	-6.746E+06	9.532E+05	-7.411E+04	-2.572E+05	-3.336E+04	1.858E+05	-9.758E+03
5)	-1.059E+07	1.495E+06	-1.163E+05	-4.030E+05	-1.811E+05	2.905E+05	-4.904E+04
6)	1.247E+07	-1.758E+06	1.367E+05	4.753E+05	-2.018E+05	-3.447E+05	-5.130E+04
7)	4.008E+06	-5.655E+05	4.397E+04	1.526E+05	4.133E+04	-1.101E+05	1.142E+04
8)	-1.825E+06	2.559E+05	-2.031E+04	-7.038E+04	-2.565E+04	5.071E+04	-7.245E+03
9)	1.808E+06	-2.533E+05	2.012E+04	6.969E+04	-2.368E+04	-5.043E+04	-6.202E+03

	8	9	10	11	12	13	14
1)	2.189E+02	-8.539E+03	-7.448E+05	4.586E+03	-5.602E+02	4.295E+01	1.687E+02
2)	-8.403E+02	2.886E+04	1.359E+06	-1.146E+04	1.603E+03	-9.014E+01	-4.089E+02
3)	-4.549E+03	7.345E+05	5.121E+06	-1.575E+04	2.161E+03	-2.458E+02	-6.535E+02
4)	-6.339E+03	7.167E+05	4.201E+06	-2.767E+04	3.977E+03	-2.538E+02	-1.015E+03
5)	-3.437E+04	4.380E+06	6.496E+06	-3.709E+04	5.227E+03	-3.777E+02	-1.388E+03
6)	-3.831E+04	4.985E+06	-8.192E+06	4.256E+04	-5.993E+03	4.412E+02	1.603E+03
7)	7.855E+03	-9.796E+05	-2.494E+06	1.398E+04	-1.966E+03	1.430E+02	5.240E+02
8)	-5.754E+03	7.016E+04	1.107E+06	-1.032E+04	1.503E+03	-2.588E+02	-5.088E+02
9)	-5.307E+03	9.033E+04	-1.117E+06	9.428E+03	-1.401E+03	2.365E+02	4.615E+02

	15	16	17	18	19	20	21
1)	6.620E+01	-1.206E+02	1.991E+01	1.126E+01	-5.478E+01	-2.526E+03	-5.580E-01
2)	-1.536E+02	2.917E+02	-3.756E+01	-2.730E+01	1.964E+02	4.612E+03	2.715E+00
3)	2.348E+01	4.800E+02	9.393E+00	7.781E+00	3.760E+03	1.728E+04	-4.629E+00
4)	-2.408E+02	7.281E+02	-7.007E+01	-4.693E+01	3.808E+03	1.418E+04	4.216E+00
5)	-8.680E+02	9.960E+02	-2.327E+02	-1.660E+02	2.287E+04	2.157E+04	3.232E+00
6)	-9.682E+02	-1.161E+03	-2.465E+02	-1.832E+02	2.591E+04	-2.831E+04	-2.387E+00
7)	3.114E+02	-3.763E+02	8.691E+01	5.634E+01	-5.124E+03	-8.356E+03	-1.119E+00
8)	-3.309E+03	3.682E+02	-9.388E+02	-6.411E+02	3.829E+02	3.715E+03	2.129E+00
9)	-3.412E+03	-3.611E+02	-9.647E+02	-6.521E+02	4.008E+02	-3.780E+03	-2.979E+00

	22
1)	1.060E-01
2)	-6.187E-02
3)	5.157E-02
4)	1.111E-02
5)	-3.674E-02
6)	3.316E-02
7)	2.294E-02
8)	4.825E-02
9)	-3.134E-01

Figures 4-1. Output power spectral density from closed-loop linear quadratic regulator (LQR) (LOS-output formulation).

(On following pages)

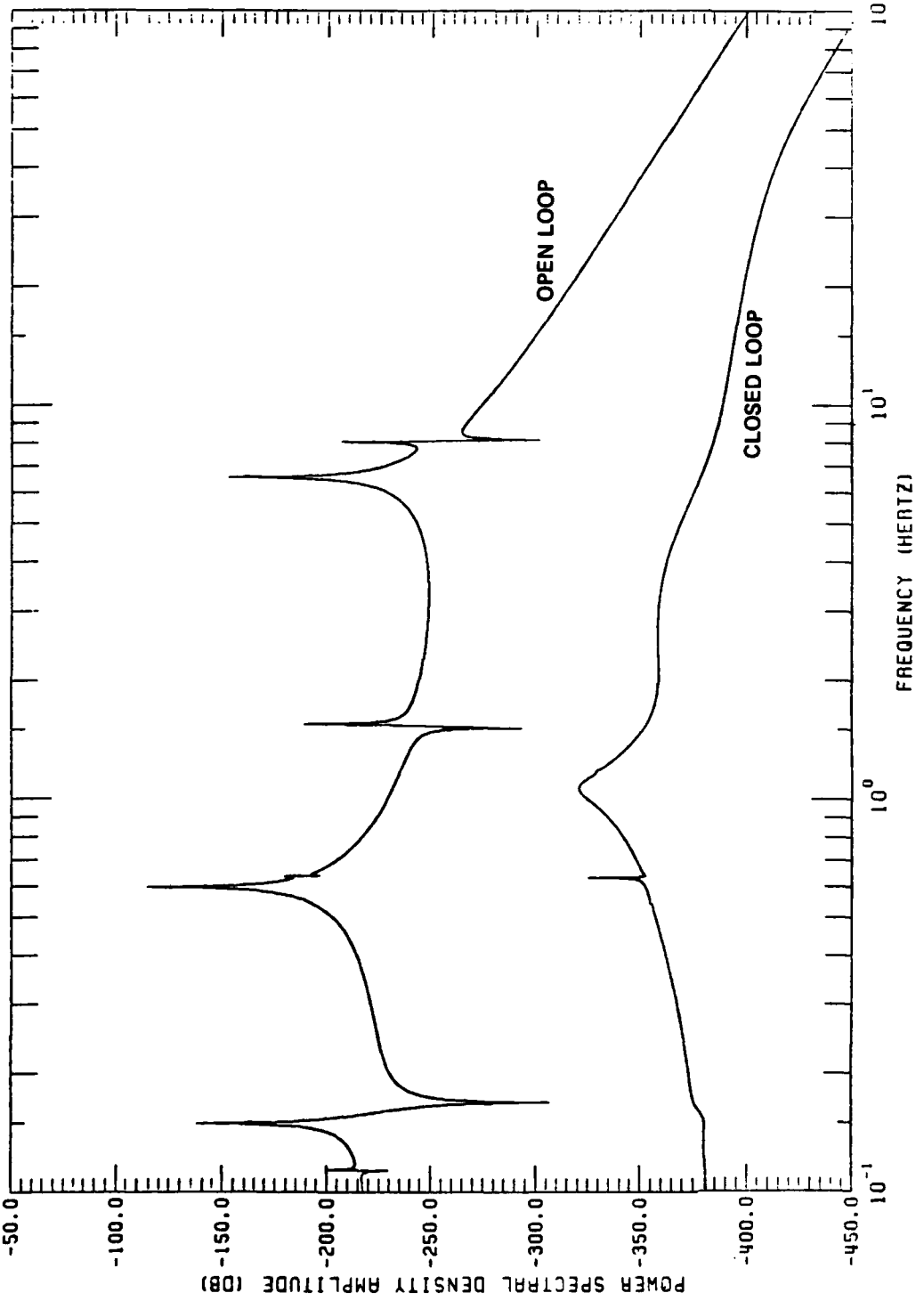

Figure 4-1a. Disturbance at node 37, output LOS-X.

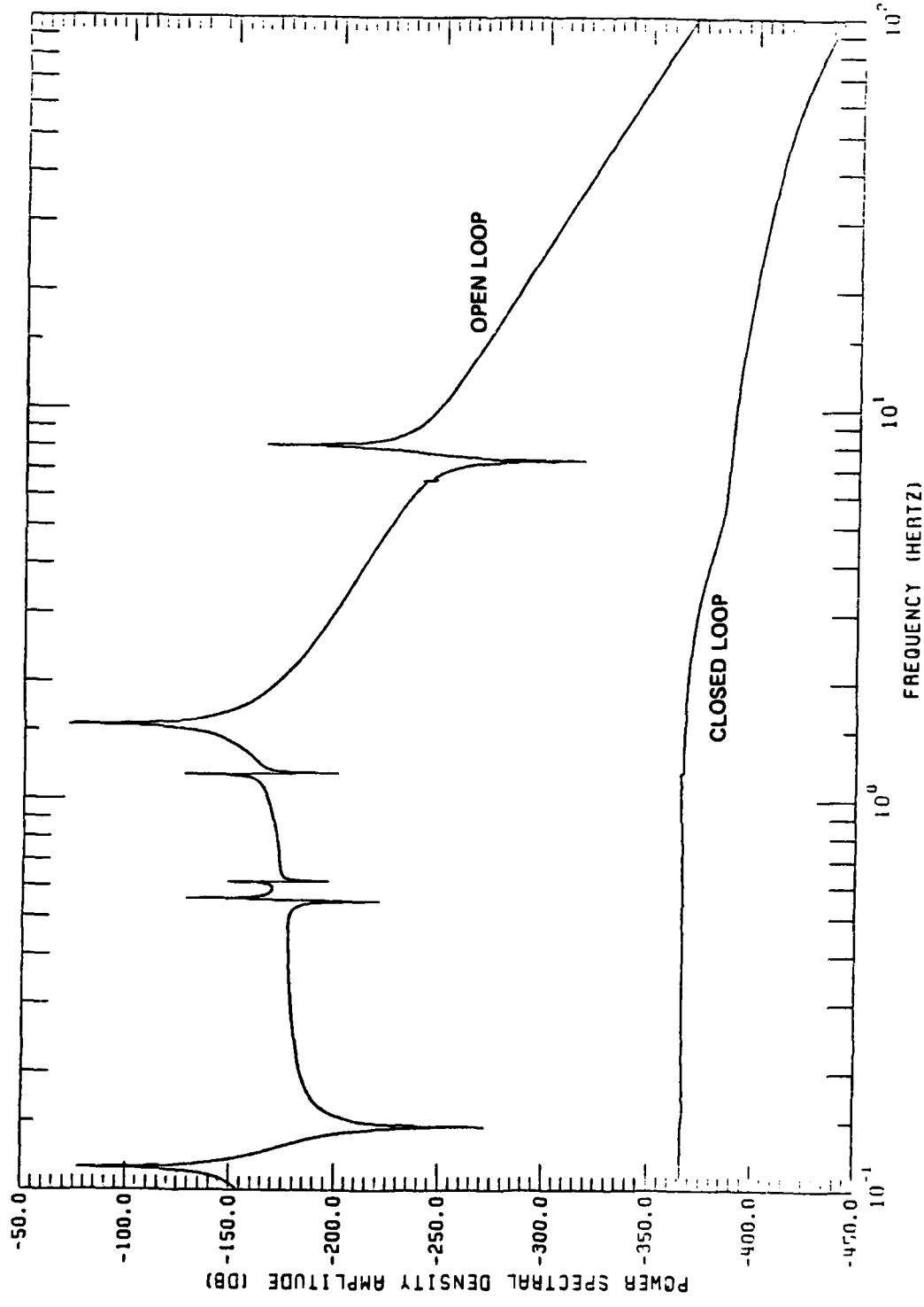

Figure 4-1b. Disturbance at node 37, output LOS-Y.

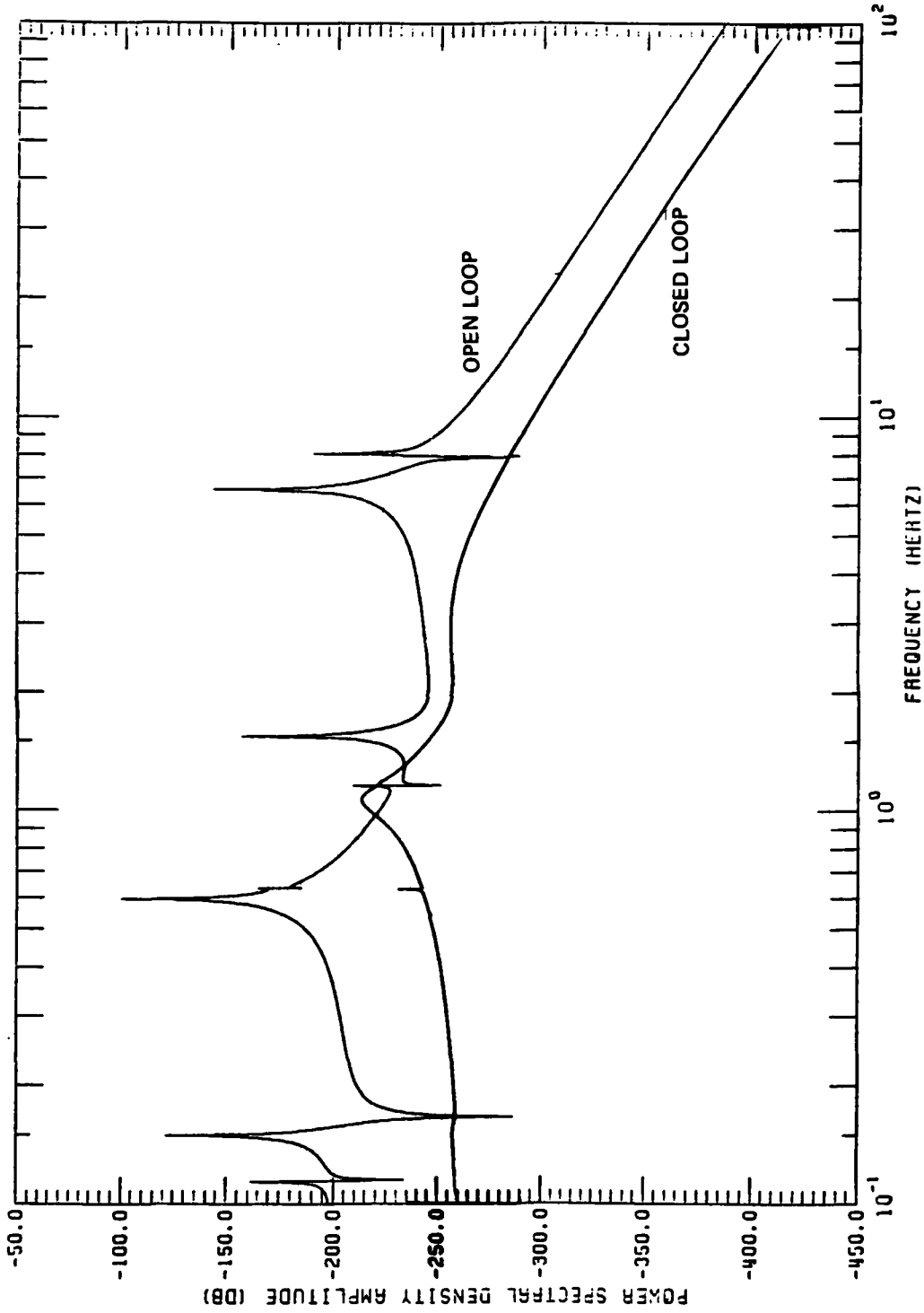

Figure 4-1c. Disturbance at node 37, output LOS-Z.

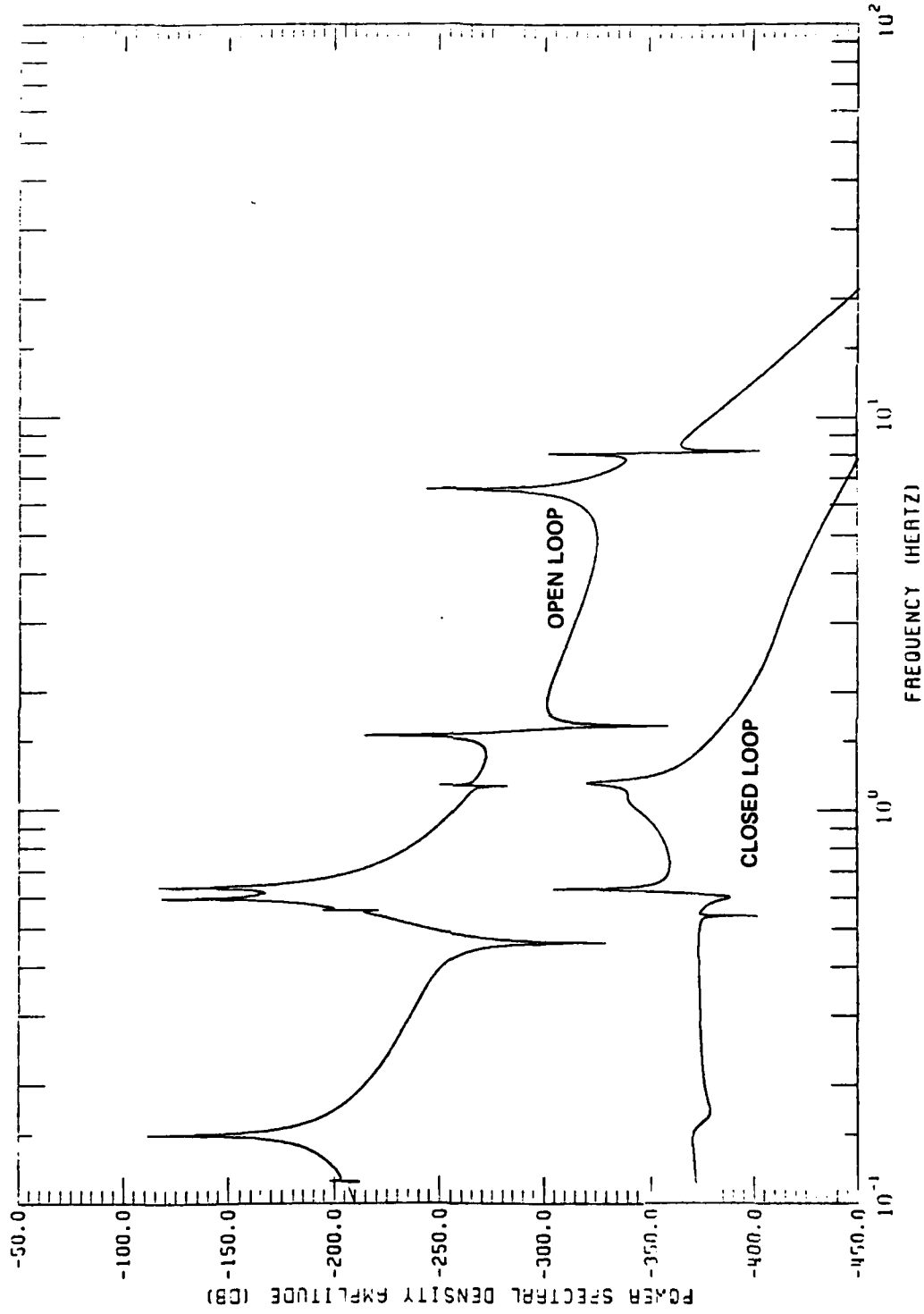

Figure 4-1d. Disturbance at node 46, output LOS-X.

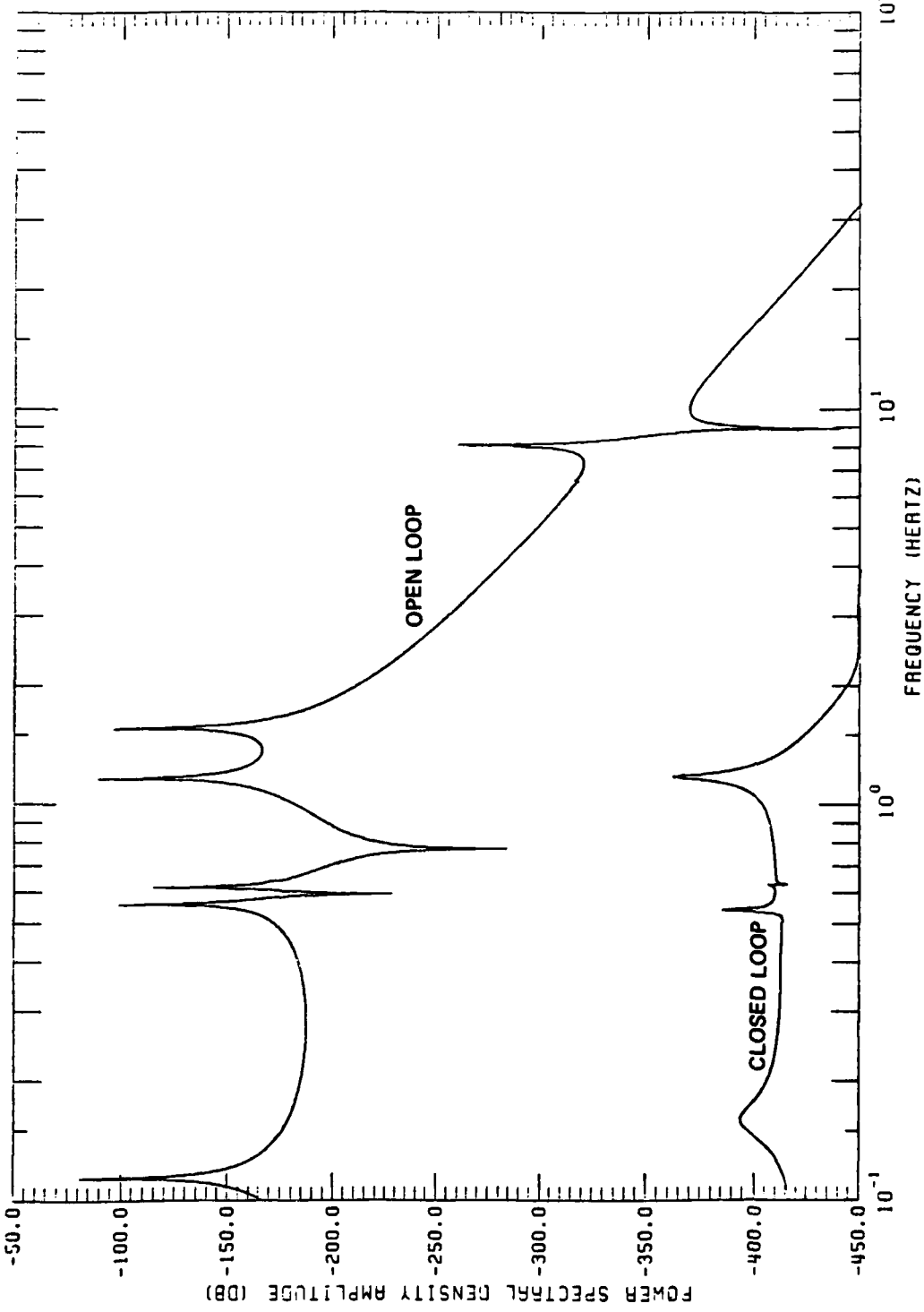

Figure 4-1e. Disturbance at node 46, output LOS-Y.

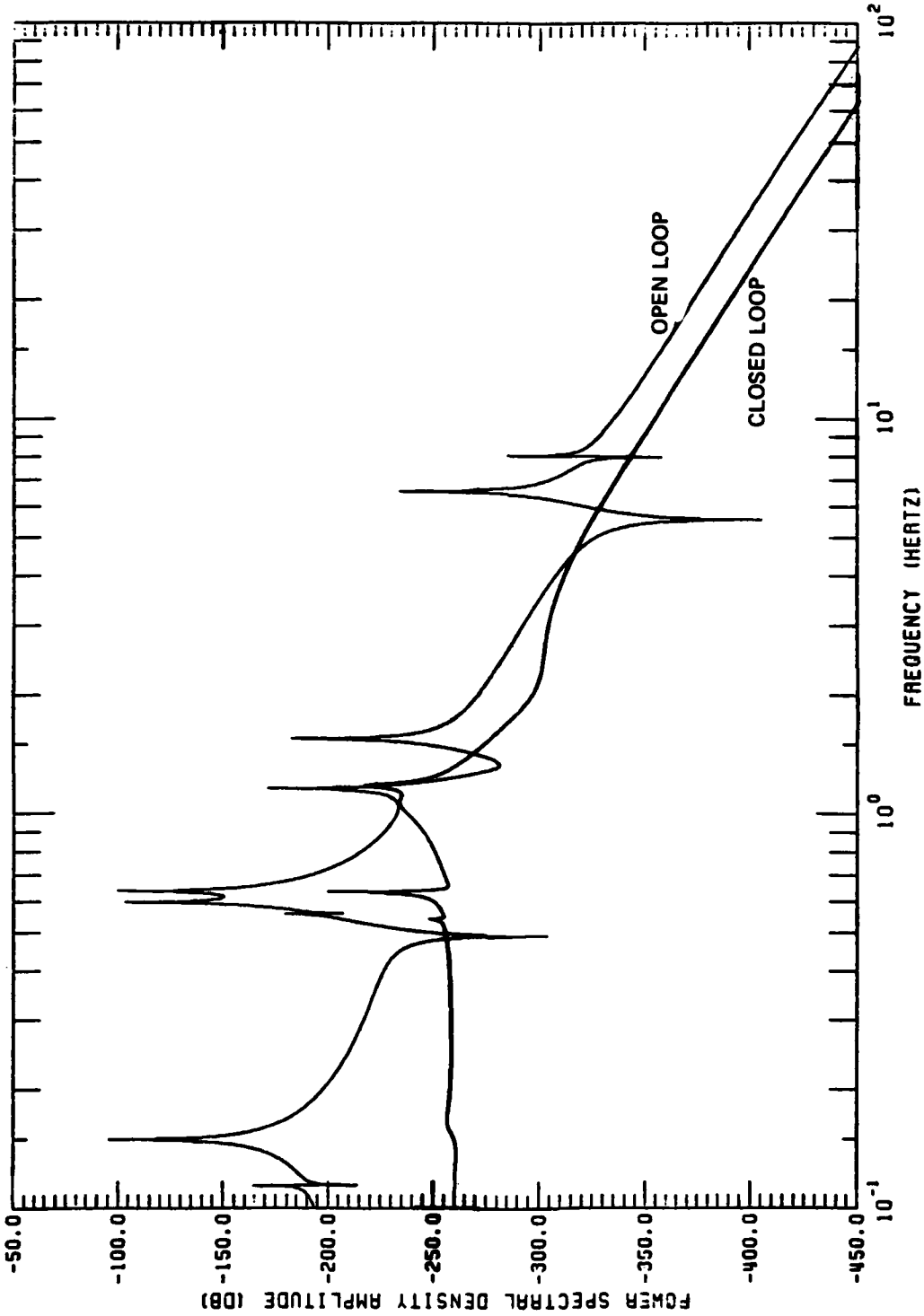

Figure 4-1f. Disturbance at node 46, output LOS-Z.

Figures 4-2. Comparison of output power spectral densities of closed-loop linear quadratic gaussian regulator (OBS/LQR) with linear quadratic regulator (LQR).

(On following pages)

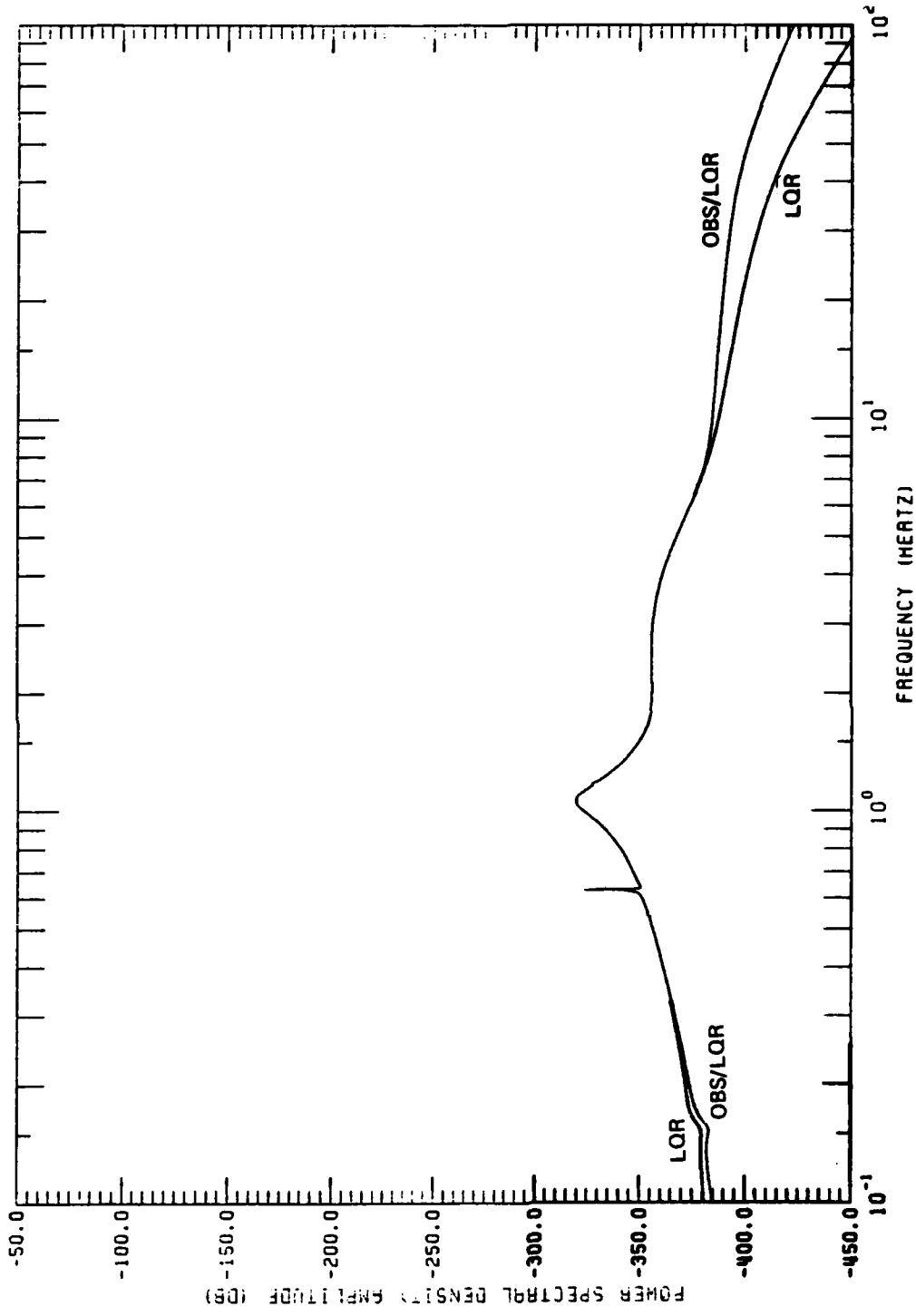

Figure 4-2a. Disturbance at node 37, output LOS-x.

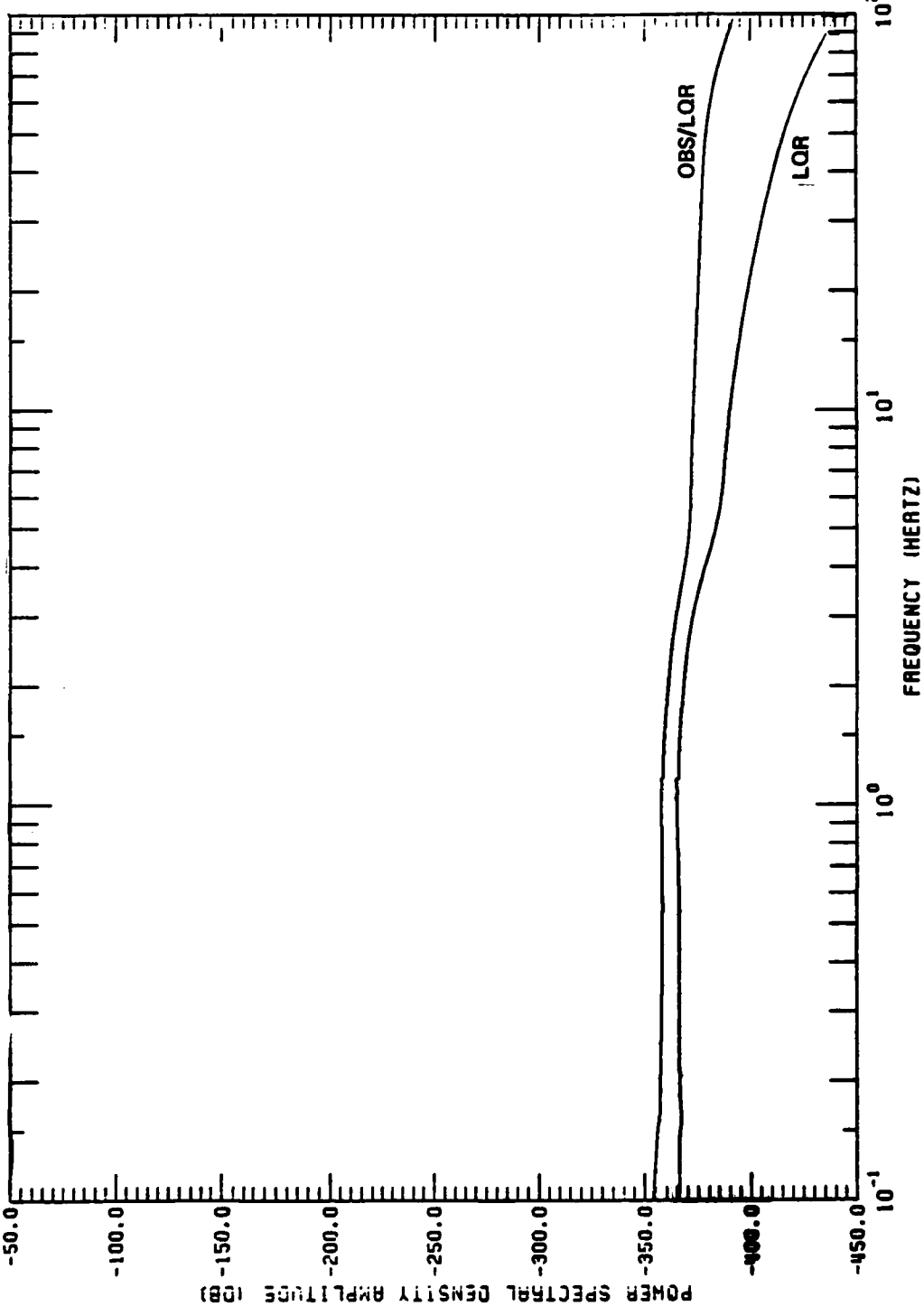

Figure 4-2b. Disturbance at node 37, output LOS-Y.

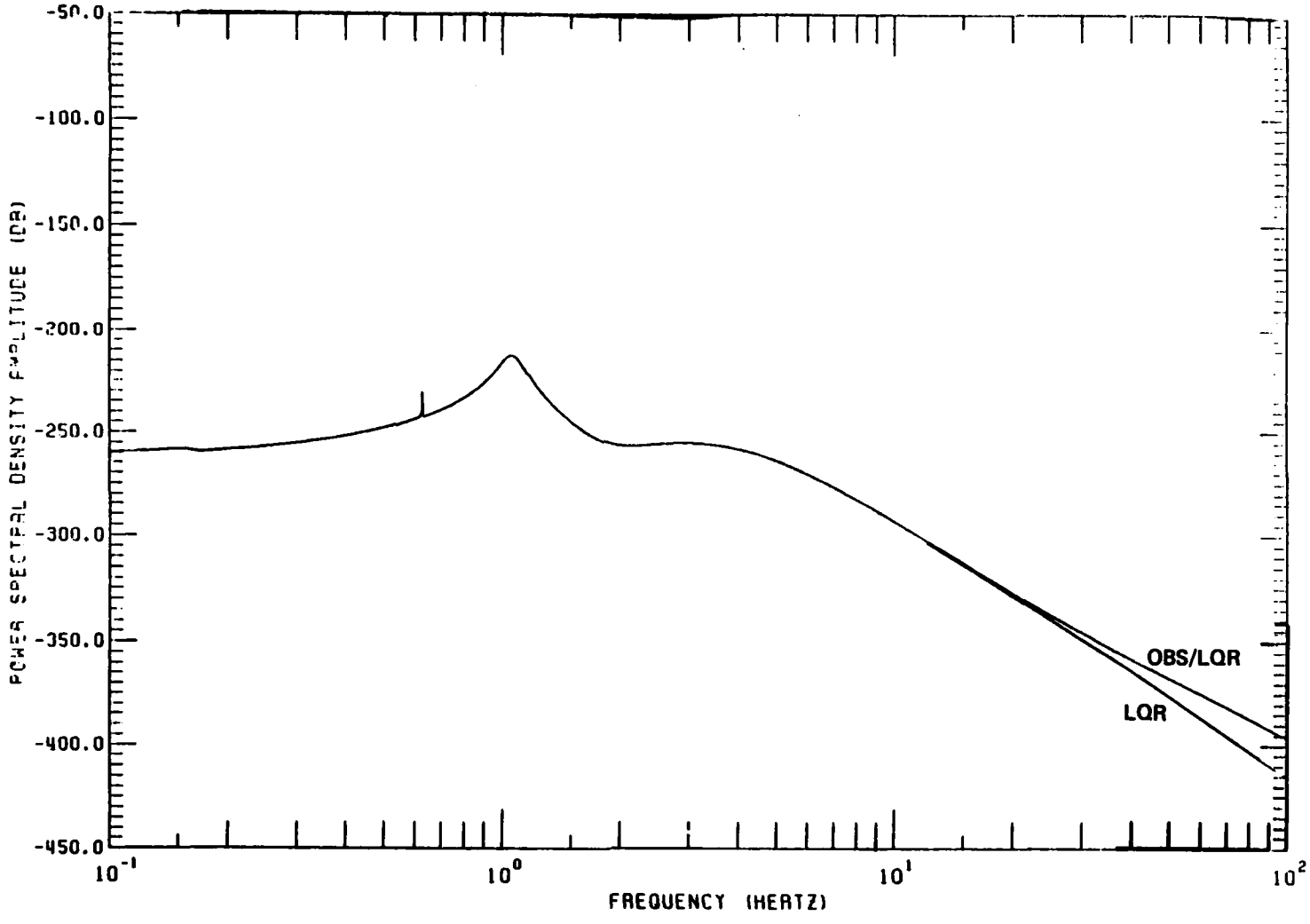

Figure 4-2c. Disturbance at node 37, output LOS-Z.

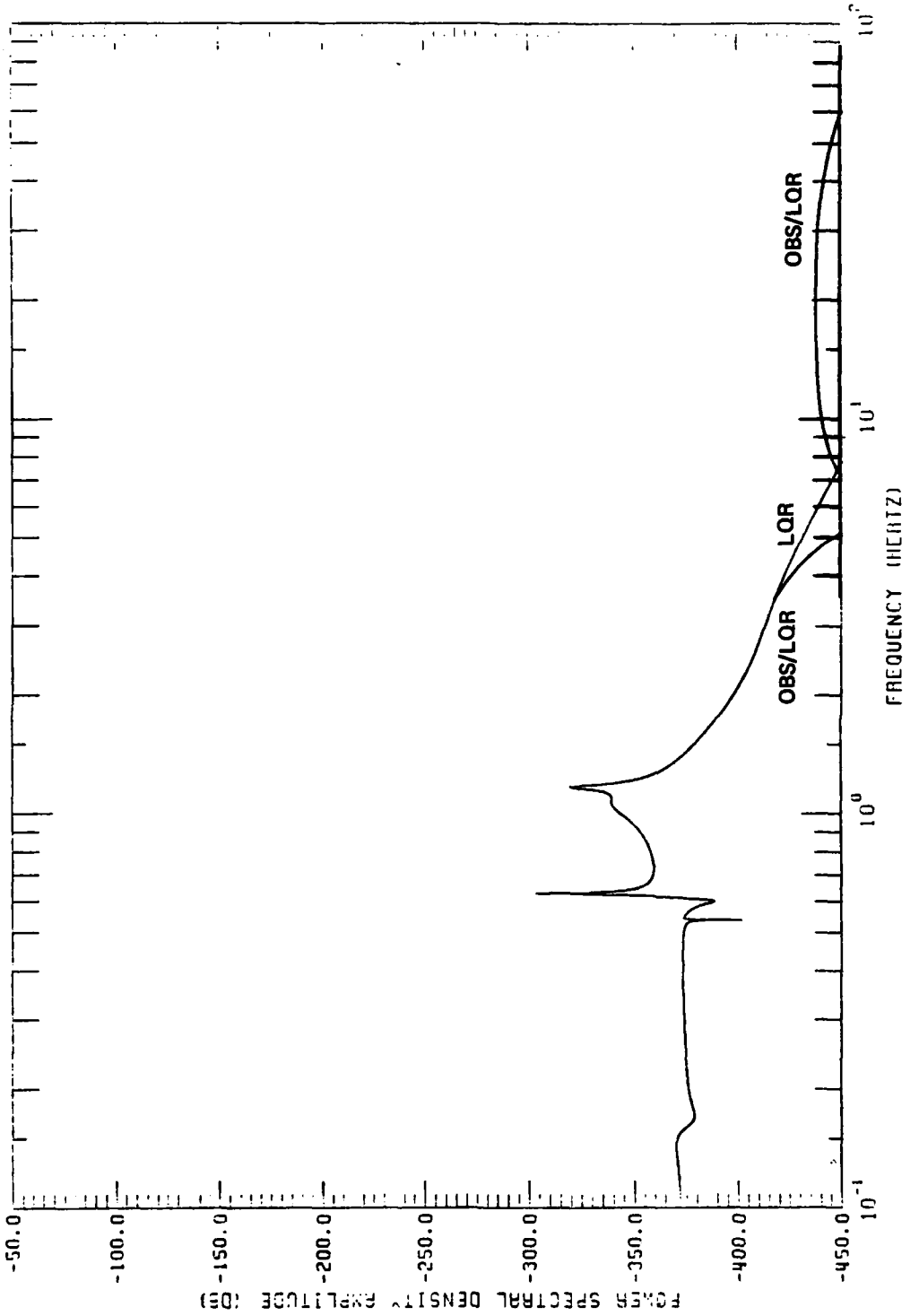

Figure 4-2d. Disturbance at node 46, output LOS-X.

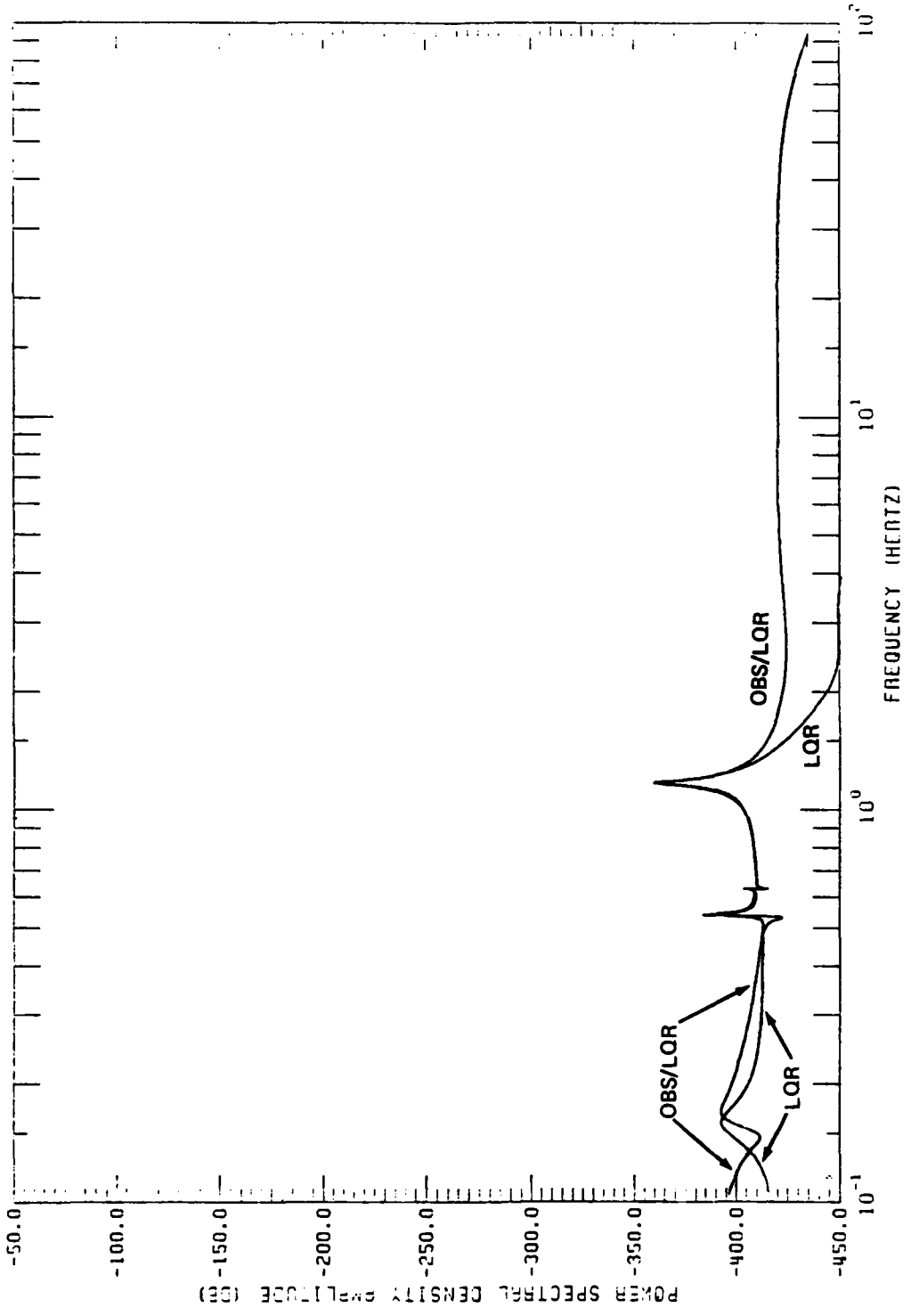

Figure 4-2e. Disturbance at node 46, output LOS-Y.

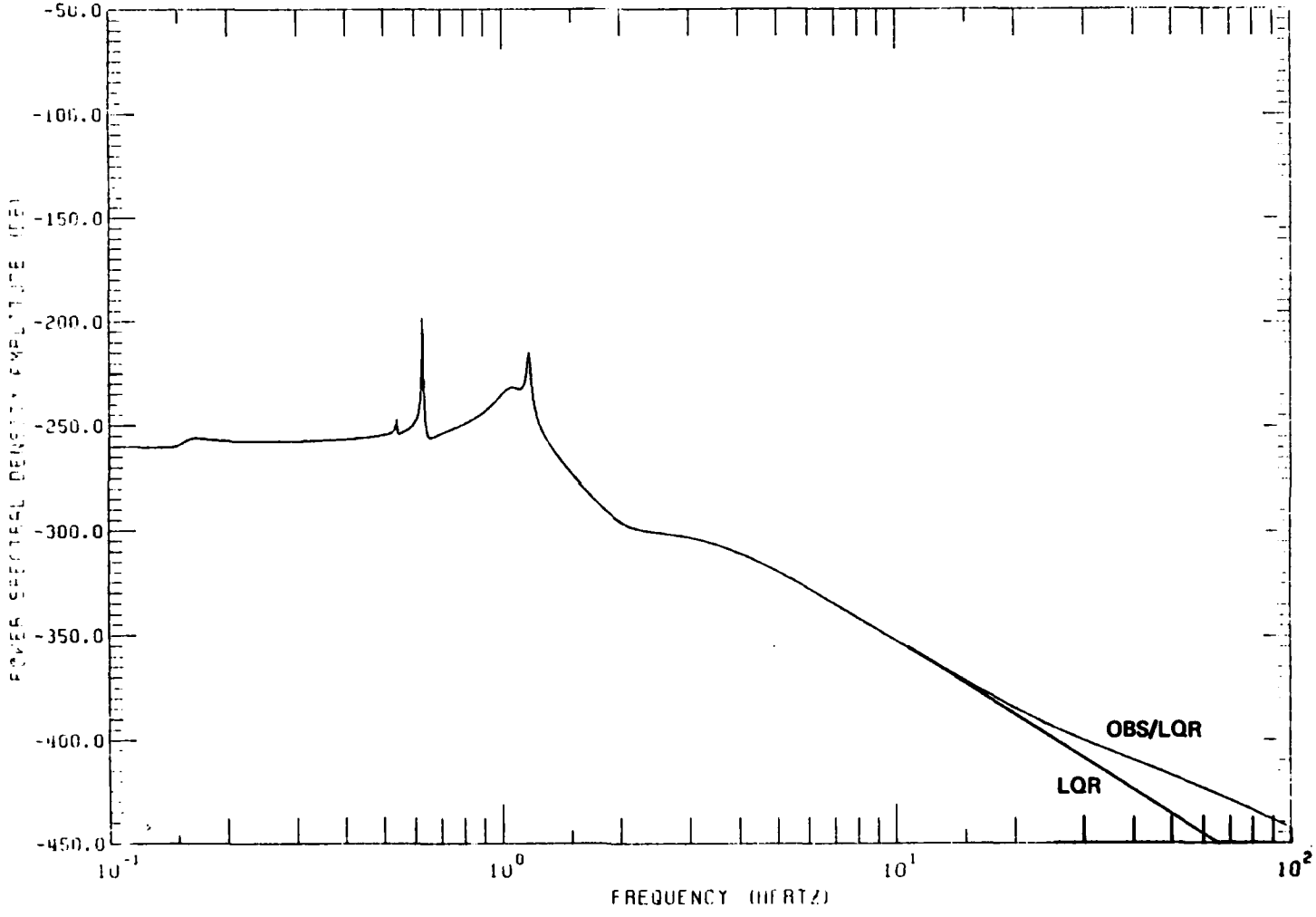

Figure 4-2f. Disturbance at node 46, output LOS-Z.

SECTION 5

LINEAR-QUADRATIC OPTIMAL CONTROL DESIGN

5.1 The Design Problem

Preceding sections have described a flexible structure model, and a general model of a disturbance containing both broad-band and discrete frequency components. A reduced-order subsystem (design model) is defined which consists of the ten modes that display the largest mean-square line-of-sight (LOS) rotation error when the disturbance is applied to the full open-loop structural model. Using the same criterion for ranking, a twenty-mode subsystem for evaluation of the design (evaluation model) is also defined. The problem treated in the present section is to design a linear-quadratic regulator for the ten-mode reduced-order subsystem which is asymptotically stable with respect to the larger twenty-mode reduced order subsystem, and, in addition, which assures that the steady-state LOS rotation error is within the specified tolerance in spite of the disturbance.

5.2 Description of Design Philosophy

The disturbance-rejection controller presented in Section 4 assumes full knowledge of the statistics of the disturbance. With such an assumption, it is possible to include a dynamic model of the disturbance as part of the model of the reduced-order system to be controlled. In contrast, for the purpose of the present procedure, no information about the disturbance is used explicitly in the design process. Instead, the LOS errors generated by the disturbance acting on the open-loop system are translated into desired values for modal

damping ratio and characteristic frequency of the closed-loop ten-mode subsystem. If such values can be attained, a closed-loop system that meets the overall design objectives in stability and performance, at least with respect to itself, if not with respect to the evaluation model, can be expected. These desired parameter values, which indirectly reflect certain effects of the disturbance, are used as explicit objectives of a linear-quadratic design. Well-known connections between such parameter objectives and the weighting matrices in the quadratic cost functional are exploited.

The approach just outlined embodies a systematic analytical procedure for selection of weighting matrices that is explicitly and directly connected with the system performance specifications. It avoids to a substantial degree the trial-and-error process often associated with the selection of weighting matrices for linear-quadratic regulator design.

5.2.1 Generation of Desired Closed-Loop Characteristics

First the transfer matrix connecting the LOS-error outputs and the disturbance inputs for the open-loop structure is generated. Next, using spectral density concepts, the mean-square-value of these errors due to the disturbance, as a function of open-loop modal parameters, is developed. Finally, these relations are used to generate implicit relations for desired closed-loop modal parameters by imposing an allowable tolerance on LOS-errors.

5.2.1.1 Transfer Matrix: Disturbance Inputs to LOS-Error Outputs

The open-loop structural model in modal coordinates with disturbance inputs is:

$$\ddot{\eta} + 2Z\Omega\dot{\eta} + \Omega^2\eta = (\Phi^T B_D R_D) w_D \qquad (5\text{-}1)$$

$$y_{LOS} = C_{LOS}\Phi\eta \qquad (5\text{-}2)$$

where $\eta \equiv (\eta_1,\ldots,\eta_N)^T$ is the modal coordinate vector, N being the number of modes to be controlled, $\Omega \equiv \text{diag}\,(\omega_1,\ldots,\omega_N)$: N×N is the matrix of modal characteristic frequencies, $Z \equiv \text{diag}\,(\zeta_1,\ldots,\zeta_N)$: N×N is the matrix of modal damping ratios, $\Phi \equiv \left[\phi^1 \mid \cdots \mid \phi^N\right]$: 6ν×N is the matrix whose columns are the mode shape vectors, B_D: 6ν×δ_1 is the

structural influence matrix of the disturbances, $u_D \triangleq R_D w_D$: δ_1×1 is the disturbance input to the structure, $y_{LOS} \equiv (y_{LOS,1},\ldots,y_{LOS,\ell})^T$ is the vector of LOS-error outputs, and C_{LOS}: ℓ×6ν is the combination matrix defining the LOS-error outputs. The actuator equivalence matrix R_D: $\delta_1\times\delta_2$ reflects simplifying assumptions on the disturbance allowing a lower-dimensional disturbance vector w_D: δ_2×1 (cf. Section 2.3; esp. Eq. (2-5)). Superscript "T" denotes matrix transpose.

Since the system of Eq. (5-1) is diagonal in the modal coordinates, and Eq. (5-2) can be written in the form:

$$y_{LOS} = \sum_{\alpha=1}^{N}(C_{LOS}\phi^{\alpha})\eta_{\alpha} \triangleq \sum_{\alpha=1}^{N} y_{LOS}^{\alpha} \quad ,$$

it makes sense to consider each single-mode channel connecting the disturbance input w_D to the channel output y_{LOS}^{α}. The corresponding transfer matrix $H_{\alpha}(s)$: ℓ×δ_2 is

$$H_{\alpha}(s) = \frac{C_{LOS}\phi^{\alpha}\phi^{\alpha T}B_D R_D}{s^2 + 2\zeta_{\alpha}\omega_{\alpha}s + \omega_{\alpha}^2} \triangleq \frac{K_{\alpha}}{L_{\alpha}(s)}$$

5.2.1.2 Mean-Square-Value of LOS-Error Outputs

It is assumed that the components of the input disturbance vector w_D are uncorrelated wide-sense-stationary random processes. The associated spectral density matrix is thus:

$$S_{w_D}(\omega) = S_I(\omega)\, I_{\delta_2}$$

where $S_I(\omega)$ is a second order approximation to the specified disturbance density:

$$S_I(\omega) \triangleq \frac{G\omega_c^2}{\omega_c^2 + \omega^2}, \quad -\infty < \omega < +\infty$$

and I_{δ_2} is the $\delta_2 \times \delta_2$ identity matrix. Values for the amplitude G and bandwidth frequency ω_c are specified in Section 2.2.

The mean-square-value matrix for the LOS-error output random process is obtained by integrating the output spectral density over all frequencies [Ref. 5-1]:

$$E_{y_{LOS}\alpha,\, y_{LOS}\alpha}^{T}(t) = \frac{1}{2\pi}\int_{-\infty}^{+\infty} S_{y_{LOS}\alpha}(\omega)\, d\omega = \frac{1}{2\pi i}\int_{-i\infty}^{+i\infty} S_{y_{LOS}\alpha}(-is)ds \qquad (5\text{-}3)$$

where

$$S_{y_{LOS}\alpha}(\omega) = H_\alpha(i\omega)\, S_{\omega_D}(\omega)\, H_\alpha^T(-i\omega).$$

Eq. (5-3) reduces to the evaluation of a single scalar complex integral:

$$M_\alpha\left(\frac{1}{2\pi i}\int_{-i\infty}^{+i\infty} F(s)F(-s)ds\right) \qquad (5\text{-}4)$$

where

$$M_\alpha \triangleq G\,\omega_c^2\,K_\alpha K_\alpha^T$$

and

$$F(s) \triangleq \frac{1}{(\omega_c + s)L_\alpha(s)}$$

The complex integral in Eq. (5-4) may be evaluated using the residue theorem; convenient tabulations of such integrals with F a general rational function have been compiled [Ref. 5-2]. The result, as a function of the modal parameters, is:

$$I(\omega_\alpha, \zeta_\alpha) = \frac{\omega_c + 2\zeta_\alpha\omega_\alpha}{2\omega_c(2\zeta_\alpha\omega_\alpha)\omega_\alpha^2\left[\omega_c^2 + \omega_c(2\zeta_\alpha\omega_\alpha) + \omega_\alpha^2\right]} \qquad (5\text{-}5)$$

The root-mean-square (RMS) value for the errors associated with LOS rotation is of principal concern and is defined by:

$$RMS_{LOS,\alpha} = \left(e_{11}^\alpha + e_{22}^\alpha\right)^{1/2}$$

where the e_{ii} are the upper-left diagonal elements of the mean-square-value matrix in Eq. (5-4). It follows that

$$RMS_{LOS,\alpha} = I(\omega_\alpha, \zeta_\alpha)^{1/2} m_\alpha \tag{5-6}$$

where m_α is a constant independent of the modal frequency and damping ratio.

5.2.1.3 Implicit Relations for Desired Closed-Loop Modal Parameters

The RMS LOS-rotation error induced by the input disturbance acting on the α-th mode open-loop subsystem is:

$$\rho_{\alpha 0} \triangleq [RMS_{LOS,\alpha}]_0 = I(\omega_{\alpha 0}, \zeta_{\alpha 0})^{1/2} m_\alpha \tag{5-7}$$

where $\omega_{\alpha 0}$ is the characteristic frequency and $\zeta_{\alpha 0}$ is the assumed modal damping ratio. For each of the ten modes selected to be controlled, the values in Eq. (5-7) exceed the allowable value of 0.05 μ-radians. A desired value $[RMS_{LOS,\alpha}]_d$ for the RMS LOS rotation error is chosen, and we seek a strategy for compensation of the structural open-loop system leading to corresponding parameters $\omega_{\alpha d}$, $\zeta_{\alpha d}$ of the closed-loop compensated system which achieves the desired error reduction, i.e.,

$$\rho_{\alpha d} \triangleq [RMS_{LOS,\alpha}]_d = I(\omega_{\alpha d}, \zeta_{\alpha d})^{1/2} m_\alpha \tag{5-8}$$

Equation (5-8) does not reflect any modal coupling effects that result from compensation. Combining Eqs. (5-7) and (5-8) leads to an implicit relation for the parameters $\omega_{\alpha d}$ and $\zeta_{\alpha d}$. In view of the form of Eq. (5-5), it is convenient to express the implicit relation in terms of new variables γ, κ defined by:

$$\gamma \leftarrow 2\zeta_\alpha \omega_\alpha \quad , \quad \kappa \leftarrow \omega_\alpha^2$$

where the mode subscript "α" has been suppressed with the new variables. The implicit relation for the desired modal parameters (in the new variables) is:

$$(2\omega_c^2\pi_0)\gamma_d^2\kappa_d + (2\omega_c\pi_0)\gamma_d\kappa_d^2 + (2\omega_c^3\pi_0)\gamma_\alpha\kappa_d + (-1)\gamma_d + (-\omega_c) = 0 \qquad (5\text{-}9)$$

where

$$\pi_0 \triangleq \left(\frac{\rho_{\alpha d}}{\rho_{\alpha 0}}\right)^2 I(\omega_{\alpha 0}, \zeta_{\alpha 0})$$

Instead of seeking a general solution of Eq. (5-9), we look for solutions which also satisfy some simpler and physically meaningful constraints on γ_d and κ_d. Several special cases are of interest.

Special Case 1: $\kappa_d = a^2, \quad -\infty < \gamma_d < +\infty; \quad a > 0$

This corresponds to fixing the closed-loop natural frequency $\omega_{\alpha d}$ at the value a, without further constraining the damping ratio $\zeta_{\alpha d}$. Equation (5-9) reduces to a quadratic in γ_d:

$$(2\omega_c^2\pi_0 a^2)\gamma_d^2 + [2\omega_c\pi_0 a^2(a^2 + \omega_c^2) - 1]\gamma_d + (-\omega_c) = 0 \qquad (5\text{-}10)$$

which has two real roots of opposite sign. Using the positive root, $(\gamma_d)_+$, one obtains the desired closed-loop modal parameter pair $(\zeta_{\alpha d}, \omega_{\alpha d}) \triangleq ((\gamma_d)_+/2a, a)$ sought. Choosing $a = \omega_{\alpha 0}$ corresponds to leaving the α-th mode natural frequency unchanged.

Special Case 2: $\kappa_d = (b\gamma_d)^2$, $-\infty < \gamma_d < +\infty$; $b > 0$

This corresponds to fixing the closed-loop damping ratio $\zeta_{\alpha d}$ at the value 1/2b, without further constraining the natural frequency $\omega_{\alpha d}$. Equation (5-9) becomes a quintic equation in γ_d:

$$(2\omega_c\pi_0 b^4)\gamma_d^5 + (2\omega_c^2\pi_0 b^2)\gamma_d^4 + (2\omega_c^3\pi_0 b^2)\gamma_d^3 + (-1)\gamma_d + (-\omega_c) = 0 \quad (5\text{-}11)$$

which has at least one positive real root. If $(\gamma_d)_+$ is a positive real root of Eq. (5-11), then the closed-loop system with modal parameter pairs $(\zeta_{\alpha d}, \omega_{\alpha d}) \triangleq (1/2b,\ b(\gamma_d)_+)$ satisfies the RMS LOS-error specifications. Choosing $b = 1/2\zeta_{\alpha 0}$ corresponds to leaving the α-th mode damping ratio unchanged.

Results of calculations performed to determine modal parameter objectives for the design are shown in Table 5-1. The first set of three columns shows the open-loop modal parameters and the RMS LOS-rotation error that result from applying the disturbance to the full open-loop structural model. The second set of three columns shows the closed-loop modal damping ratios that would be required to reduce the RMS error in LOS rotation to the allowable level of $\rho_{\alpha d} = 0.05$ μ-radians without changing the modal frequencies. These correspond to solutions of Eq. (5-10) with $a = \omega_{\alpha 0}$. Implementation of these ratios is not desirable, since each represents real poles, one of which would have a very large time constant (i.e., damping ratio far in excess of critical). The next set of three columns shows that a much more reasonable set of modal damping ratios is obtained by raising the allowable RMS error to $\rho_{\alpha d} = 5.0$ μ-radians. The parameters listed in the final set of three columns reflect changes associated with the first four (overdamped) modes, whose parameters are adjusted so as to fix the desired damping ratio at the "optimal" value of $1/\sqrt{2}$. These correspond to solutions of Eq. (5-11) with $b = 1/\sqrt{2}$. These parameter values are used in subsequent calculations.

It should be observed that the implicit relation of Eq. (5-9) allows considerably more flexibility in design than is actually implemented with Special Cases 1 and 2. These special cases impose restrictions on variations in the free parameters ($\rho_{\alpha d}$, γ_α, κ_d) for the sake of convenience, as indicated. However, it is quite conceivable that there may be an advantage in dropping such restrictions and focusing directly on pole assignment instead of attempting explicit assignment of characteristic frequencies and damping ratios.

5.3 Generation of Weighting Matrices for Linear-Quadratic Design

In the preceding subsection, an approach to generating desired values for the closed-loop poles was developed so as to ensure that the effects of the disturbance on the LOS rotation are kept at an acceptable level. In the present section, these parameter objectives are used to guide the selection of weighting matrices for a full-state-feedback linear-quadratic controller design.

5.3.1 Relationships between Closed-Loop Modal Parameters and Weighting Matrices

The open-loop structural model in modal coordinates with actuator inputs is:

$$\ddot{\eta} + 2Z\Omega\dot{\eta} + \Omega^2\eta = \Phi^T B_A u \tag{5-12}$$

$$y_{LOS} = C_{LOS}\Phi\eta \tag{5-2}$$

where B_A: $6\nu \times m$ is the structural influence matrix of the actuators, and $u \equiv (u_1,\ldots,u_m)^T$ is the actuator input to the structure. (Remaining notation is as in Eqs. (5-1) and (5-2)). Defining state variables by

$$x_{2\alpha-1} \triangleq \eta_\alpha , \quad x_{2\alpha} \triangleq \dot{\eta}_\alpha , \quad \alpha = 1,\ldots,N$$

leads to a set of N systems of state equations of the form

$$\dot{s}_\alpha = A_\alpha s_\alpha + B_\alpha w_\alpha , \tag{5-13}$$

where

$$s_\alpha \triangleq \begin{bmatrix} x_{2\alpha-1} \\ x_{2\alpha} \end{bmatrix}, \quad w_\alpha \triangleq \phi^{\alpha T} B_A u \quad \text{(scalar)},$$

$$A_\alpha = \begin{bmatrix} 0 & 1 \\ -\omega_\alpha^2 & -2\zeta_\alpha\omega_\alpha \end{bmatrix}, \quad B_\alpha = \begin{bmatrix} 0 \\ 1 \end{bmatrix} .$$

For each α, consider the problem of minimizing the functional

$$J_\alpha \triangleq \frac{1}{2} \int_0^{+\infty} [s_\alpha^T Q_\alpha s_\alpha + r_\alpha w_\alpha^2] \, dt \tag{5-14}$$

along the trajectories of the system Eq. (5-13), with "full-state" feedback of the form

$$w_\alpha = F_\alpha s_\alpha \tag{5-15}$$

Note particularly that the effects of coupling between modes is not modeled by the functionals in Eq. (5-14).

The connection between the modal parameters of the second-order closed-loop system corresponding to Eqs. (5-13) and (5-15) and the weighting matrices in Eq. (5-14) is well-known [Refs. 5-3, 5-4]. These connections have been exploited in multivariable applications [Ref. 5-5]. Essentially, one simply solves the Riccati equation associated with the optimization problem analytically and makes the appropriate connections. Denoting the closed-loop modal parameters by ω_α^c, ζ_α^c, the results are:

$$\left(\omega_\alpha^c\right)^4 - \omega_\alpha^4 = q_D^\alpha / r_\alpha \tag{5-16}$$

$$\left(2\zeta_\alpha^c \omega_\alpha^c\right)^2 - \left(2\zeta_\alpha \omega_\alpha\right)^2 - 2\left[\left(\omega_\alpha^c\right)^2 - \omega_\alpha^2\right] = q_V^\alpha / r_\alpha \tag{5-17}$$

where

$$Q_\alpha \equiv \begin{bmatrix} q_D^\alpha & q_S^\alpha \\ q_S^\alpha & q_V^\alpha \end{bmatrix}$$

Since the off-diagonal elements of Q_α do not enter into Eqs. (5-16) or (5-17), there is no loss of generality (at the level of the second-order system (5-13)) in assuming that Q_α is diagonal.

An appropriate quadratic cost functional for the full N-mode design model that is consistent with Eqs. (5-16) and (5-17) is the following augmented-state regulator formulation:

$$J \triangleq \sum_{\alpha=1}^{N} J_\alpha + \frac{1}{2}\int_0^{+\infty} y_{LOS}^T Q_L y_{LOS}\, dt = \frac{1}{2}\int_0^{+\infty}[\tilde{y}^T Q \tilde{y} + u^T R u]dt \qquad (5\text{-}18)$$

where the augmented-state vector $\tilde{y}$ is defined by:

$$\tilde{y}_\alpha \triangleq y_{LOS,\alpha}\ , \quad \alpha = 1,\ldots,\ell$$

$$\tilde{y}_{\ell+\alpha} \triangleq \eta_\alpha\ , \qquad \tilde{y}_{\ell+N+\alpha} \triangleq \dot{\eta}_\alpha\ , \quad \alpha = 1,\ldots,N$$

The augmented-state weighting matrix Q in Eq. (5-18) has the structure:

$$Q \equiv \begin{bmatrix} Q_L & 0 & 0 \\ 0 & Q_D & 0 \\ 0 & 0 & Q_V \end{bmatrix} \qquad (5\text{-}19)$$

where $Q_L \triangleq \text{diag}\,(q_L^\alpha)$: $\ell\times\ell$ weights the LOS-error outputs that are unavailable for feedback, $Q_D \triangleq \text{diag}\,(q_D^\alpha)$: N×N weights the displacement states and $Q_V \triangleq \text{diag}\,(q_V^\alpha)$: N×N weights the velocity states, both assumed available for feedback for the purpose of this design. The control weighting matrix R: m×m in Eq. (5-18) is:

$$R = (\Phi^T B_A)^T \text{diag}\,(r_\alpha)(\Phi^T B_A) \qquad (5\text{-}20)$$

In general, R is a fully populated matrix.

Motivation for the use of the cost functional (5-18) incorporating an augmentation of the state with LOS-error outputs is connected with the stringent tolerance on those outputs. This is discussed below in Section 5.5.3.

5.3.2 Application in Design

The relationships developed above and in the preceding subsection provide the foundation for a rational systematic approach to the selection of weighting matrices for linear-quadratic design in the presence of broad-band stochastic disturbance inputs. The first step is to determine a set of closed-loop modal parameters $\omega_{\alpha d}$, $\zeta_{\alpha d}$ for each mode to be controlled based on considerations of attenuating the effects of the disturbance input. Such determinations are discussed in Section 5.2. Next, these desired values are used with Eqs. (5-16) and (5-17) (in the place of ω_α^c and ζ_α^c) to determine the elements of the matrices Q_D and Q_V in Eq. (5-19) as a function of the free parameters r_α. For the designs reported on here, parameters r_α were chosen as (cf. Eq. (5-7)):

$$r_\alpha \triangleq \left(\frac{\rho_{\alpha 0}}{\left|\left| \phi^{\alpha^T} B_A \right|\right|} \right)^2 \tag{5-21}$$

which includes the average effect of the disturbance upon the α-th mode and a measure of the modal actuator influence.

Calculation of the parameters q_D^α, q_V^α, and r_α which generate the weighting matrices are shown in Table 5-2 corresponding to the closed-loop modal parameter objectives listed for $\rho_{\alpha d} = 5.0$ in Table 5-1. The LOS-error weighting parameters q_L^α were determined independently so as not to dominate the displacement weighting q_D^α associated with the lowest-frequency mode in the design model (mode 7).

For a single mode subsystem represented by Eqs. (5-13), any choice of weighting matrices for the functional in Eq. (5-14) satisfying Eqs. (5-16) and (5-17) ensures that the closed-loop system formed by the feedback law Eq. (5-15) will have the desired modal parameters ω_α^c and ζ_α^c used in Eqs. (5-16) and (5-17). However, since the above analysis does not account for the effect of coupling between modes when full-state feedback is implemented on the N-mode design model, the weighting matrix determination is not completely effective in achieving the desired closed-loop modal parameters. Nevertheless, it is quite helpful in generating a starting point for the design.

5.4 Design Results

Numerical experience substantially validates the selection procedure outlined in Section 5.3. Plots of spectral density of the LOS-error outputs for the final design run are shown in Figures 5-1a through 5-1f. The RMS-error values associated with each plot, e.g.,

$$\text{RMS}\ (y^{37}_{\text{LOS-X}}) \equiv \left(\frac{1}{2\pi} \int_{-\infty}^{+\infty} S_{y^{37}_{\text{LOS-X}}}(\omega)\, d\omega \right)^{1/2}$$

are listed in Table 5-3 (last column). The final closed-loop pole locations, along with associated damping ratio and characteristic frequency, are listed in Table 5-4. The weighting matrices Q and R used for the final run are listed in Table 5-5. (The column order reflects the ordering of the modes shown in Table 5-1.) The final matrix Q includes adjustments in the weighting associated with modes 7 and 9 so as to keep the closed-loop characteristic frequencies associated with

these modes above the natural frequency of the isolator springs. The optimal state-feedback gain matrix is listed in Table 5-6.

5.5 Numerical Experience in the Design Process

Although the properties of the control system generated by the final design run are of principal interest, some observations made while proceeding toward the final design are worth mentioning. The principal observations are outlined below.

5.5.1 Optimal vs. Nonoptimal Design

The intitial design run incorporates weighting on velocity states only (i.e., $Q_L = 0$, $Q_D = 0$ in Eq. (5-19)) using appropriately scaled values for the parameters listed for $\omega_{\alpha d} = \omega_{\alpha 0}$, $\rho_{\alpha d} = 5.0$, in Table 5-2. It turns out that the control weighting matrix R generated with these parameters by Eq. (5-20) is ill-conditioned with respect to inversion. This results in failure to obtain a solution for the Riccati equation associated with the optimization of criterion Eq. (5-18). Nevertheless, a stable design (relative to the design model) is obtained which gives surprisingly close agreement with the damping objectives calculated for the corresponding data in Table 5-1 (seven of ten pole pairs in close agreement). None of the subsequent design runs produces such close agreement. Although the RMS LOS-error values for this first run are quite unsatisfactory, this observation suggests that other design techniques (e.g., direct pole assignment) could be worth investigating.

5.5.2 Conditioning of the Control Weighting Matrix

Satisfactory solution of the Riccati equation asociated with Eq. (5-18) is achieved on subsequent design runs by using a well-conditioned control weighting matrix $\tilde{R}$ obtained from the matrix of Eq. (5-20) by adding a scalar factor to the diagonal elements:

$$\tilde{r}_{ii} \leftarrow r_{ii}(1+\alpha)$$

This modification leads to some deterioration in the agreement with the modal parameter objectives of Table 5-1. The final value of $\alpha = 0.1$ gives an acceptable level of conditioning to the matrix $\tilde{R}$ as well as reasonable agreement with the modal parameter objectives.

5.5.3 State vs. Augmented-State Weighting

No substantial reduction in the RMS LOS-error values is obtained until explicit weighting on those outputs is incorporated into the cost functional in Eq. (5-18) (i.e., $Q_L \neq 0$ in Eq. (5-19)). This is immediately evident from a comparison of the columns in Table 5-3. This emphasizes the importance of formulating the design problem as an augmented-state regulator, in which weighting on the specific linear combinations of the state variables that are of principal interest is employed in addition to the usual weighting on the state variables themselves. This is to be distinguished from an output regulator in which weighting is placed only on the outputs of interest, and not necessarily on all of the state variables (cf. Section 4, Eq. (4-9)).

5.5.4 Active Damping vs. Active Stiffness-Damping Augmentation

As discussed in Section 5.2, the augmentation of damping by active control beyond the point of critical damping is likely to be counter-productive. This constitutes a fundamental constraint in the design of vibration controllers. Often, as in the present design problem, the incorporation of subcritical damping alone is not sufficient to meet the design specifications. Active stiffening in concert with active damping can overcome this constraint and lead to an acceptable design. In the case of a design directed toward attenuating the effects of a broad-band

disturbance input, such stiffening has the effect of moving the poles associated with the most disturbance-sensitive modes outside of the disturbance bandwidth (cf. Table 5-1, last three columns). This is completely consistent with the corresponding observation noted in the disturbance-rejection control design of Section 4.

5.6 Work in Progress

Questions of substantial importance have not been discussed in this section. One is the question of stability of the reduced-order controller when connected to evaluation models of larger order. Another is the question of the effect upon the stability and performance of the system of incorporating a state observer into the controller. Both questions are under investigation and will be discussed in subsequent reports.

References

5-1. Davenport, W. B., Probability and Random Processes, McGraw-Hill, New York, 1970.

5-2. Newton, G. C., Jr., Gould, L. A., and Kaiser, J. F., Analytical Design of Linear Feedback Controls, Wiley, New York, 1957.

5-3. Rynaski, E. G., Reynolds, P. A., and Shed, W. H., "Design of Linear Flight Control Systems Using Optimal Control Theory," ASD-TDR-63376, USAF Flight Dynamics Laboratory, April 1964.

5-4. Jacobs, O.L.R., "The Damping Ratio of an Optimal System," IEEE Trans. Automatic Control, Vol. AC-10, pp. 473-476, October 1965.

5-5. Herther, J. G., "Vibration Control of Large Space Structures Using Linear Quadratic Techniques," M.S. Thesis, Dept. of Aeronautics and Astronautics, Massachusetts Institute of Technology, Cambridge, MA, February 1982 (also Report CSDL-T-767, Charles Stark Draper Laboratory).

Table 5-1. Calculation of desired closed-loop modal parameter objectives.

	OPEN LOOP			$\omega_{\alpha d} = \omega_{\alpha 0}$; $\rho_{\alpha d} = 0.05$		
MODE	$\omega_{\alpha 0}$	$\zeta_{\alpha 0}$	$\rho_{\alpha 0}$	$\omega_{\alpha d}$	$\zeta_{\alpha d}$	$\rho_{\alpha d}$
23	9.74569	0.001	1746.220	9.74569	1467.56	0.05
22	7.28061	0.001	513.582	7.28061	488.72	0.05
7	0.71608	0.001	403.338	0.71608	1184.17	0.05
12	3.50193	0.001	202.140	3.50193	270.21	0.05
13	3.74593	0.001	108.935	3.74593	139.99	0.05
14	3.86272	0.001	83.232	3.86272	104.92	0.05
15	3.99818	0.001	76.559	3.99818	94.79	0.05
9	0.93994	0.001	50.996	0.93994	123.81	0.05
33	41.2344	0.001	30.690	41.2344	19.27	0.05
34	50.6740	0.001	25.829	50.6740	16.72	0.05

	$\omega_{\alpha d} = \omega_{\alpha 0}$; $\rho_{\alpha d} = 5.0$			$\zeta_{\alpha d} \leq 0.707$; $\rho_{\alpha d} = 5.0$		
MODE	$\omega_{\alpha d}$	$\zeta_{\alpha d}$	$\rho_{\alpha d}$	$\omega_{\alpha d}$	$\zeta_{\alpha d}$	$\rho_{\alpha d}$
23	9.74569	13.8275	5.0	35.59	0.707	5.0
22	7.28061	3.89206	5.0	14.77	0.707	5.0
7	0.71608	5.25117	5.0	1.468	0.707	5.0
12	3.50193	1.27616	5.0	4.357	0.707	5.0
13	3.74593	0.43109	5.0	3.74593	0.43109	5.0
14	3.86272	0.26071	5.0	3.86272	0.26071	5.0
15	3.99818	0.22215	5.0	3.99818	0.22215	5.0
9	0.93994	0.10399	5.0	0.93994	0.10399	5.0
33	41.2344	0.03643	5.0	41.2344	0.03643	5.0
34	50.6740	0.02610	5.0	50.6740	0.02610	5.0

Table 5-2. Quadratic weights to achieve desired closed-loop modal parameter objectives.

		$\omega_{\alpha d} = \omega_{\alpha 0}$; $\rho_{\alpha d} = 5.0$		$\zeta_{\alpha d} \leq 0.707$; $\rho_{\alpha d} = 5.0$	
MODE	r_α	q_D^α	q_V^α	q_D^α	q_V^α
23	7.5162×10^{1}	0	5.46×10^{6}	1.20×10^{8}	1.43×10^{4}
22	8.7760×10^{1}	0	2.819×10^{5}	3.93×10^{6}	9.31×10^{3}
7	1.9080×10^{0}	0	1.079×10^{2}	8.36×10^{0}	1.96×10^{0}
12	8.4371×10^{-2}	0	6.7403×10^{0}	1.78×10^{1}	2.07×10^{0}
13	1.0980×10^{-2}	0	1.145×10^{-1}	0	1.145×10^{-1}
14	3.8073×10^{-4}	0	1.5445×10^{-3}	0	1.5445×10^{-3}
15	8.9494×10^{-3}	0	2.824×10^{-2}	0	2.824×10^{-2}
9	3.1965×10^{-5}	0	1.2215×10^{-6}	0	1.2215×10^{-6}
33	7.9410×10^{-4}	0	7.162×10^{-3}	0	7.162×10^{-3}
34	3.4933×10^{-4}	0	2.441×10^{-3}	0	2.441×10^{-3}

Table 5-3. Summary of results for RMS error in LOS output.

RMS Error (μ-radians)		$\omega_{\alpha d} = \omega_{\alpha 0}$; $\rho_{\alpha d} = 5.0$	$\zeta_{\alpha d} \leq 0.707$; $\rho_{\alpha d} = 5.0$	
		$Q_L=0$, $Q_D=0$	$Q_L=0$, $Q_D\neq 0$	$Q_L\neq 0$, $Q_D\neq 0$
INPUT	LOS-X	87.8635	89.0878	0.599137
AT	LOS-Y	282.896	290.835	12.7934
NODE 37	LOS-Z	178.351	165.763	40.9001
INPUT	LOS-X	139.392	49.0196	1.33162
AT	LOS-Y	376.895	174.084	25.3192
NODE 46	LOS-Z	339.485	104.179	79.9046

Table 5-4. Closed-loop poles for final design run.

NUMBER	REAL	IMAG	DAMPING	FREQUENCY (Rad/Sec)
2	-8.769678834E-01	1.461512935E+00	5.145216919E-01	1.704433257E+00
4	-1.087287502E-01	3.408435863E+00	3.188367784E-02	3.410169640E+00
6	-1.948704685E-02	3.950036962E+00	4.933323384E-03	3.950085030E+00
8	-3.869225121E+00	2.685924262E+00	8.214731632E-01	4.710105326E+00
10	-1.089833479E+00	4.813085291E+00	2.208407490E-01	4.934929283E+00
12	-4.373151345E+00	5.428774954E+00	6.273270603E-01	6.971086729E+00
14	-9.748363547E+00	1.021557284E+01	6.903695724E-01	1.412050000E+01
16	-2.495696740E+01	2.510249821E+01	7.050481302E-01	3.539753718E+01
18	-2.906650868E+01	5.839874058E+01	4.455834609E-01	6.523246759E+01
20	-5.089422278E+01	6.547852743E+01	6.136887361E-01	8.293165539E+01

Table 5-5. Quadratic weighting matrices for final design run.

Q:

	1	2	3	4	5
q_L^α	4.67×10^{8}	4.67×10^{8}	0	-	-
q_D^α	1.2×10^{8}	3.93×10^{6}	2.26×10^{2}	1.78×10^{1}	0
q_V^α	1.43×10^{4}	9.31×10^{3}	1.96×10^{0}	2.07×10^{0}	1.145×10^{-1}

	6	7	8	9	10
q_L^α	-	-	-	-	-
q_D^α	0	0	3.77×10^{-3}	0	0
q_V^α	1.5445×10^{-3}	2.824×10^{-2}	0	7.162×10^{-3}	2.441×10^{-3}

R:

	1	2	3	4	5
1	1.620421000D-06	-5.293120000D-06	1.260330000D-05	-6.155860000D-06	-2.252290000D-06
2	-5.293120000D-06	3.575187000D-05	-8.262220000D-05	4.143380000D-05	1.289720000D-05
3	1.260330000D-05	-8.262220000D-05	2.323739000D-04	-1.061430000D-04	-3.254450000D-05
4	-6.155860000D-06	4.143380000D-05	-1.061430000D-04	5.873912000D-05	1.630920000D-05
5	-2.252290000D-06	1.289720000D-05	-3.254450000D-05	1.630920000D-05	5.734795000D-06
6	2.347330000D-06	-1.347010000D-05	3.401670000D-05	-1.702410000D-05	-5.356450000D-06
7	8.753020000D-07	-4.914010000D-06	1.237770000D-05	-6.196310000D-06	-1.984090000D-06
8	-3.382550000D-06	5.789460000D-06	-1.129750000D-05	5.000640000D-06	2.888830000D-06
9	3.382870000D-06	-5.795660000D-06	1.131790000D-05	-5.016640000D-06	-2.894830000D-06

	6	7	8	9
1	2.347330000D-06	8.753020000D-07	-3.382550000D-06	3.382870000D-06
2	-1.347010000D-05	-4.914010000D-06	5.789460000D-06	-5.795660000D-06
3	3.401670000D-05	1.237770000D-05	-1.129750000D-05	1.131790000D-05
4	-1.702410000D-05	-6.196310000D-06	5.000640000D-06	-5.016640000D-06
5	-5.356450000D-06	-1.984090000D-06	2.888830000D-06	-2.894830000D-06
6	6.255150000D-06	2.051690000D-06	-3.002940000D-06	3.000600000D-06
7	2.051690000D-06	8.322370000D-07	-1.160950000D-06	1.171620000D-06
8	-3.002940000D-06	-1.160950000D-06	2.433101000D-05	-2.010080000D-05
9	3.000600000D-06	1.171620000D-06	-2.010080000D-05	2.436027000D-05

Table 5-6. Optimal state-feedback gain for final design run.

	1	2	3	4	5
1	1.144313484D+06	1.407339279D+06	-1.416721841D+04	-1.733328386D+04	-1.652267215D+03
2	-3.414945591D+05	3.717630183D+04	5.070409140D+02	2.197571365D+03	3.908391212D+02
3	1.462723313D+05	-2.688283115D+04	-2.006663467D+02	-1.200756597D+03	-2.140064726D+02
4	-2.484187585D+05	7.367340194D+04	-1.825211424D+02	8.544417170D+02	9.131745236D+01
5	-3.865174310D+05	6.137741439D+04	-1.912858416D+03	-6.654043762D+03	-1.356031467D+04
6	5.159962810D+05	-7.188184249D+04	2.567752977D+03	9.001277670D+03	-1.684614893D+04
7	1.129457080D+06	-6.833478611D+04	4.648471786D+03	1.680715455D+04	1.958921023D+04
8	-1.781965711D+04	-3.583341839D+04	-1.713324388D+03	-1.393940960D+03	8.042224918D+02
9	1.418127977D+04	3.213697646D+04	1.650157668D+03	1.021669300D+03	7.537874782D+02

	6	7	8	9	10
1	1.286079066D+04	-5.036440543D+02	-3.284856047D+02	3.378861938D+04	7.184882487D+04
2	-1.585683635D+03	1.112271974D+02	7.573418947D+01	-7.675293008D+03	-2.456426166D+04
3	8.612570396D+02	-6.120784479D+01	-4.168905515D+01	4.072982921D+03	1.401937615D+04
4	-5.903657759D+02	2.848773273D+01	1.894633167D+01	-1.572672893D+03	-1.322054021D+04
5	4.737991580D+03	-3.568243387D+03	-2.544120399D+03	2.697154258D+05	5.809774694D+04
6	-6.577729000D+03	-4.404342403D+03	-3.210045828D+03	3.355627147D+05	-1.080100690D+05
7	-1.196554974D+04	5.321669793D+03	3.889474657D+03	-3.865942538D+05	-1.668806893D+05
8	9.693403422D+02	1.159564413D+02	-2.722791800D+02	1.173415606D+03	-1.426292043D+03
9	-9.099325445D+02	1.107982887D+02	-2.817513591D+02	1.675947036D+03	1.798783094D+03

	11	12	13	14	15
1	5.723268572D+04	1.980957932D+05	-1.191934263D+04	1.668398221D+03	-5.445847648D+01
2	-1.647717885D+04	6.307019006D+03	-1.836269961D+02	1.504470420D+02	-9.691134587D+00
3	7.280685219D+03	-4.442784277D+03	1.819116519D+02	-4.870813329D+01	-8.133924155D+00
4	-1.156838091D+04	1.101234533D+04	-5.453769727D+02	1.380731668D+02	9.170943242D+00
5	-1.162926738D+04	5.198523514D+03	-3.336647373D+01	-5.403490472D+01	-1.326848676D+02
6	1.601101745D+04	-5.482161119D+03	2.712467297D+01	2.157965752D+02	-2.846416115D+02
7	3.576376606D+04	-5.685054733D+02	-3.588538303D+02	1.165881555D+03	6.459121099D+02
8	-5.076060309D+02	-2.528100485D+03	-1.832011843D+03	2.947803427D+02	-3.756881147D+02
9	4.472140048D+02	2.436132720D+03	1.577621460D+03	-2.506201741D+02	-3.766558164D+02

	16	17	18	19	20
1	2.650760810D+02	5.884763240D+00	-8.628057114D+00	6.385756866D+02	2.777572758D+03
2	-3.440166636D+01	2.022544195D+01	1.153902143D+00	-1.417364861D+02	-8.578636238D+02
3	1.146146523D+01	1.020879443D+00	-1.085416986D+00	7.465480475D+01	4.862105075D+02
4	-1.452282154D+01	-2.421669221D+00	1.025622170D+00	-2.606454526D+01	-4.552948167D+02
5	7.348283462D+01	-3.838315274D+01	-2.525318853D+01	5.271575071D+03	2.064046150D+03
6	-1.165610061D+02	-5.475363160D+01	-5.089727134D+01	6.632870522D+03	-3.609836783D+03
7	-2.987466487D+02	1.448002603D+02	1.184486870D+02	-7.519666535D+03	-5.797681250D+03
8	5.804602006D+00	-1.053868633D+02	-1.306291251D+02	2.145757994D+01	-2.939432557D+01
9	-3.009779839D+01	-1.091790128D+02	-1.310889531D+02	3.002962251D+01	3.542901440D+01

Figures 5-1. Output power spectral density from closed-loop linear quadratic regulator (augmented-state formulation).

(On following pages)

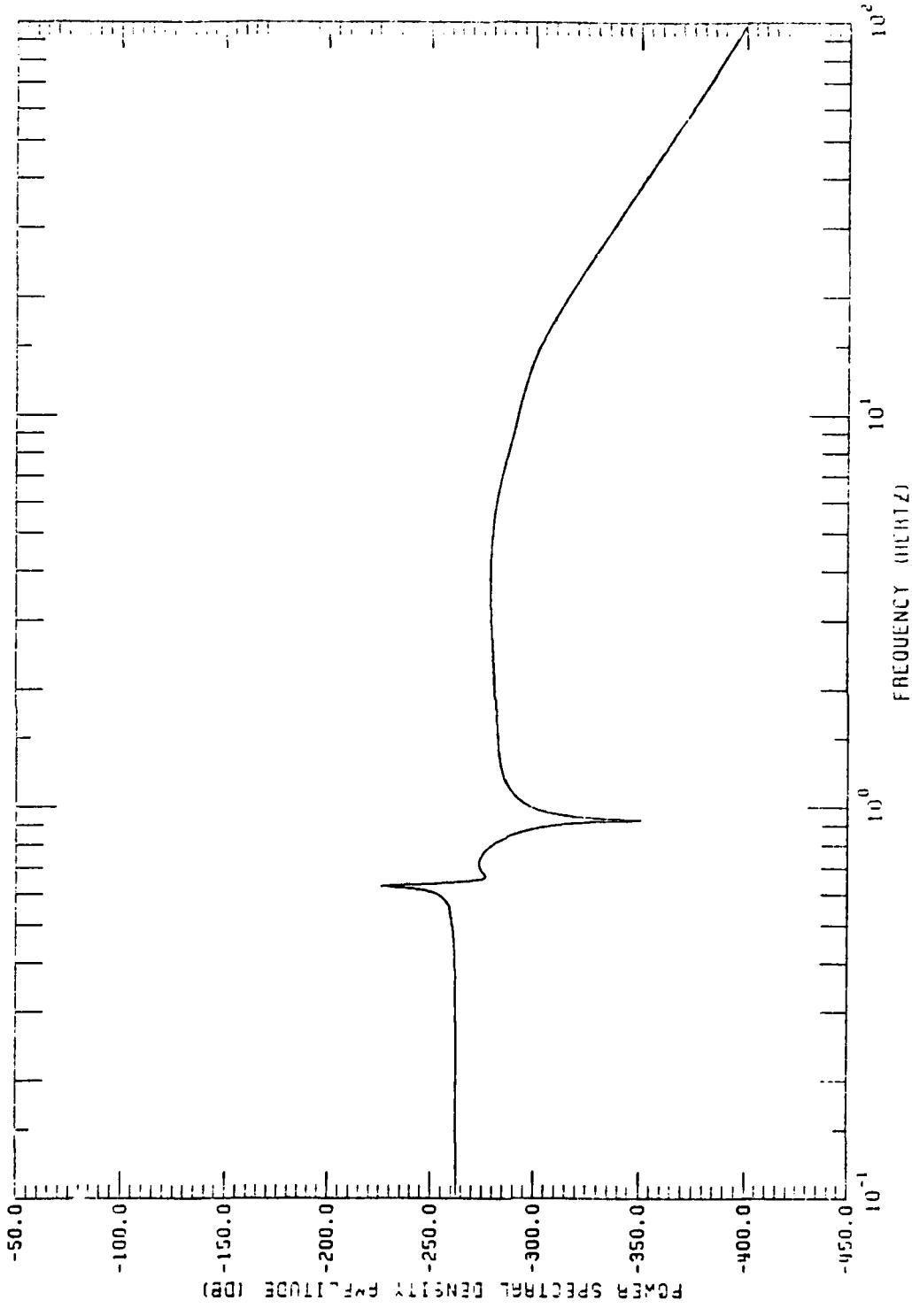

Figure 5-1a. Disturbance at node 37, output LOS-x.

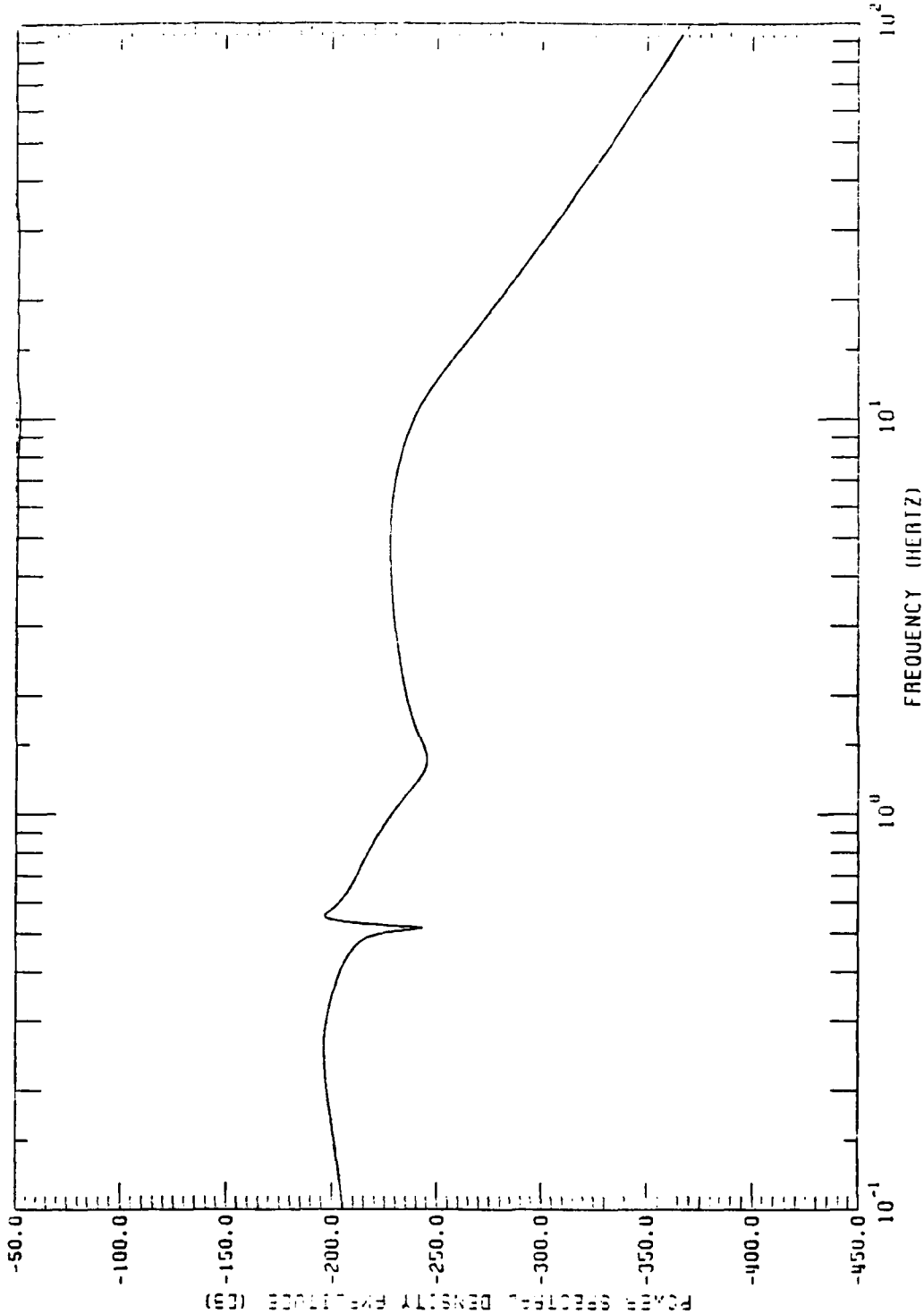

Figure 5-1b. Disturbance at node 37, output LOS-Y.

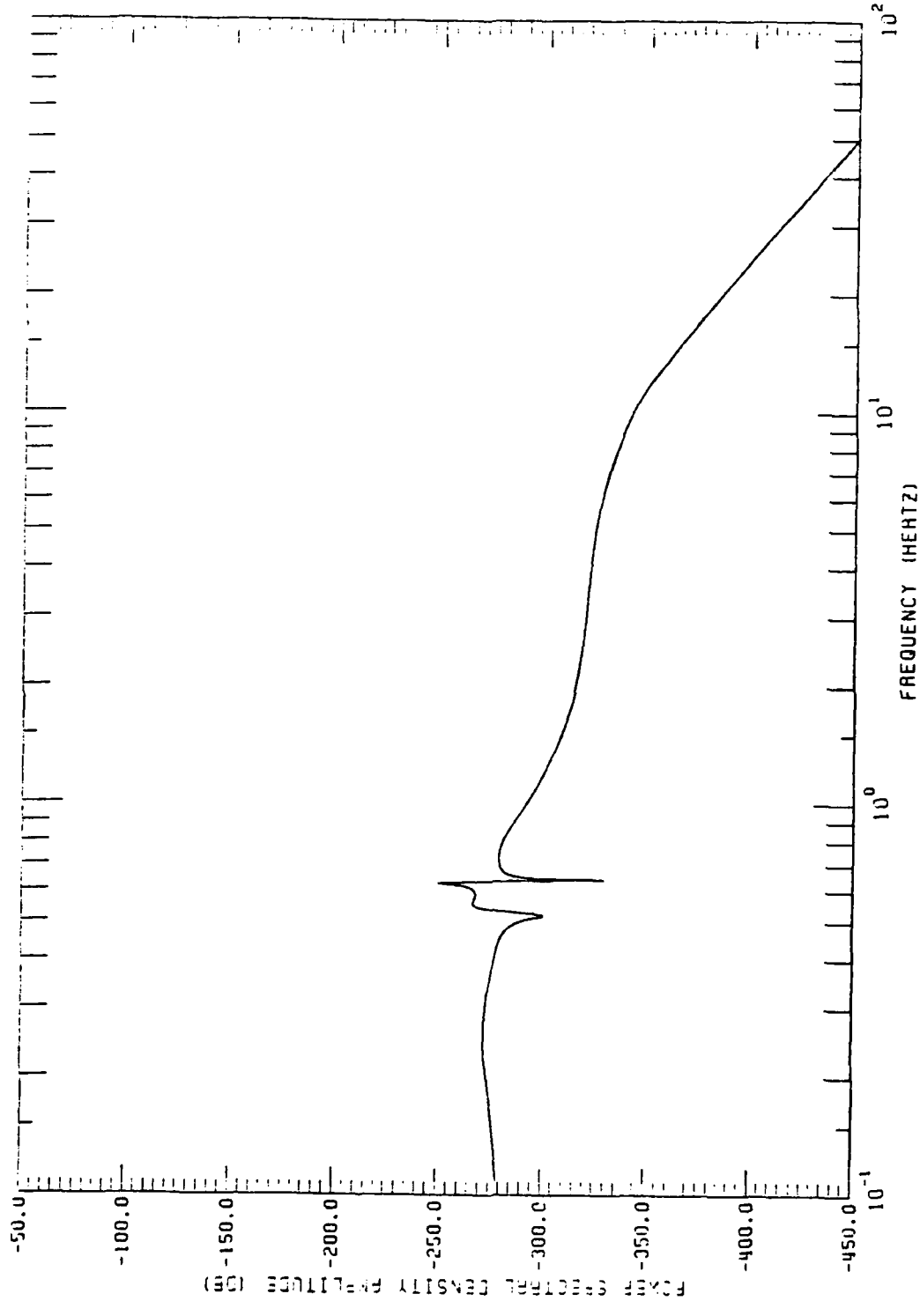

Figure 5-1c. Disturbance at node 37, output LOS-Z.

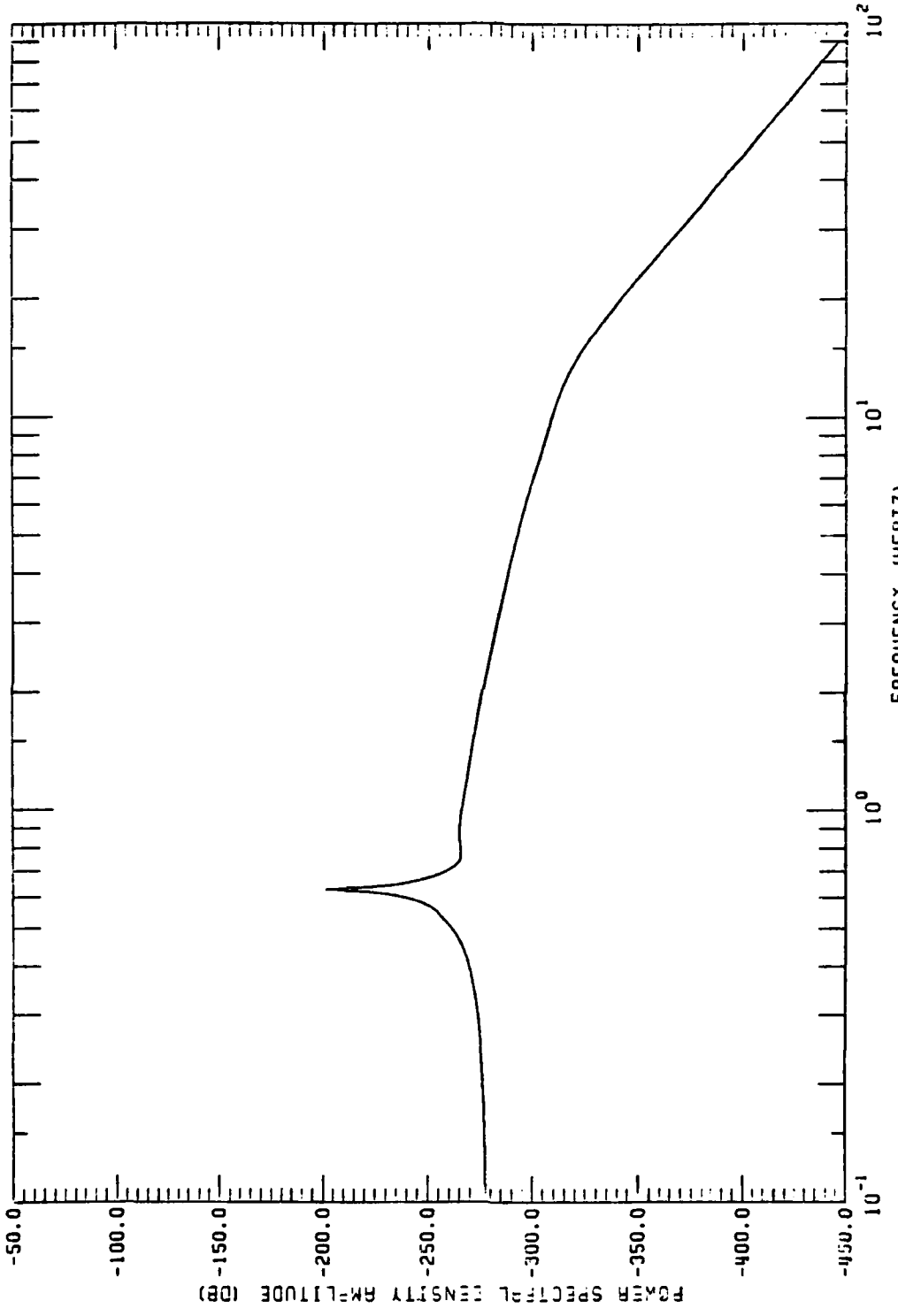

Figure 5-1d. Disturbance at node 46, output LOS-X.

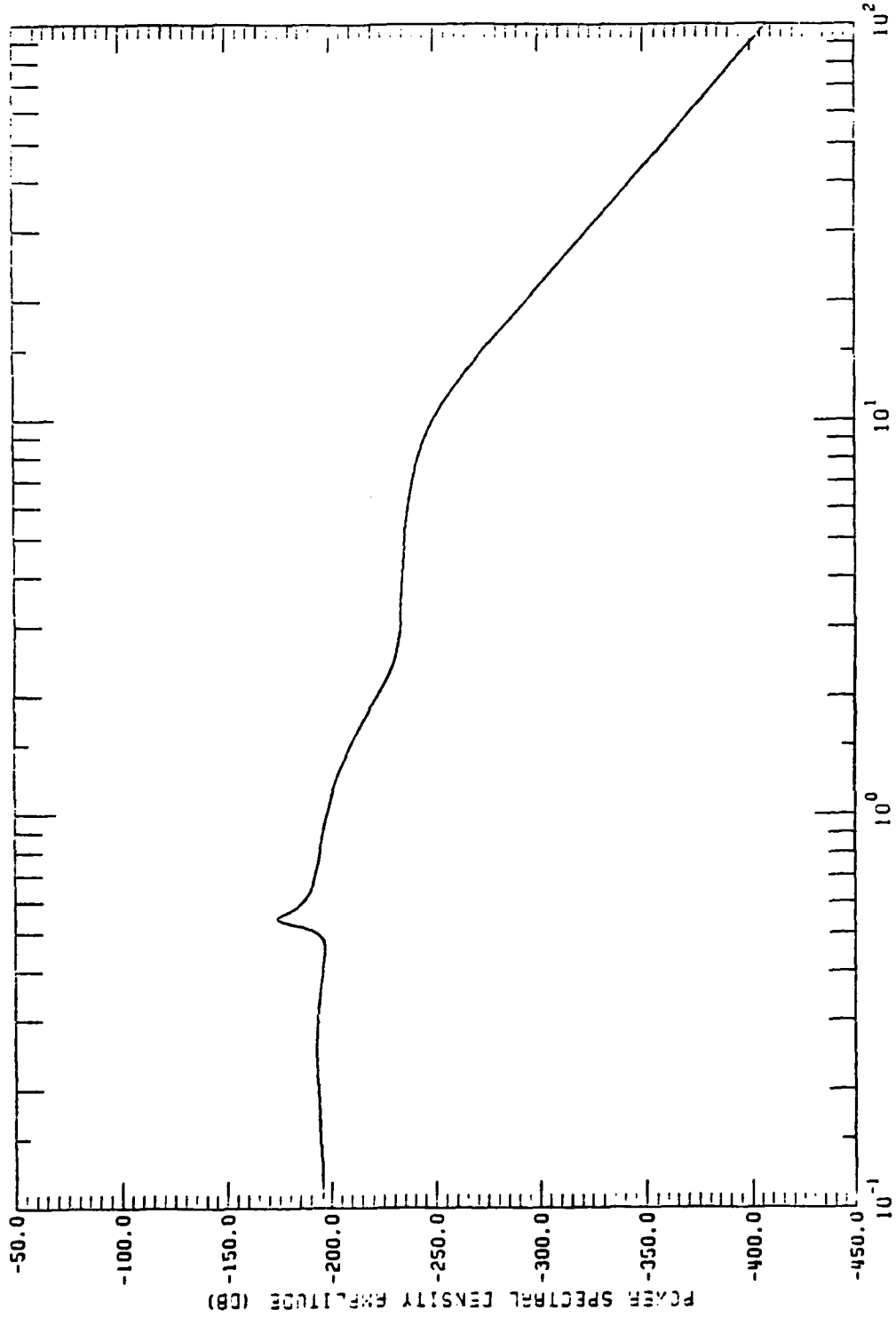

Figure 5-1e. Disturbance at node 46, output LOS-Y.

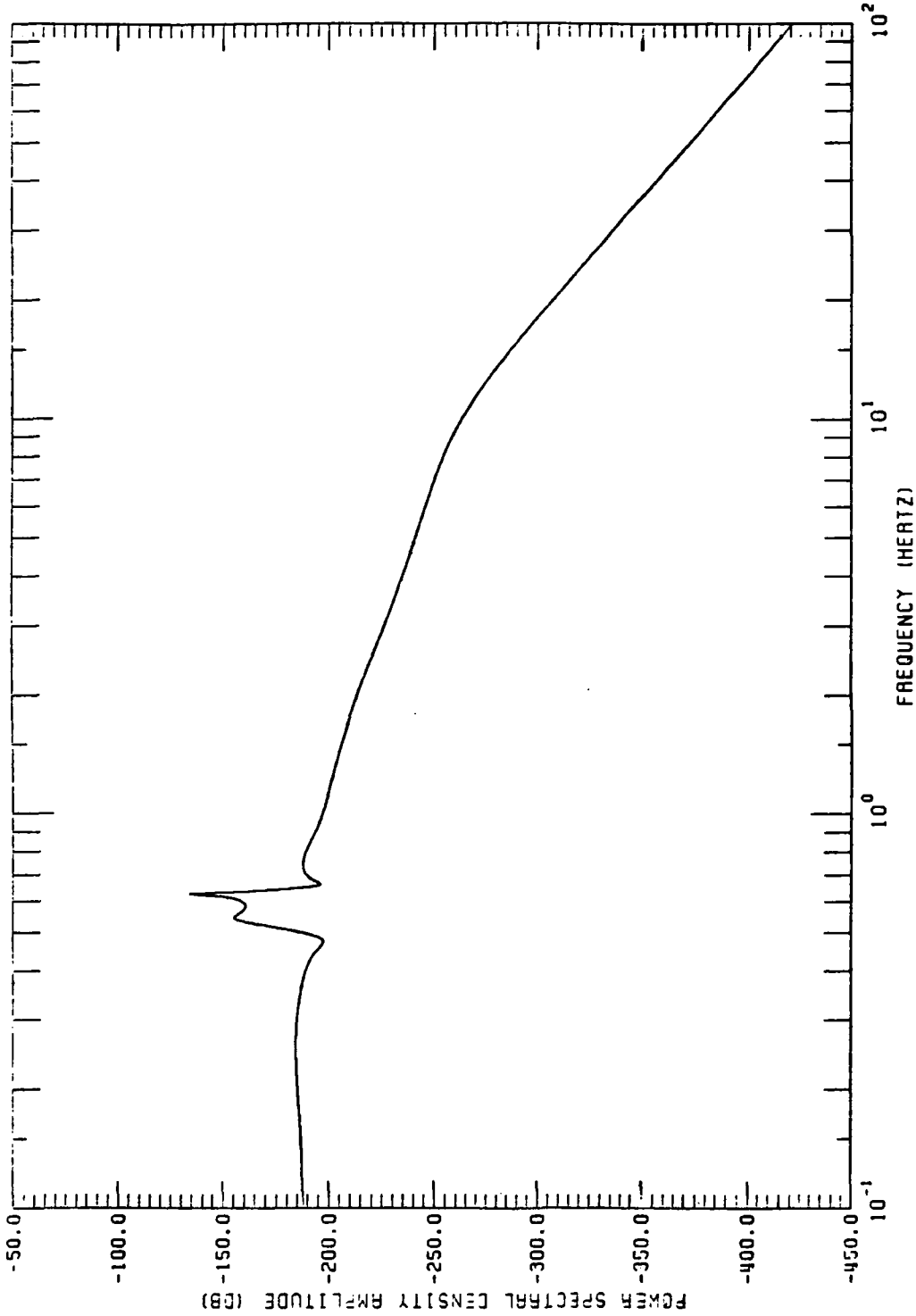

Figure 5-1f. Disturbance at node 46, output LOS-Z.

SECTION 6

LINEAR-QUADRATIC OPTIMAL CONTROL DESIGN WITH SPILLOVER REDUCTION

6.1 Introduction

Both Sections 4 and 5 describe the design of optimal control systems for the 10-mode model composed of the top 10 with respect to their RMS LOS-errors (Modes 23, 22, 7, 12, 13, 14, 15, 9, 33, and 34 in the descending order). Spillover (and possibly closed-loop instability) is expected when these control systems are applied to the 20-mode evaluation (or "truth") model, which contains, in addition, the next top 10 modes (modes 45, 40, 37, 16, 24, 10, 47, 48, 62, and 56, again in the descending order). In this section, we report a design of actuator synthesizers for preventing spillover of selected low-frequency modes and a corresponding linear-quadratic optimal control design.

6.2 A Design of Actuator Synthesizers

To demonstrate the design of a spillover-preventing synthesizer for the given six actuators, we consider modes 23, 22, 7, 12, 13, 14, 15, 9, 33, and 34 as the "primary modes" and treat modes 10, 16, 24, 37, 40, and 45 as the "secondary modes". In fact, all are critical to the LOS performance and should be actively controlled if the design model is not limited to only 10 modes. Note that the above secondary modes are of the lowest frequencies among the 10 nonprimary modes and that modes 10, 16, and 24 lie between the closely-spaced primary modes. The actuator synthesizer is designed to achieve two objectives: (1) to

prevent control spillover to the six secondary modes, and (2) to correct the modal control authority of the four most LOS-critical modes, namely, modes 23, 22, 7, and 12. Both objectives are achieved satisfactorily by a synthesizer Γ which is decomposed into two parts as

$$\Gamma = Q_2 \hat{\Gamma} \tag{6-1}$$

The matrix Q_2 is computed first (for the first objective) followed by the computation of $\hat{\Gamma}$ (for the second objective).

6.2.1 Synthesis for Prevention of Control Spillover

Ideally, we wish to synthesize to prevent control spillover to the six secondary modes exactly, but we decided to compromise with the control of the top 10 LOS-critical modes. Since the 6 x 9 actuator influence matrix $\Phi_S^T B_F$ corresponding to the six secondary modes has rank 6, an exact prevention of control spillover to the six secondary modes would require 6 independent actuators and hence result in at most 3 independent synthetic actuators (see Ref. 6-1). Note that all the nine actuators are used to control the 10 primary modes when no prevention of spillover is considered. We felt that it would be more desirable if one more independent synthetic actuator was reserved for controlling the primary modes. With such a restriction, the synthesizer could be designed in one of the following alternative ways: (1) ignore one secondary mode and prevent control spillover to the remaining 5 secondary modes exactly, or (2) prevent spillover to all the six secondary modes approximately. We took the second alternative, since a "degree-of-independence" test revealed that the actuator influences on these secondary modes have a high degree of dependence. So, some spillover to each of the six secondary modes should be expected.

The exact synthesis program previously reported in Ref. 6-2 was modified, and a 9 x 4 matrix Q_2 that provides approximate spillover prevention thus computed. The following shows the result:

$$Q_2 = \begin{bmatrix} 0.40377D-01 & 0.68237D+00 & 0.0 & 0.0 \\ -0.21362D+00 & 0.42017D+00 & -0.70978D+00 & 0.35879D+00 \\ 0.71674D+00 & 0.78608D-01 & 0.11774D+00 & 0.45053D+00 \\ 0.13984D+00 & 0.82051D-01 & 0.81981D-01 & 0.39338D-01 \\ -0.91406D-01 & 0.38219D+00 & 0.29262D+00 & -0.31405D+00 \\ 0.54240D-01 & -0.40540D+00 & -0.30018D+00 & 0.29277D+00 \\ -0.37592D+00 & -0.18267D+00 & -0.17103D+00 & -0.14506D+00 \\ -0.36513D+00 & 0.23773D-01 & 0.36782D+00 & 0.48031D+00 \\ -0.36542D+00 & 0.23737D-01 & 0.36790D+00 & 0.48028D+00 \end{bmatrix}$$

6.2.2 Synthesis for Correction of Modal Control Authority

Modes 23, 22, 7, and 12 are the most LOS-critical primary modes: their individual contributions to LOS errors not only rank the highest among the 20 modes (also among all the 156 modes of the VCOSS model structure), but are also disproportionately large compared with other LOS-critical modes. For example, they are, respectively, 34, 10, 8, and 4 times larger than that of Mode 9. Therefore, the control authority of the 9 actuators on these four modes not only should rank the highest but also should have the similar proportions as compared with that on mode 9, for example. By whatever measure of control authority, the situations are just the opposite, however. As can be seen from Tables 6-1 through 6-4, these four modes all have very disappointingly small values, and all lie at or near the bottom, even with the nonprimary modes included for comparison.

The free parameter matrix $\hat{\Gamma}$ is useful for trying to correct the situation. We calculated the matrix $\hat{\Gamma}$ column by column using a least-

squares optimization technique in such a way that each column tried to elevate the relative control authority on one of these four modes. The results are shown below:

$$\hat{\Gamma} = \begin{bmatrix} -0.58244D+01 & 0.97129D+00 & -0.24545D+00 & 0.11582D+00 \\ 0.23931D+02 & -0.45118D+01 & 0.53743D+00 & -0.90634D+00 \\ -0.19278D+02 & 0.34960D+01 & -0.52266D+00 & 0.60541D+00 \\ 0.91904D+01 & -0.16749D+01 & 0.22756D+00 & -0.29022D+00 \end{bmatrix}$$

Forming the matrix product of Q_2 and $\hat{\Gamma}$ as in Eq. (6-1), we obtained the synthesizer Γ:

$$\Gamma = \begin{bmatrix} 0.16094D+02 & -0.30395D+01 & 0.35681D+00 & -0.61378D+00 \\ 0.28280D+02 & -0.51856D+01 & 0.73087D+00 & -0.93940D+00 \\ -0.42270D+00 & -0.14559D-02 & -0.92692D-01 & -0.47700D-01 \\ -0.69848D-01 & -0.13651D-01 & -0.24123D-01 & -0.19953D-01 \\ 0.11511D+01 & -0.26415D+00 & 0.34306D-02 & -0.88683D-01 \\ -0.15400D+01 & 0.34201D+00 & -0.76766D-02 & 0.10702D+00 \\ -0.21796D+00 & 0.10408D+00 & 0.50477D-01 & 0.60575D-01 \\ 0.19005D-01 & 0.19527D-01 & 0.19451D-01 & 0.19446D-01 \\ 0.17885D-01 & 0.19762D-01 & 0.19451D-01 & 0.19506D-01 \end{bmatrix}$$

The synthesized actuator influences are thus given by post-multiplying the unsynthesized influence matrix by the matrix Γ. Tables 6-5 through 6-8 show the ranking of the synthesized control authority using the same measures as before. Observe that the synthesized control authority on the two most LOS-critical modes, namely 23 and 22, have been greatly improved, compared with that on mode 9, for instance, though improvement in modes 12 and 7 are rather small. The proportions of the synthesized control authority among the primary modes are also improved.

The difficulties in improving the control authority on modes 12 and 7 manifest two levels of improper placement of the actuators. The first level, shown even clearer by modes 23 and 22, is the undesirably small magnitude of actuator influences on the most important modes. The second level is the undesirably high dependence of the primary-mode actuator influences on the secondary-mode influences.

6.3 Optimal Control Design with Spillover Reduction

With the spillover-preventing synthesizer Γ included, the dynamic equations become

$$\ddot{\eta}_i + 2\zeta_i\omega_i\dot{\eta}_i + \omega_i^2\eta_i = \phi_i^T B_F \Gamma u \qquad (6\text{-}2)$$

for each primary mode. The only difference is the replacement of the unsynthesized influence matrix B_F by the synthesized matrix $B_F\Gamma$. Thus, any controller design technique that is applicable to the unsynthesized case is equally applicable to the synthesized case. In particular, both the disturbance-rejection design presented in Section 4 and the linear-quadratic optimal control design presented in Section 5 can be mimicked here for the synthesized case. We chose to mimic the latter in our first attempt of reduced-order modern-controller design with spillover-preventing synthesizers. The analytical and one-shot nature is both cost-effective and time-effective, and hence is more attractive than the regular trial-and-error approach. It is based on the analytical procedure, jointly developed with J.G. Herther earlier [Ref. 6-3], for selecting the weight matrices in the linear-quadratic regulator design.

6.3.1 A Linear-Quadratic Optimal Control Design

Like the design of Section 5, the objective is to attenuate the individual contribution to the RMS LOS-error from each primary mode to 5 μrad. Note that the defocus error (i.e., the "LOS-Z" error) has not been used in the ranking and selection of the 10 control-system design model modes, i.e., the 10 primary modes. Note also that the total contribution to the RMS LOS-error from all the 10 primary modes is

$$\sqrt{10 \times 5^2} = 15.81 \text{ μrad}$$

if all the individual contributions are reduced to 5 μrad.

Following the same analytical procedure as sketched in Section 5 (see Eqs. (5-18) to (5-21), and refer to Eqs. (5-11), (5-12), (5-16), (5-17), and the case of $\zeta_{\alpha d} \leq 0.707$ in Table 5-1), we selected *a priori* the weight matrices Q and R as shown in Table 6-9.

6.3.2 Design Results

Table 6-10 shows the resulting state-feedback gains. Table 6-11 lists the resulting closed-loop poles, modal damping and modal frequencies. The power spectral density of the LOS-errors subject to the broad-band random disturbances at nodes 37 and 46 are shown in Figures 6-1a through 6-1f. Table 6-12 summarizes the RMS LOS-errors.

Observe that the total LOS-Y error contributed from all the 10 modes subject to either or both disturbances is very close to the design objective of 5 μrad for each mode. Although the total LOS-X error has also been reduced, it requires further reduction to meet the design objective. Some analysis and adjustment of the LOS weighting are required after this preliminary design.

Recall that in this design, only four control inputs are used for controlling the 10 primary modes, in contrast with the designs presented in Sections 4 and 5, in which all nine control inputs are used. Lower performance should be expected.

Other detailed discussions as well as the follow-on design activities will be reported later.

References

6-1. Lin, J.G., "Reduction of Control and Observation Spillover in Vibration Control of Large Flexible Space Structures," in Actively Controlled Structures Theory - Final Report, Charles Stark Draper Laboratory, Cambridge, MA, Report R-1338, December 1979.

6-2 Kissel, G.J., and Lin, J.G., "Spillover Prevention via Proper Synthesis/Placement of Actuators and Sensors," in Active Control of Space Structures - Final Report, Charles Stark Draper Laboratory, Cambridge, MA, Report R-1454, February 1981.

6-3 Herther, J.G., "Vibration Control of Large Space Structures Using Linear Quadratic Techniques," M.S. Thesis, Dept. of Aeronautics and Astronautics, Massachusetts Institute of Technology, Cambridge, MA, February 1982 (also Report CSDL-T-767, Charles Stark Draper Laboratory).

Table 6-1. The root-sum-square (RSS) values for each mode's control influence.

RANK	MODE	RSS
1	9	0.9019900897D-01
2	10	0.7050992633D-01
3	14	0.4265642533D-01
4	48	0.2493147623D-01
5	45	0.2274967529D-01
6	56	0.2232548603D-01
7	16	0.2098430635D-01
8	62	0.1669896495D-01
9	47	0.1439991647D-01
10	34	0.1381960835D-01
11	40	0.1279961879D-01
12	33	0.1089109832D-01
13	13	0.1039577065D-01
14	37	0.8236123765D-02
15	15	0.8092834171D-02
16	12	0.6959151462D-02
17	7	0.2920009766D-02
18	24	0.2240694139D-02
19	23	0.2014182207D-02
20	22	0.5482287245D-03

Table 6-2. The terms with the greatest absolute value in each row.

RANK	MODE	MAX
1	9	0.6378167887D-01
2	10	-0.4985987593D-01
3	14	-0.3017647834D-01
4	48	-0.2247462268D-01
5	45	-0.1536239079D-01
6	16	-0.1486552989D-01
7	56	0.1270583963D-01
8	47	-0.1187121992D-01
9	40	0.1001187826D-01
10	62	-0.9874167696D-02
11	34	-0.8062187492D-02
12	33	-0.7477476226D-02
13	13	-0.7405826176D-02
14	15	-0.5954319418D-02
15	37	-0.5741676334D-02
16	12	0.4922065292D-02
17	7	-0.2066678837D-02
18	23	-0.1653198503D-02
19	24	-0.1298867108D-02
20	22	0.3189018984D-03

Table 6-3. The damped degree-of-controllability (DOC) values for each mode's control influence with delta = .06.

RANK	MODE	DOC
1	9	0.8453719188D-05
2	10	0.5165528493D-05
3	14	0.1884632443D-05
4	16	0.4559450893D-06
5	45	0.2046270947D-06
6	48	0.1975475353D-06
7	34	0.1133468352D-06
8	13	0.1119594247D-06
9	56	0.1116967443D-06
10	33	0.8376070304D-07
11	47	0.6933173299D-07
12	15	0.6781903938D-07
13	40	0.6642650620D-07
14	62	0.5449112199D-07
15	12	0.5019237498D-07
16	37	0.3597169420D-07
17	7	0.8860244364D-08
18	24	0.5068259371D-08
19	23	0.4123635709D-08
20	22	0.3085356173D-09

Table 6-4. The undamped DOC values for each mode's control influence with delta = 1.

RANK	MODE	DOC
1	9	0.2214876900D-02
2	10	0.1324474663D-02
3	14	0.2320624786D-03
4	16	0.5358790490D-04
5	13	0.1425833015D-04
6	15	0.8042876959D-05
7	12	0.6879592027D-05
8	45	0.3478015216D-05
9	48	0.3291040802D-05
10	7	0.2378865193D-05
11	34	0.1884357812D-05
12	56	0.1860633769D-05
13	33	0.1438250407D-05
14	47	0.1162451603D-05
15	40	0.1128703537D-05
16	62	0.8998399631D-06
17	37	0.5991474092D-06
18	24	0.2244366462D-06
19	23	0.2080305574D-06
20	22	0.2050291577D-07

Table 6-5. The RSS values for each mode's control influence.

RANK	MODE	RSS
1	62	0.7665261412D-01
2	34	0.1964353669D-01
3	56	0.1949282657D-01
4	48	0.1868951163D-01
5	23	0.1835832973D-01
6	47	0.5885492914D-02
7	9	0.4915413610D-02
8	15	0.3291047618D-02
9	22	0.2916199034D-02
10	33	0.2021945935D-02
11	14	0.1310011534D-02
12	13	0.1175811702D-02
13	12	0.8784900923D-03
14	16	0.4230897846D-03
15	7	0.2314815954D-03
16	10	0.1249775007D-03
17	24	0.5528453623D-04
18	40	0.1373992454D-05
19	37	0.7473887318D-06
20	45	0.6335282574D-06

Table 6-6. The terms with the greatest absolute value in each row.

RANK	MODE	RSS
1	62	-0.7520285819D-01
2	56	0.1913919301D-01
3	34	-0.1883667488D-01
4	48	0.1850321486D-01
5	23	0.1805516365D-01
6	47	-0.5652007766D-02
7	15	-0.3257844598D-02
8	22	-0.2857453201D-02
9	9	0.2504911298D-02
10	33	0.1996049546D-02
11	14	-0.1287734647D-02
12	13	0.9680597192D-03
13	12	0.8641993619D-03
14	16	-0.4168865235D-03
15	7	-0.2276252051D-03
16	10	-0.1231451046D-03
17	24	-0.5447396499D-04
18	40	0.1353847241D-05
19	37	-0.7364306620D-06
20	45	0.6242395879D-06

Table 6-7. The damped DOC values for each mode's control influence with delta = .06 .

RANK	MODE	DOC
1	62	0.1768509174D-06
2	23	0.2564113362D-07
3	34	0.1999705975D-07
4	48	0.1336721607D-07
5	56	0.1322839465D-07
6	9	0.2965294086D-08
7	47	0.1430819156D-08
8	15	0.1060278071D-08
9	22	0.6542220180D-09
10	33	0.2121223747D-09
11	14	0.1839420675D-09
12	13	0.1519726159D-09
13	12	0.8737861122D-10
14	16	0.1719216811D-10
15	7	0.7320702038D-11
16	10	0.1883760480D-11
17	24	0.2228680891D-12
18	40	0.8565986263D-16
19	37	0.2704895235D-16
20	45	0.1695593384D-16

Table 6-8. The undamped DOC values for each mode's control influence with delta = 1.

RANK	MODE	DOC
1	62	0.1896007763D-04
2	23	0.1728207773D-04
3	9	0.6577580881D-05
4	34	0.3807248873D-05
5	48	0.1849410073D-05
6	56	0.1418432560D-05
7	15	0.1330082178D-05
8	22	0.5801314068D-06
9	14	0.2188709486D-06
10	47	0.1941872078D-06
11	13	0.1824025239D-06
12	12	0.1096285936D-06
13	33	0.4957129057D-07
14	16	0.2178425043D-07
15	7	0.1494975784D-07
16	10	0.4161087073D-08
17	24	0.1366268180D-09
18	40	0.1300632226D-13
19	37	0.4933794416D-14
20	45	0.2697199398D-14

Table 6-9. Weight matrices Q and R.

Q	1	2	3	4	5	6	7	8	9	10
q_L^α	5.06×10^{8}	7.42×10^{10}	0	-	-	-	-	-	-	-
q_D^α	1.444×10^{6}	1.389×10^{5}	3.593×10^{3}	1.117×10^{3}	0	0	0	1.268	0	0
q_V^α	1.719×10^{2}	3.289×10^{2}	3.112×10^{2}	1.299×10^{2}	8.950	1.641	1.705×10^{-1}	0	2.029×10^{-1}	1.199×10^{-3}

R	1	2	3	4
1	3.424070000D-04	-6.143100000D-05	1.062240000D-05	-1.043410000D-05
2	-6.143100000D-05	1.122140000D-05	-1.740180000D-06	2.046220000D-06
3	1.062240000D-05	-1.740180000D-06	4.666030000D-07	-1.795070000D-07
4	-1.043410000D-05	2.046220000D-06	-1.795070000D-07	4.697060000D-07

Table 6-10. Optimal gain matrix.

	1	2	3	4	5
1	1.283624137D+08	-2.244407096D+07	3.136988189D+06	5.176059599D+06	-1.511163745D+05
2	6.652330835D+08	-1.332554214D+08	3.230360821D+07	2.805351541D+07	-6.889690382D+05
3	-5.380428510D+08	5.321046979D+07	2.575730214D+07	-1.867430050D+07	8.855481209D+05
4	-2.477150444D+08	1.017223063D+08	-6.107728439D+07	-1.421156014D+07	-4.160035410D+03

	6	7	8	9	10
1	-4.121562317D+06	-3.023919487D+04	5.465859104D+04	-2.434634411D+06	-8.038570492D+07
2	-2.283446699D+07	-2.465911148D+05	4.123034680D+05	-2.749401100D+07	-4.141778210D+08
3	1.371155020D+07	-8.454549902D+04	7.786582198D+04	-2.568671909D+07	3.420646134D+08
4	1.307193146D+07	3.723150654D+05	-5.533903551D+05	5.580528791D+07	1.473528024D+08

	11	12	13	14	15
1	5.947530104D+05	-9.127381772D+05	4.764969750D+05	-1.940950043D+05	4.640822705D+04
2	2.881309690D+06	-8.519704710D+06	2.510982226D+07	-1.994928163D+06	3.264905454D+05
3	-3.012787211D+06	-5.310112498D+06	5.314144562D+07	-1.566191603D+06	8.530630888D+03
4	-4.164464872D+05	1.477051133D+07	-7.822185119D+07	3.781866370D+06	-3.894136313D+05

	16	17	18	19	20
1	-6.639072548D+04	1.367770331D+04	2.399409845D+04	-9.582599280D+04	-6.537916873D+05
2	-6.128150618D+05	9.404542739D+04	1.587542711D+05	-9.542236739D+05	-3.483910690D+06
3	-3.698057429D+05	-2.628879580D+03	-2.014194308D+04	-7.028686219D+05	2.503952479D+06
4	1.049377386D+06	-1.074208919D+05	-1.672575042D+05	1.757172886D+06	1.595800404D+06

Table 6-11. Closed-loop poles, modal damping, and modal frequencies.

NUMBER	REAL	IMAG	DAMPING	FREQUENCY (Rad/Sec)
2	-9.388419259E-01	1.228878347E+00	6.070874800E-01	1.546468930E+00
4	-2.366773605E+00	2.184081130E+00	7.349013937E-01	3.220532204E+00
6	-1.439333048E+00	3.420759862E+00	3.878311123E-01	3.711236675E+00
8	-1.842932432E-01	3.773380762E+00	4.878220423E-02	3.777878555E+00
10	-3.876810259E-02	3.950171868E+00	9.813809867E-03	3.950362104E+00
12	-9.924175509E-01	4.373982227E+00	2.212671818E-01	4.485154748E+00
14	-1.029484799E+00	7.291612342E+00	1.398010229E-01	7.363928944E+00
16	-2.428900197E+01	2.530290863E+01	6.925052645E-01	3.507410444E+01
18	-2.438190124E+01	4.766324692E+01	4.554173884E-01	5.353748421E+01
20	-1.296556899E+02	1.388700371E+02	6.824410440E-01	1.899881184E+02

Table 6-12. Summary of results for RMS LOS-errors.

RMS errors (μ-rad)	LOS-X	LOS-Y	Total
Disturbance at Node 37	453.87	6.66	453.92
Disturbance at Node 46	408.41	5.25	408.44
Total	610.57	8.48	610.63

Figures 6-1. Output power spectral density from closed-loop linear-quadratic regulator with actuator synthesizers.

(On following pages)

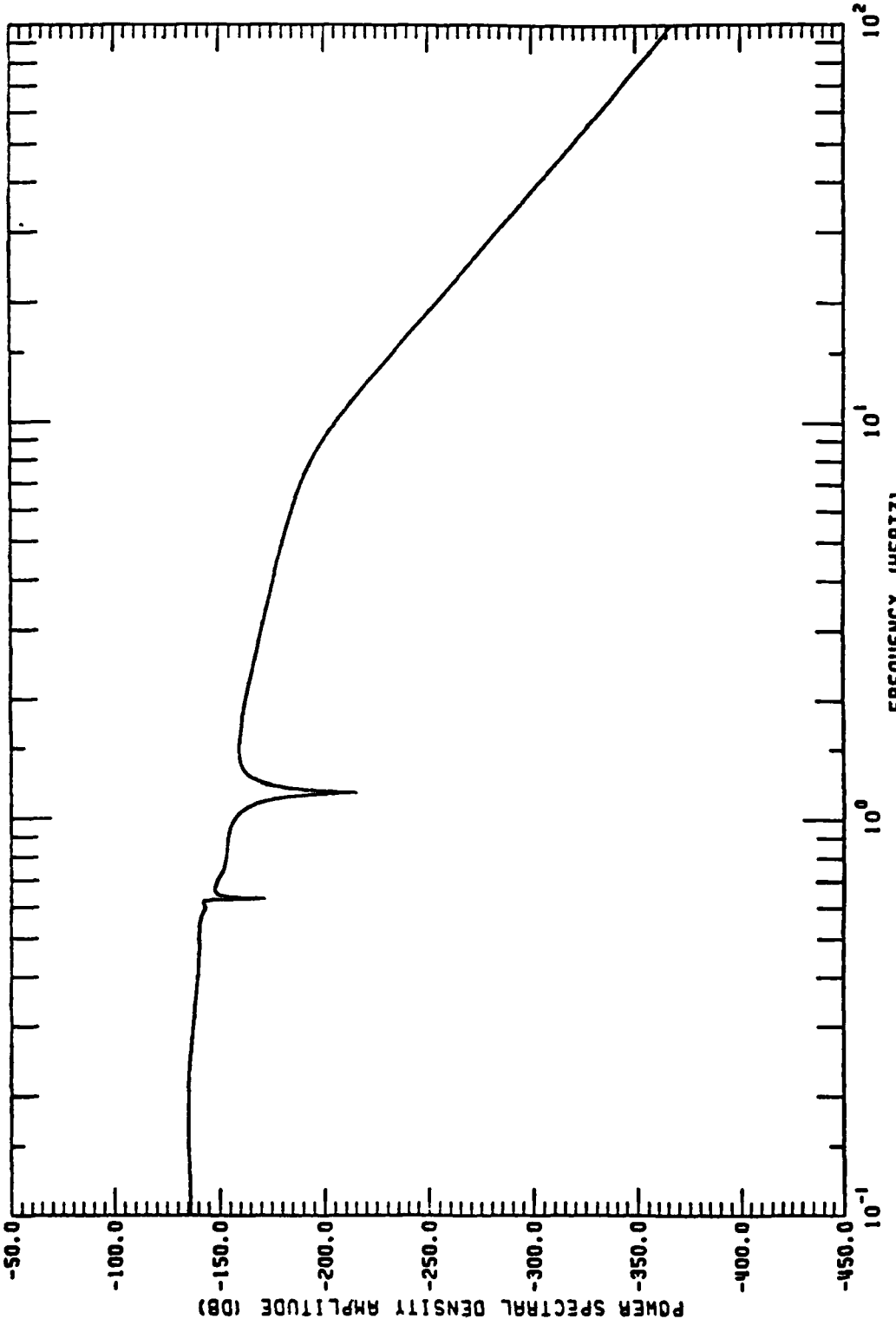

Figure 6-1a. Disturbance at node 37, output LOS-X.

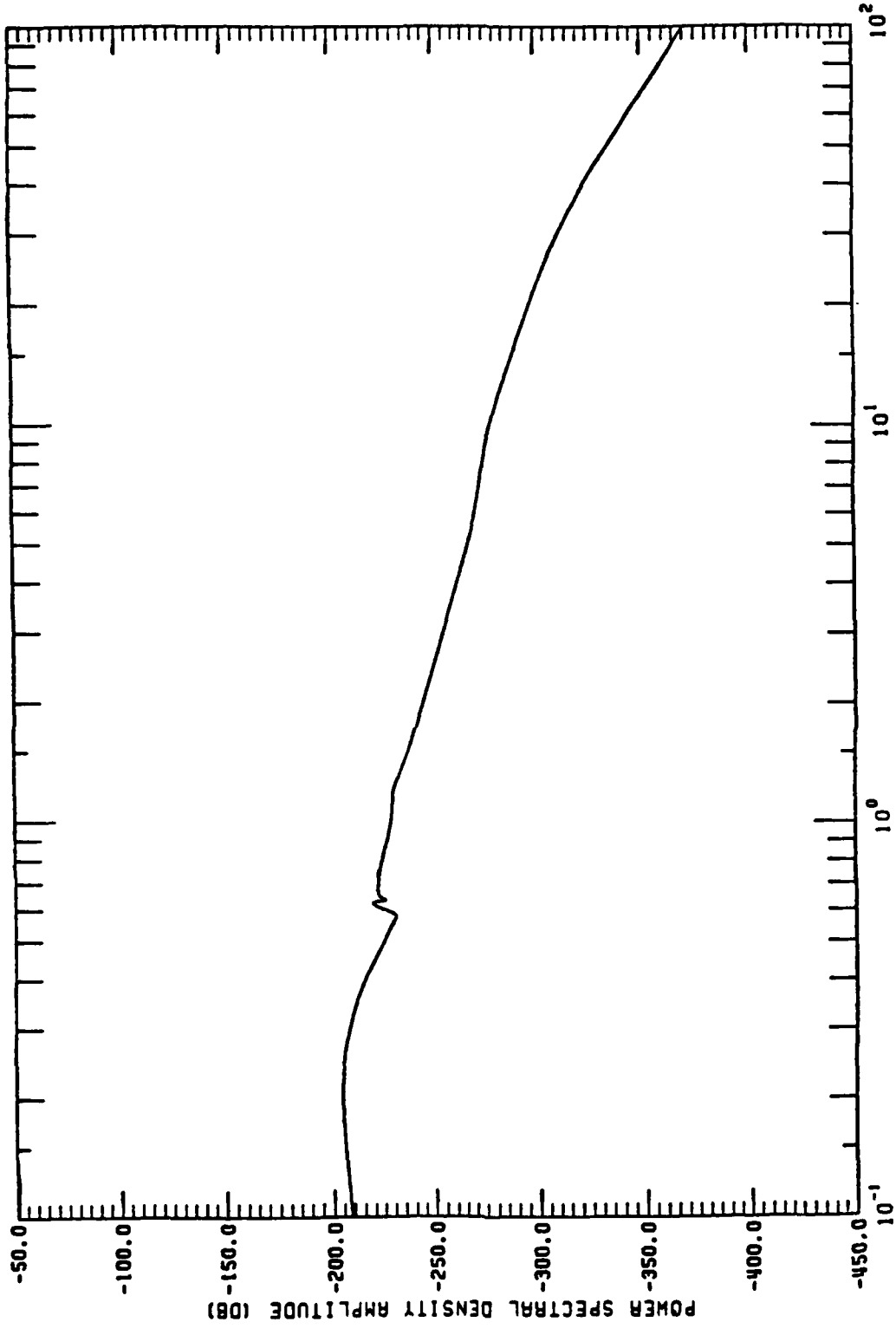

Figure 6-1b. Disturbance at node 37, output LOS-Y.

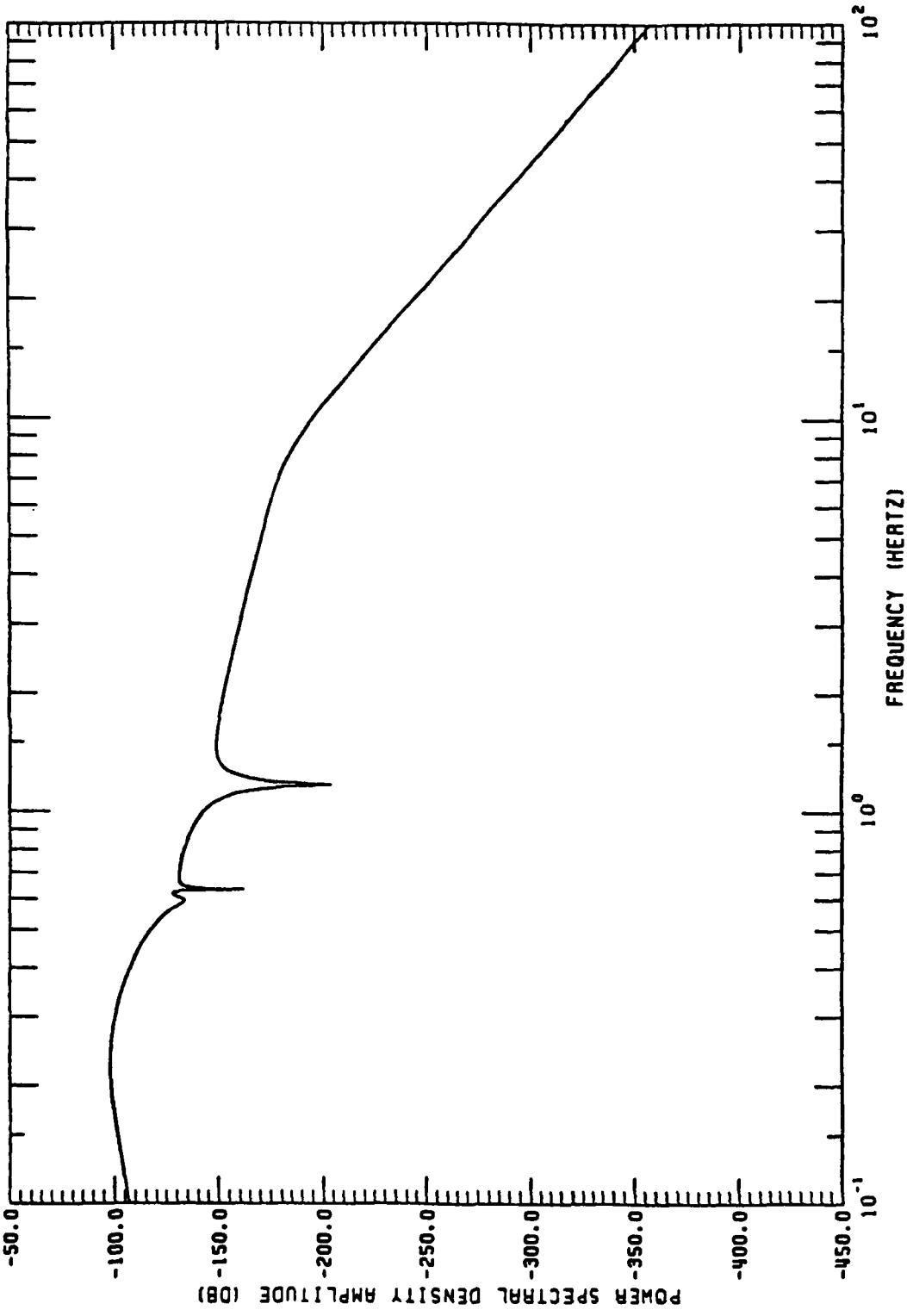

Figure 6-1c. Disturbance at node 37, output LOS-Z.

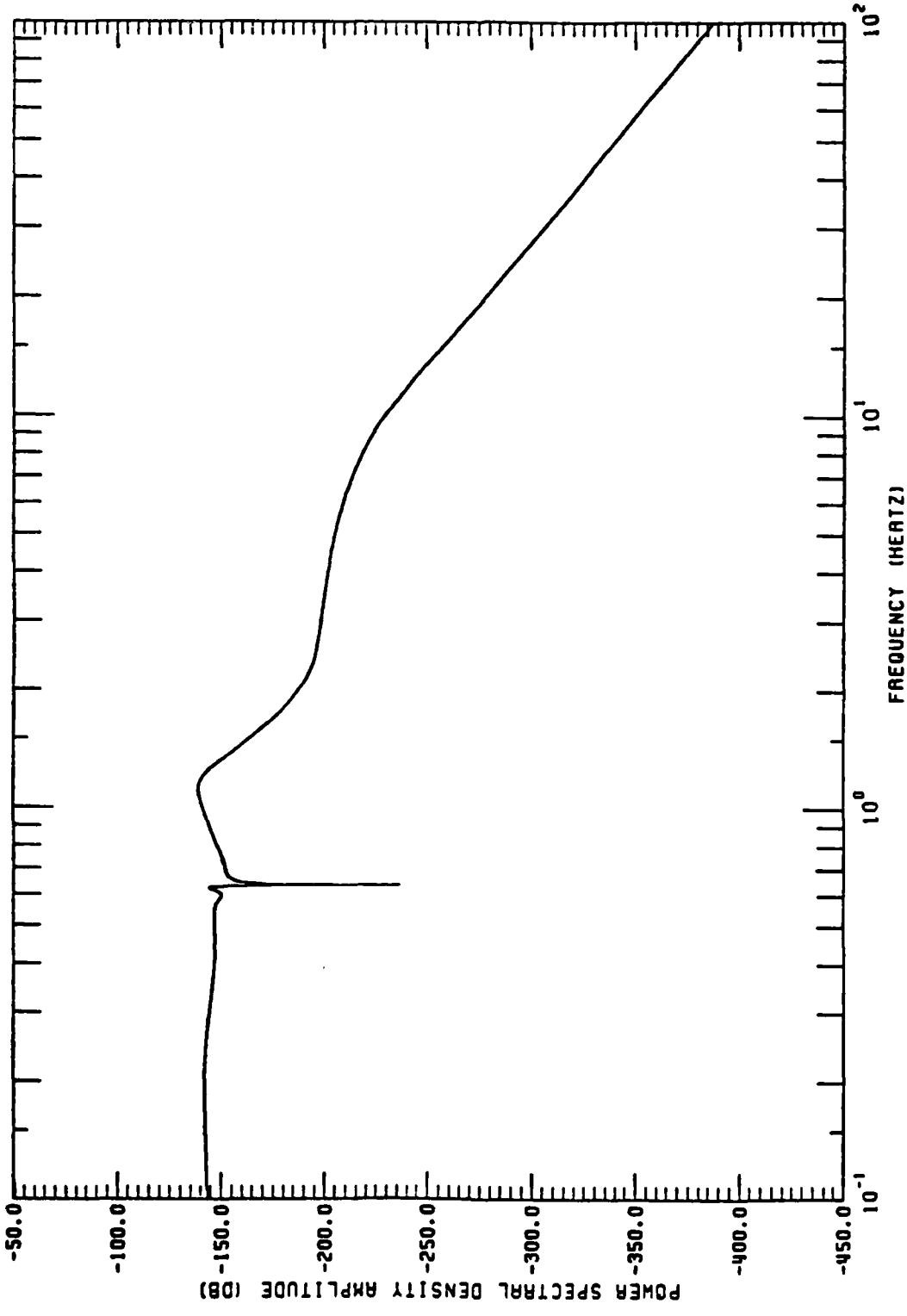

Figure 6-1d. Disturbance at node 46, output LOS-X.

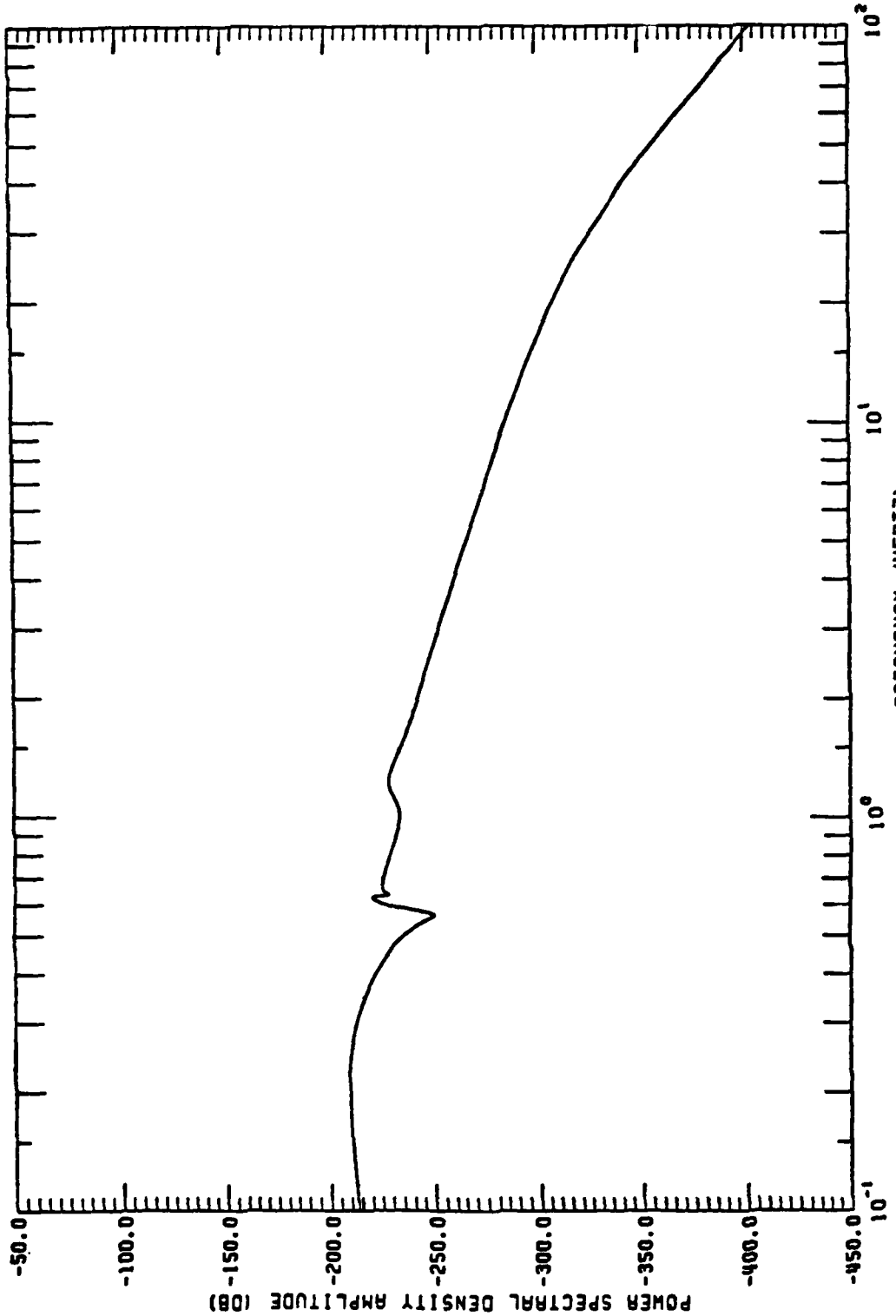

Figure 6-1e. Disturbance at node 46, output LOS-Y.

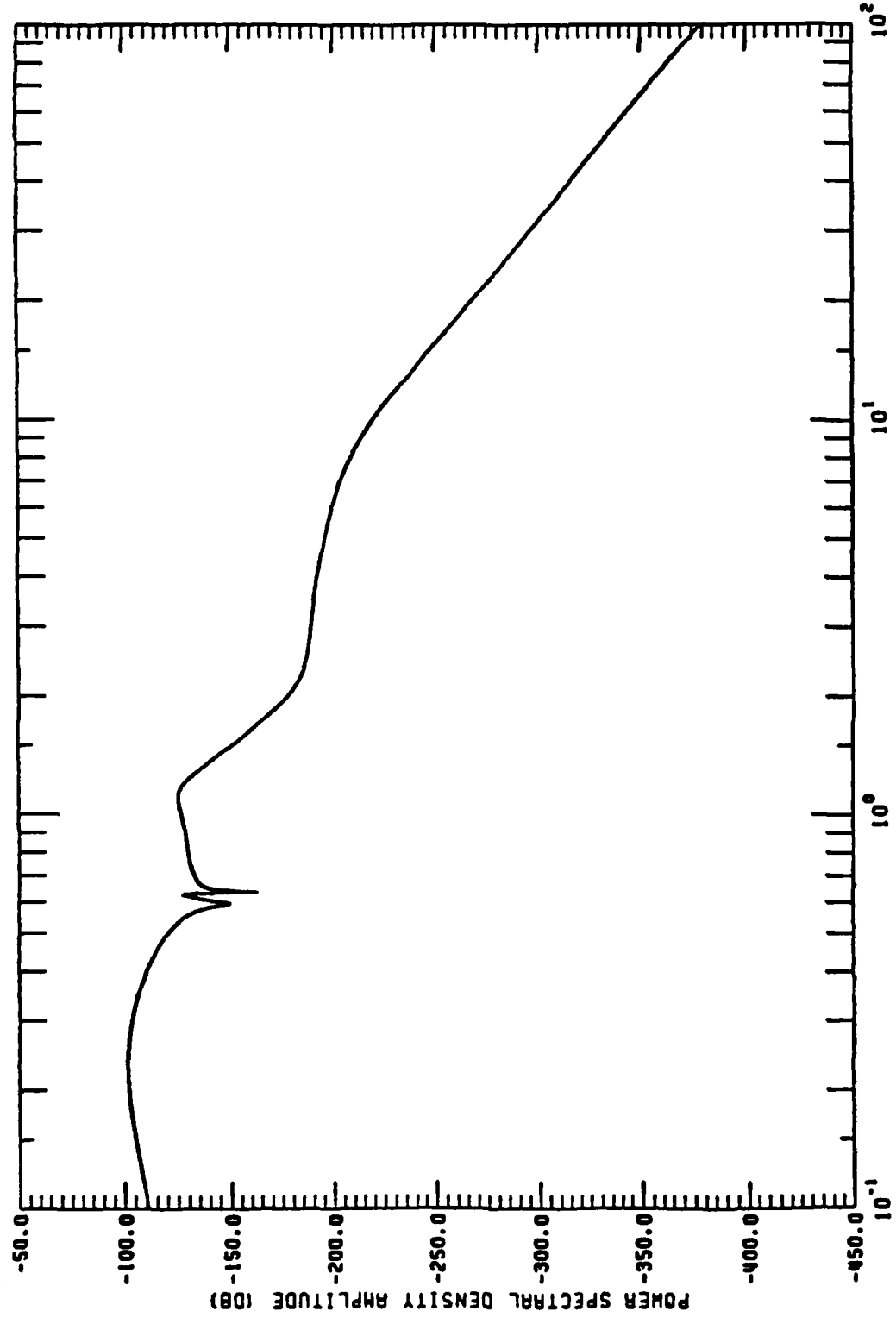

Figure 6-1f. Disturbance at node 46, output LOS-Z.

SECTION 7

LARGE-ANGLE SPACECRAFT SLEWING MANEUVERS

7.1 Introduction

This section presents some recent extensions for the problem of maneuvering a flexible spacecraft through large angles. In particular, this section addresses specific control issues in the following four areas:

(1) Selection of a reduced order model;

(2) Retargeting maneuvers;

(3) Optimal control employing state and control feedback; and

(4) Fixed time maneuvers using feedback control.

The remainder of this section is presented in four parts. Section 7.2 presents a method for selecting a reduced order plant model using a degree-of-controllability measure and a residual energy method. Section 7.3 presents a technique for slewing a flexible spacecraft to engage a moving target. This material represents an extension to the work first presented in Ref. 7-1. Section 7.4 presents a control design using integral precompensation, where the state, controls, and control rates are fed through optimal gains into a cascade of integrators. The output of the last integrator is the control which maneuvers the vehicle. This material represents an extension to the feedback case of the open-loop control-rate penalty technique presented in Ref. 7-1.

7.2 Reduced-Order Model Selection

Given the typically high dimension of finite element models used to characterize flexible spacecraft, it is necessary to reduce the flexible-body plant description to a manageable number of degrees of freedom. The reduced-order model selection procedure presented in this section consists of: (1) computing a relative degree-of-controllability for each flexible mode; and (2) using a residual energy technique to minimize the number of degrees of freedom retained in the plant description.

For a structure with many vibration modes, the relative degree-of-controllability measure is obtained by checking the rank of the controllability matrix

$$C_i = \left[B_i : A_i B_i : A_i^2 B_i : A_i^3 B_i\right]; \quad i = 1, \cdots, N \qquad (7\text{-}1)$$

where

$$A_i = \begin{bmatrix} 0 & 0 & 1 & 0 \\ 0 & 0 & 0 & 1 \\ 0 & 0 & 0 & 0 \\ 0 & -\omega_i^2 & 0 & 0 \end{bmatrix} \qquad (4 \times 4)$$

$$B_i = \begin{bmatrix} 0 \\ --- \\ V \end{bmatrix} \qquad (4 \times N_c)$$

and ω_i is the frequency of the i-th mode, V $(2 \times N_c)$ is the matrix of control influence coefficients for the rigid body and the i-th mode, N is the number of modes in the plant model before model reduction, and N_c is the number of independent controls.

To determine the rank of the controllability matrix, a Gram-Schmidt orthogonalization process is carried out on the columns of the C_i. As a result, the rank of C_i is found by computing the number of non-zero columns. Numerically, the number of non-zero columns is established by computing the sum of the squares of the coefficients of each column and comparing the result with a prescribed tolerance ε. By varying the tolerance ε and observing the rank of C_i as a function of ε, one obtains a rough indication of the relative degree-of-controllability of the i-th mode. In practice all modes which have been found to be uncontrollable are removed from the candidate set of modes considered for the reduced-order model.

Using this approach on an 84-mode subset of the ACOSS Model No. 2 structure, 20 modes were eliminated.

To further reduce the number of degrees of freedom in the plant model, a residual energy method is next presented.

The first step in the residual energy method consists of arbitrarily selecting several of the significant modes identified in the degree-of-controllability measure as a candidate reduced-order model. Next, basing a control design on the candidate reduced-order model, the resulting control is applied to all the modes remaining after the degree-of-controllability measure. At the end of the maneuver the control is turned off and the residual energy of the i-th mode

$$E_i = \frac{1}{2}\dot{\eta}_i^2(t_f) + \frac{1}{2}\omega_i^2\eta_i^2(t_f) \quad (i=1,\cdots,n^*) \tag{7-2}$$

is computed, where η_i is the i-th modal amplitude, $\dot{\eta}_i$ is the time derivative of the i-th modal amplitude, ω_i is the i-th modal frequency, and n* is the number of modes remaining after the degree-of-controllability measure. If any uncontrolled modes are observed to have unacceptably large residual energies, then the candidate reduced-order model is expanded to include these modes.

As a check on the new reduced-order model, a new control design is established, and the resulting control is applied to the structure. As before, the energy in the i-th residual mode is computed using Eq. (7-2), the residual mode energies E_i for i=1, •••, n^* are ranked according to magnitude, and the reduced-order plant model is refined as necessary. Typically, only one or two iterations of the residual energy method are required before a suitable reduced-order model has been found.

7.3 Retargeting Maneuvers For Flexible Spacecraft

The problem of slewing a flexible spacecraft to engage a moving target is presented in this section. This material represents an extension to the rigid body retargeting maneuvers first presented in Ref. 7-1. In particular, the results of this section are valid for the special case of a single-axis maneuver.

The target motion complicates the slewing control problem, because the terminal control state must be set in order to have the spacecraft track the target motion at the end of the maneuver. To obtain the terminal control, the spacecraft's attitude motion is constrained to osculate the target attitude motion through (k+1) time derivatives, where k denotes the highest time derivative of the control appearing in the performance index. In addition to the rigid body attitude motion constraints, it is convenient to impose the vibration constraint that the flexible body response is zero through (k+1) time derivatives. Subject to the desired target motion constraints above, the required terminal control state is shown in this section to be a function of the target attitude motion.

The assumed target motion kinematics and geometry is shown in Figure 7-1.

7.3.1 Optimal Control Problem

The optimal control problem for the retargeting maneuver is to seek the torque time history $\underline{u}(t)$ which minimizes the performance index

$$J = \frac{1}{2} \int_{t_o}^{t_f} [\underline{s}^T W_{ss} \underline{s} + \underline{u}^T W_{uu} \underline{u} + \dot{\underline{u}}^T W_{vv} \dot{\underline{u}}] dt \qquad (7\text{-}3)$$

subject to

$$\dot{\underline{s}} = A\underline{s} + B\underline{u}, \quad \text{given } \underline{s}(t_o) \text{ and } \underline{s}(t_f) \qquad (7\text{-}4)$$

where $\underline{s} = [\theta\ \eta_1 \cdots \eta_n\ \dot{\theta}\ \dot{\eta}_1 \cdots \dot{\eta}_n]^T$, θ is the rigid body angle, $\dot{\theta}$ is the angular rate, η_i for i=1, •••, n denotes the generalized coordinates for the flexible degrees of freedom, $\dot{\eta}_i$ for i=1, •••,n denotes the time derivative of the generalized coordinates for the flexible body degrees of freedom, n is the number of flexible body generalized coordinates, $\underline{u}$ denotes a distributed set of independent controls, A is the plant dynamics matrix, B is the control influence matrix, W_{ss} is the state weight matrix, W_{uu} is the control weight matrix, and W_{vv} is the control-rate weight matrix.

As shown in Ref. 7-1, the necessary conditions for the optimal control problem follow as:

State: $$\dot{\underline{s}} = A\,\underline{s} + B\,\underline{u} \qquad (7\text{-}5)$$

Costate: $$\dot{\underline{\lambda}} = -W_{ss}\underline{s} - A^T\underline{\lambda} \qquad (7\text{-}6)$$

Control: $$\dot{\underline{U}} = C\underline{U} + D\underline{\lambda} \qquad (7\text{-}7)$$

where

$$C = \begin{bmatrix} 0 & I \\ W_{vv}^{-1} W_{uu} & 0 \end{bmatrix} \qquad (2N_c \times 2N_c)$$

$$D = \begin{bmatrix} 0 \\ W_{vv}^{-1} B \end{bmatrix} \qquad (N_c \times 2N)$$

$$\underline{U} = \begin{bmatrix} \underline{u}^T & \dot{\underline{u}}^T \end{bmatrix}^T$$

N_c is the number of independent controls, and $N = 1 + n$.

The necessary conditions of Eq. (7-5), (7-6), and (7-7) define a two-point boundary-value problem; since $\underline{s}$ is known initially and finally, $\underline{\lambda}$ is unknown initially and finally, and $\underline{u}$ is unknown initially and finally. However, as shown in Ref. 7-1, the terminal boundary conditions for $\underline{u}$ can be specified to suit the needs of individual problems. In particular, in this section the final value of the control is set in order to enforce the desired target attitude motion constraints and the vibration suppression constraints.

Assuming that $\underline{u}(t_o)$ is given, the equation defining the solution for $\underline{\lambda}(t_o)$ and $\dot{\underline{u}}(t_o)$ is given by [Ref. 7-1]

$$\begin{bmatrix} \phi_{s\lambda} & \phi_{su_b} \\ \phi_{u_a\lambda} & \phi_{u_a u_b} \end{bmatrix} \begin{Bmatrix} \underline{\lambda}(t_o) \\ \underline{u}_b(t_o) \end{Bmatrix} = \begin{Bmatrix} \underline{s}(t_f) \\ \underline{u}_a(t_f) \end{Bmatrix} - \begin{bmatrix} \phi_{ss} & \phi_{su_a} \\ \phi_{u_a s} & \phi_{u_a u_a} \end{bmatrix} \begin{Bmatrix} \underline{s}(t_o) \\ \underline{u}_a(t_o) \end{Bmatrix} \qquad (7\text{-}8)$$

where $\underline{u}_a \triangleq \underline{u}$, $\underline{u}_b \triangleq \dot{\underline{u}}$, and ($\phi_{s\lambda}$, ϕ_{su_b}, $\phi_{u_a\lambda}$, $\phi_{u_au_b}$, ϕ_{ss}, ϕ_{su_a}, ϕ_{u_as}, $\phi_{u_au_a}$) denote blocks of the state transition matrix for Eqs. (7-3), (7-4), and (7-5).

Before Eq. (7-8) can be inverted for $\underline{\lambda}(t_o)$ and $\underline{u}_b(t_o)$, the terminal control, $\underline{u}_a(t_f)$, must be specified. The terminal control for the retargeting maneuver is obtained from the vehicle's equation of motion.

In order to illustrate the technique, the vehicle's equation of motion is assumed to be given by

$$\begin{bmatrix} \hat{I} & \underline{M}_{\theta\eta}^T \\ \underline{M}_{\theta\eta} & \underline{M}_{\eta\eta} \end{bmatrix} \begin{Bmatrix} \ddot{\theta}(t) \\ \ddot{\underline{\eta}}(t) \end{Bmatrix} + \begin{bmatrix} 0 & \underline{0}^T \\ \underline{0} & K_{\eta\eta} \end{bmatrix} \begin{Bmatrix} \theta(t) \\ \underline{\eta}(t) \end{Bmatrix} = \begin{bmatrix} 1 & 4\underline{r}^T \\ 0 & F \end{bmatrix} \begin{Bmatrix} u_R(t) \\ \underline{u}_E(t) \end{Bmatrix} \quad (7\text{-}9)$$

where $\underline{u} = (u_R, \underline{u}_E^T)^T$, u_R is the rigid body control, $\underline{u}_E$ is the vector of elastic body controls, $\hat{I}$ is moment of inertia of the undeformed structure, $\underline{M}_{\theta\eta}$ is the vector of elastic angular momentum coupling coefficients, $M_{\eta\eta}$ is the modal mass matrix, $K_{\eta\eta}$ is the modal stiffness matrix, F is the modal control influence matrix, $\underline{r} = [1, \cdots, 1]^T$ $(n \times 1)$,

$$\begin{bmatrix} \hat{I} & \underline{M}_{\theta\eta}^T \\ \underline{M}_{\theta\eta} & M_{\eta\eta} \end{bmatrix} = \text{system mass matrix}$$

$$\begin{bmatrix} 0 & \underline{0}^T \\ \underline{0} & K_{\eta\eta} \end{bmatrix} = \text{system stiffness matrix}$$

$$\begin{bmatrix} 1 & 4\underline{r}^T \\ \underline{0} & F \end{bmatrix} = \text{system control influence matrix}$$

In Eq. (7-9), $\theta(t_f)$ and $\underline{\eta}(t_f)$ are prescribed and $\ddot{\theta}(t_f)$, $\ddot{\underline{\eta}}(t_f)$, $u_R(t_f)$, $\underline{u}_E(t_f)$ are unknown. Thus to obtain a solution for $\underline{u}(t_f)$, the following dynamical constraints are imposed on $\ddot{\theta}(t_f)$ and $\ddot{\underline{\eta}}(t_f)$, namely:

$$\ddot{\theta}(t_f) \triangleq \ddot{\theta}_{target}(t_f) \tag{7-10}$$

$$\ddot{\underline{\eta}}(t_f) \triangleq \underline{0} \tag{7-11}$$

As a result, the rigid body motion osculates the target motion through two time derivatives, and the flexible body response is zero through two time derivatives, where $\underline{s}_f$ is given by

$$\underline{s}_f = [\theta_{target}(t_f)\ 0\cdots0\ \dot{\theta}_{target}(t_f)\ 0\cdots0].$$

Subject to the given boundary conditions of $\underline{s}(t_f)$ and the constraints of Eq. (7-10) and (7-11), the solution for $\underline{u}(t_f)$ in Eq. (7-9) follows as

$$\underline{u}(t_f) = P^* \ddot{\theta}_{target}(t_f) \tag{7-12}$$

where

$$P^* = (B^T W B)^{-1} B^T W \begin{Bmatrix} \hat{I} \\ \underline{M}_{\theta\eta} \end{Bmatrix}$$

$$W = \text{diag}\left[W_{\theta\theta}, W_{\eta_1\eta_1}, \cdots, W_{\eta_n\eta_n}\right]$$

$$= \text{diag}\left[10^5, 10^3, 1, \cdots, 1\right]$$

$W_{\theta\theta}$ denotes the least-squares weighting penalty on the rigid body accelerations

$W_{\eta_i\eta_i}$ for $i = 1,\cdots,n$ denotes the least-squares weighting penalty on the i-th modal amplitude accelerations

$$B = \begin{bmatrix} 1 & 4\underline{r}^T \\ \underline{0} & F \end{bmatrix} = \text{control influence matrix}$$

In Eq. (7-12), P* is the weighted least-squares pseudo-inverse operator corresponding to B^{-1}, since B is in general rectangular.

Assuming that the spacecraft control system is turned off at the start of the retargeting maneuver, $\underline{u}_a(0)$ is given by

$$\underline{u}_a(0) \triangleq \underline{0} \tag{7-13}$$

Substituting Eq. (7-12) and (7-13) into Eq. (7-8), leads to

$$\begin{bmatrix} \phi_{s\lambda} & \phi_{su_b} \\ \phi_{u_a\lambda} & \phi_{u_au_b} \end{bmatrix} \begin{Bmatrix} \underline{\lambda}(t_o) \\ \underline{u}_b(t_o) \end{Bmatrix} = \begin{Bmatrix} \underline{s}(t_f) - \phi_{ss}\underline{s}(t_o) \\ P^* \theta_{target}(t_f) - \phi_{u_as}\underline{s}(t_o) \end{Bmatrix} \tag{7-14}$$

Equation (7-14) is in the standard form for the linear algebraic equation $A\underline{x} = \underline{b}$, which can be solved via Gaussian elimination for $\underline{x}$, yielding $\underline{\lambda}(t_o)$ and $\underline{u}_b(t_o)$.

The optimal control time histories for the retargeting maneuver are obtained by integrating Eq. (7-5), (7-6), and (7-7) subject to the initial conditions given by $\underline{s}(t_o)$, $\underline{\lambda}(t_o)$, and $\underline{U}(t_o) = [\underline{0}^T , \underline{u}_b^T(t_o)]^T$.

7.4 Optimal Integral Pre-Compensation LQ Regulator Design

In this section the open-loop control-rate penalty technique presented in Ref. 7-1 is extended to the closed-loop case. In particular, for the results of this section it is assumed that the performance index penalizes the states, controls, and first time-derivatives of the controls.

The first step in the problem formulation consists of adding the control to the state equation given by

$$\dot{\underline{s}} = A\underline{s} + B\underline{u} \quad (2N\times 1) \tag{7-15}$$

where $\underline{s}$ is the state, $\underline{u}$ is the control, A is the system dynamics matrix, and B is the control influence matrix. As a result, the augmented state equation becomes

$$\dot{\underline{\Sigma}} = \tilde{A}\underline{\Sigma} + \tilde{B}\underline{u}_2 \quad [(2N+N_c)\times 1] \tag{7-16}$$

where

$$\tilde{A} = \begin{bmatrix} A & B \\ 0 & 0 \end{bmatrix}, \qquad \tilde{B} = \begin{bmatrix} 0 \\ I \end{bmatrix}, \qquad \underline{\Sigma} = \begin{Bmatrix} \underline{s} \\ \underline{u}_1 \end{Bmatrix}$$

$$\underline{u}_1 = \underline{u} \ (N_c\times 1) \qquad \underline{u}_2 = \dot{\underline{u}}_1 \ (N_c\times 1)$$

and N_c is the number of independent controls.

7.4.1 Optimal Control Problem

The optimal control problem is to seek a solution of Eq. (7-16) which minimizes

$$J = \frac{1}{2}\underline{\Sigma}^T(t_f)\mathscr{S}_f\underline{\Sigma}(t_f) + \frac{1}{2}\int_{t_0}^{t_f}[\underline{\Sigma}^T Q\underline{\Sigma} + \underline{u}_2^T R\,\underline{u}_2]dt \qquad (7\text{-}17)$$

subject to prescribed initial conditions

$$\underline{\Sigma}(t_o) = \begin{Bmatrix} \underline{s}(t_o) \\ \text{-----} \\ \underline{u}_1(t_o) \end{Bmatrix}$$

where $\mathscr{S}_f$ is the augmented terminal state weight matrix, Q is the augmented state weight, and R is the weight matrix for the control-rate. As shown in what follows, the commanded control becomes the control rate, and the solution follows as a standard LQ regulator design.

The initial control, $\underline{u}_1(t_o)$, in Eq. (7-17) can be prescribed since the resulting commanded control satisfies a first order differential equation with a free boundary condition. As shown in Ref. 7-1, it is convenient to select $\underline{u}_1(t_o) = \underline{0}$, since this choice minimizes the initial control jump discontinuity which can excite the residual plant dynamics of flexible space structures.

From Pontryagin's principle it easily follows that the necessary conditions for the augmented state, augmented costate, and control-rate are given by

$$\underline{\text{State}}: \quad \dot{\underline{\Sigma}} = \tilde{A}\underline{\Sigma} - \tilde{B}R^{-1}\tilde{B}^T\underline{\lambda} \qquad (7\text{-}18)$$

Costate: $$\dot{\underline{\Lambda}} = -Q\,\underline{\Sigma} - \tilde{A}^T\underline{\Lambda} \tag{7-19}$$

Control-Rate: $$\underline{u}_2 = -R^{-1}\tilde{B}^T\underline{\Lambda} \tag{7-20}$$

7.4.2 The Integral Pre-Compensation Regulator Design

Since the final augmented states are free, Pontryagin's principle provides the following terminal boundary condition relating the augmented states and costates

$$\underline{\Lambda}(t_f) = \mathscr{S}_f\,\underline{\Sigma}(t_f) \tag{7-21}$$

As a result, it can be shown that a feedback solution can be obtained by letting

$$\underline{\Lambda}(t) = \mathscr{S}(t)\underline{\Sigma}(t) \tag{7-22}$$

for $t \in [t_o, t_f]$.

Upon taking the time derivative of Eq. (7-22) and introducing $\dot{\underline{\Sigma}}$ and $\dot{\underline{\Lambda}}$ from Eq. (7-18) and (7-19), one finds that the matrix $\mathscr{S}(t)$ satisfies the following differential matrix Riccati equation

$$\dot{\mathscr{S}} = -\mathscr{S}\tilde{A} - \tilde{A}^T\mathscr{S} + \mathscr{S}\tilde{B}R^{-1}\tilde{B}^T\mathscr{S} - Q \tag{7-23}$$

which is subject to the boundary condition given by

$$\mathscr{S}(t_f) = \mathscr{S}_f \tag{7-24}$$

where $\mathscr{S}_f$ is defined in Eq. (7-17).

Substituting Eq. (7-22) into Eq. (7-20) yields the required control-rate command as the following linear combination of the augmented states:

$$\underline{u}_2(t) = -R^{-1}\tilde{B}^T\mathcal{S}(t)\underline{\Sigma}(t) \qquad (7\text{-}25)$$

By partitioning the matrix $\mathcal{S}(t)$ as follows:

$$\mathcal{S} = \begin{bmatrix} \mathcal{S}_{11} & \mathcal{S}_{12} \\ \mathcal{S}_{21} & \mathcal{S}_{22} \end{bmatrix} \begin{matrix} \} \ 2N \\ \} \ N_C \end{matrix} \qquad \mathcal{S}_{21} = \mathcal{S}_{12}^T \qquad (7\text{-}26)$$

$$\underbrace{\qquad}_{2N} \quad \underbrace{\qquad}_{N_C}$$

and carrying out the implied matrix multiplication in Eq. (7-25), the control-rate command can be written as:

$$\underline{u}_2(t) = -G\underline{s}(t) - G_u\underline{u}_1(t) \qquad (7\text{-}27)$$

where $$G = R^{-1}\mathcal{S}_{21}(t)$$

$$G_u = R^{-1}\mathcal{S}_{22}(t)$$

From Eq. (7-27) it follows that the control-rate command is obtained by feeding back the current states and controls through time-varying gains. Alternatively, if the infinite time problem is of interest, then $\dot{\mathcal{S}}$ in Eq. (7-23) is set to zero and the optimal gains are obtained from the solution for the algebraic matrix Riccati equation:

$$\mathcal{S}\tilde{A} + \tilde{A}^T\mathcal{S} - \mathcal{S}\tilde{B}R^{-1}\tilde{B}^T\mathcal{S} + Q = 0$$

The block diagram for the integral pre-compensation LQ regulator design is shown in Figure 7-2.

From Eq. (7-27) it follows that since $\underline{u}_2$ is integrated to provide $\underline{u}(t)$, one can interpret the control scheme of this section to be an integral pre-compensation strategy. However, given the high-frequency roll-off characteristics of this approach, Eq. (7-27) can also be validly interpreted as a low-pass filter for the control. Of special interest is the observation that a single solution of the Riccati equation yields both the regulator gains and the low-pass filter gains.

The results of this section can be generalized for the case of n-th order time derivatives appearing in the performance index, leading to a k-th order commanded control of the form

$$\underline{u}^{(k)} = -G_u \underline{u} - G_{\dot{u}} \dot{\underline{u}} - \cdots - G_{u_{(k-1)}} \underline{u}_{(k-1)} - G\underline{s}$$

where $(*)_{(k)} \triangleq \dfrac{d^k}{dt^k}(*)$, $G = R^{-1}\mathscr{S}_{k+1,1}$,

$G_u = R^{-1}\mathscr{S}_{k+1,2}$, $G_{\dot{u}} = R^{-1}\mathscr{S}_{k+1,3}, \cdots, G_{u_{(k-1)}} = R^{-1}\mathscr{S}_{k+1,k+1}$

and

$$\mathscr{S} = \underbrace{\begin{bmatrix} \mathscr{S}_{11} & \mathscr{S}_{12} & \cdots & \mathscr{S}_{1,k+1} \\ \mathscr{S}_{21} & \mathscr{S}_{22} & \cdots & \mathscr{S}_{2,k+1} \\ \vdots & \vdots & & \vdots \\ \mathscr{S}_{k+1,1} & \mathscr{S}_{k+1,2} & \cdots & \mathscr{S}_{k+1,k+1} \end{bmatrix}}_{2N \qquad\qquad kN_C} \left.\begin{matrix} \\ \\ \\ \\ \end{matrix}\right\} \begin{matrix} 2N \\ \\ \\ kN_C \end{matrix}$$

The block diagram for the k-th order integral pre-compensation LQ regulator design is shown in Figure 7-3.

7.4.3 Some Frequency Domain Features of the Integral Pre-Compensation LQ Regulator Design

After some reductions, the block diagram in Figure 7-2 can be written as shown in Figure 7-4. The loop transfer matrix broken at the plant input, (a), is given by

$$G_{loop}(s) = (sI_{N_c} + G_u)^{-1} G(sI_{2N} - A)^{-1} B \qquad (7\text{-}28)$$

where I_{N_c} = diag(1,•••,1) is $(N_c \times N_c)$ and I_{2N} = diag(1,•••,1) is $(2N \times 2N)$.

From Eq. (7-28) it follows that $G_{loop}(s)$ has the following properties:

(1) A two pole roll-off in each channel;

(2) The poles of $G_{loop}(s)$ consist of the original plant poles, plus the eigenvalues of $-G_u$; and

(3) For scalar input, G_u, as determined from the Riccati equation, is a break frequency.

The high frequency roll-off characteristics of $G_{loop}(s)$ are believed to be particularly significant for the residual plant dynamics of flexible space structures.

7.4.4 Observer-Based Compensation Design

Assuming that the commanded control is known and the state must be estimated, the block diagram structure for the observer-based integral pre-compensation control is shown in Figure 7-5.

At the present time the following two approaches are being considered for generating the observer gains K required in the state estimator. The first approach employs a standard root square locus technique. The second approach employs the Doyle-Stein loop transfer recovery procedure to improve the crossover properties of the loop transfer function broken at the plant input.

The Doyle-Stein procedure consists of solving the Kalman-Bucy filter (KBF) Riccati equation

$$0 = A\Pi + \Pi A^T + M_o(q) - \Pi C^T N^{-1} C\Pi \qquad (7\text{-}29)$$

where $M_o(q) = M_o + q^2 B B^T$

M_o = nominal plant noise intensity matrix

N = observation noise intensity matrix

q = Doyle-Stein robustness parameter

and the observer gains are given by

$$K = -\Pi C^T N^{-1} \qquad (7\text{-}30)$$

As $q \to \infty$, in the KBF Riccati equation above, the loop transfer matrices $T_i(s)$ with the loop broken at point i in Figure 7-5, have the following significant limiting properties

$$T_2(s) \to T_1(s) \text{ as } q \to \infty \qquad (7\text{-}31)$$

where

$$T_1(s) = \phi_2(s)\, G\, \phi_1(s)\, B$$

$$T_2(s) = \phi_2(s)\left[\phi_1^{-1}(s) + B\, \phi_2(s) + KC\right]^{-1} KC\, \phi_1(s)\, B$$

$$\phi_1(s) = (sI_{2N} - A)^{-1}$$

$$\phi_2(s) = (sI_{N_c} + G_u)^{-1}$$

The robustness recovery procedure is attractive because $T_1(s)$ has the standard LQ stability robustness guarantees:

$$\sigma_{min}[I + T_1(j\omega)] \geq 1 \quad \text{for all } \omega \geq 0 \tag{7-32}$$

and

$$\sigma_{min}[I + T_1^{-1}(j\omega)] \geq \frac{1}{2} \quad \text{for all } \omega \geq 0 \tag{7-33}$$

where σ_{min} denotes the minimum singular value. In particular, $T_2(s)$ is constrained to retain a 4-pole roll-off at high frequency, where two poles are contributed by the plant, one by the integrator, and one by the rest of the compensator. In practice the design process consists of a trade-off between the low-frequency disturbance rejection properties and location of the break frequency for the high-frequency 4-pole roll-off. In the control system design, the weight matrices in the performance index of Eq. (7-17) and robustness recovery parameter q are the design variables employed in the trade-off study.

7.4.5 Closed-Loop System Stability

Since truncated dynamical models are used to characterize flexible spacecraft and generate preliminary control designs, it is important to assess the stability of the resulting control designs in the presence of unmodeled system dynamics. To this end, the equations governing the system state, control, and state estimation are summarized as follows:

Controlled State: $\dot{\underline{s}} = A\underline{s} + B\underline{u}$ (7-34)

Residual State: $\dot{\underline{s}}_R = A_R\underline{s}_R + B_R\underline{u}$ (7-35)

Measurement: $\underline{y} = C\underline{s} + C_R\underline{s}_R$ (7-36)

Control Law: $\dot{\underline{u}} = -G_u\underline{u} - G\hat{\underline{s}}$ (7-37)

Kalman-Bucy Filter: $\dot{\hat{\underline{s}}} = A\hat{\underline{s}} + B\underline{u} + K(\underline{y} - C\hat{\underline{s}})$ (7-38)

Estimation Error: $\dot{\underline{e}} = (A - KC)\underline{e} + KC_R\underline{s}_R$ (7-39)

where $\underline{e} = \hat{\underline{s}} - \underline{s}$.

In order to cast the control law of Eq. (7-37) in a useful form for the stability analysis, Eq. (7-37) is written in terms of the estimation error $\underline{e}$ as follows:

$$\dot{\underline{u}} = -G_u\underline{u} - G(\underline{e} + \underline{s}) = -G_u\underline{u} - G\underline{s} - G\underline{e} \qquad (7\text{-}40)$$

As a result, the system stability matrix is obtained by writing Eqs. (7-34), (7-35), (7-39), and (7-40) as follows:

$$\dot{\underline{X}} = \mathcal{A}\underline{X} \qquad (7\text{-}41)$$

where $\underline{X} = [\underline{s}^T \; \underline{u}^T \; \underline{e}^T \; \underline{s}_R^T]^T$

$$\mathcal{A} = \begin{bmatrix} A & B & 0 & 0 \\ -G & -G_u & -G & 0 \\ 0 & 0 & (A-KC) & KC_R \\ 0 & B_R & 0 & A_R \end{bmatrix}$$

The algebraic sign of the real part of the eigenvalues of $\mathcal{A}$ provides the desired system stability information. In particular, if the algebraic sign of all of the real parts of the eigenvalues of $\mathcal{A}$ is negative or zero, then the system is stable. Alternatively, if any of the eigenvalues of $\mathcal{A}$ have positive real parts, then the system is unstable. Clearly, if instability is indicated in the eigenvalue analysis of $\mathcal{A}$, then the control design must be modified so as to overcome the difficulty.

7.5 A Closed Form Solution for the Differential Matrix Riccati Equation for Fixed Time Slewing Maneuvers

The matrix Riccati differential equation

$$\dot{P}(t) = -A^T P(t) - P(t)A + P(t)\,BR^{-1}B^T P(t) - Q \quad (n \times n) \qquad (7\text{-}42)$$

arises in the solution for the optimal slewing control problem for the linear time-invariant system

$$\dot{\underline{x}}(t) = A\,\underline{x}(t) + Bu(t), \quad \underline{x}(t_o) = \underline{x}_o \quad (n \times 1) \qquad (7\text{-}43)$$

where the performance index is given by

$$J = \frac{1}{2}\underline{x}^T(t_f)S\underline{x}(t_f) + \frac{1}{2}\int_{t_o}^{t_f}\left[\underline{x}^T(t)Q\underline{x}(t) + u^TR\underline{u}\right]dt \qquad (7\text{-}44)$$

and $\underline{x}(t)$ is the state, $\underline{u}(t)$ is the control, A is the system dynamics matrix, B is the control influence matrix, S is the terminal state weight matrix, Q is the state weight matrix, and R is the control weight matrix. If R, Q, and S are selected to be symmetric and positive definite, then P(t) is symmetric and positive definite. The positive definiteness of P(t) is important for the results that follow.

The optimal control of Eq. (7-43) is the following linear state feedback law

$$\underline{u}(t) = -R^{-1}B^TP(t)\underline{x}(t) \qquad (7\text{-}45)$$

where P(t) is the solution for Eq. (7-42) with the terminal boundary condition

$$P(t_f) = S \qquad (7\text{-}46)$$

This section presents a simple change of variables for Eq. (7-42) which permits a closed form solution to be obtained for P(t), when R, S, and Q are selected to yield P(t) positive definite.

7.5.1 Change of Variables for the Matrix Riccati Differential Equation

Assume that the solution for P(t) can be written as

$$P(t) = P_{ss} + Z^{-1}(t) \tag{7-47}$$

where P_{ss} is the solution to the algebraic matrix Riccati equation

$$-A^T P_{ss} - P_{ss} A + P_{ss} E P_{ss} - Q = 0 , \tag{7-48}$$

$Z(t)$ is a matrix function to be determined, and $E = B R^{-1} B^T$. The substitution in Eq. (7-47) has been suggested by Potter and VanderVelde in Ref. 7-2, and is a natural consequence of the corresponding results for scalar Riccati equations. The results of this section extend the work of Potter and VanderVelde by providing an efficient analytic solution for $Z(t)$. The complete solution for $Z(t)$ can be found in Ref. 7-3.

After some algebra the linear constant-coefficient matrix differential equation for $Z(t)$ follows as:

$$\dot{Z}(t) = G Z(t) + Z(t) G^T - E \tag{7-49}$$

where $G = A - EP_{ss}$, and G is the steady-state closed-loop system matrix possessing eigenvalues with all negative real parts.

The solution for $Z(t)$ is obtained by introducing a coordinate transformation which diagonalizes the homogeneous part of $\dot{Z}$. To this end, G and G^T in Eq. (7-49) are expressed as

$$G = R \Lambda L^T \tag{7-50}$$

and

$$G^T = L \Lambda R^T \tag{7-51}$$

where R is the matrix of right eigenvectors of G, L is the matrix of left eigenvectors of G^T, Λ is the diagonal matrix of eigenvalues of G, and R and L are normalized as follows

$$R^T L = I \quad (R^T = L^{-1} \text{ and } L^T = R^{-1}) \tag{7-52}$$

Substituting Eq. (7-50) and (7-51) into Eq. (7-49) and pre-multiplying the result by L^T and post-multiplying by L, leads to

$$\dot{T}(t) = \Lambda T(t) + T(t) \Lambda - \Sigma \tag{7-53}$$

where $T(t) = L^T Z(t) L \quad (Z(t) = R\, T(t)\, R^T)$

$\Sigma = L^T E L$

Since the homogeneous part of $\dot{T}(t)$ is diagonal, the solution for T(t) is easily obtained, and after some algebra it can be shown to be

$$T(t) = e^{\Lambda(t-t_o)} \left[T(t_o) - D(t,t_o)\right] e^{\Lambda(t-t_o)} \tag{7-54}$$

where $\Lambda = \text{diag}\left[\Lambda_1 \cdots \Lambda_n\right]$

$$e^{\Lambda(t-t_o)} = \text{diag}\left[e^{\Lambda_1(t-t_o)} \cdots e^{\Lambda_n(t-t_o)}\right]$$

$$\left[D(t,t_o)\right]_{ij} = \frac{\Sigma_{ij}}{\rho_{ij}} \left\{1 - e^{-\rho_{ij}(t-t_o)}\right\}$$

$$\rho_{ij} = \Lambda_i + \Lambda_j$$

$T(t_o)$ = initial condition matrix for $T(t)$

$[*]_{ij}$ = denotes i-j element of $[*]$

As a result, the solution for $Z(t)$ is known and solution for $P(t)$ can be written as

$$P(t) = P_{ss} + \left[R\ T(t)\ R^T\right]^{-1} \tag{7-55}$$

The initial condition matrix for $T(t_o)$ is evaluated by imposing the boundary condition that $P(t_f) = S$. After carrying out the necessary algebra the solution for $T(t)$ follows as:

$$\left[T(t)\right]_{ij} = \left(H_{ij} - \frac{\Sigma_{ij}}{\rho_{ij}}\right) e^{-\rho_{ij}(t_f - t)} + \frac{\Sigma_{ij}}{\rho_{ij}} \tag{7-56}$$

where $H = L^T(S - P_{ss})^{-1}L$

Using Eq. (7-55), the integral pre-compensation control of Section 7.4.2 can be solved for fixed-time slewing maneuvers.

References

7-1 Turner, J.D., et. al., "ACOSS Eleven Semiannual Technical Report," Vol. 2, Charles Stark Draper Laboratory, Cambridge, MA, Report CSDL-R-1536, February 1982.

7-2 Potter, J.E., and VanderVelde, W.E., "Optimum Mixing of Gyroscope and Star Tracker Data," J. Spacecraft, Vol. 5, No. 5, May 1968, pp. 536-540.

7-3 Turner, J.D., and Chun, H.M., "Optimal Feedback Control of a Flexible Spacecraft During a Large-Angle Rotational Maneuver," Paper No. 82-1589, AIAA Guidance and Control Conference, San Diego, CA, August 9-11, 1982.

TARGET KINEMATICS

$(\hat{e}_x, \hat{e}_y, \hat{e}_z) \triangleq$ INERTIAL FRAME (N) UNIT VECTORS

$$\underline{R}_{TARGET}(t) = x_o\hat{e}_x + (\dot{y}_o(t - t_o) + y_o)\hat{e}_y \quad \text{(POSITION)}$$

$$\frac{d}{dt}(\underline{R}_{TARGET})_N = \dot{y}_o\hat{e}_y \quad \text{(VELOCITY)}$$

$$\theta_{TARGET}(t) = \tan^{-1}\left(\frac{\dot{y}_o(t - t_o) + y_o}{x_o}\right) \quad \text{(ORIENTATION)}$$

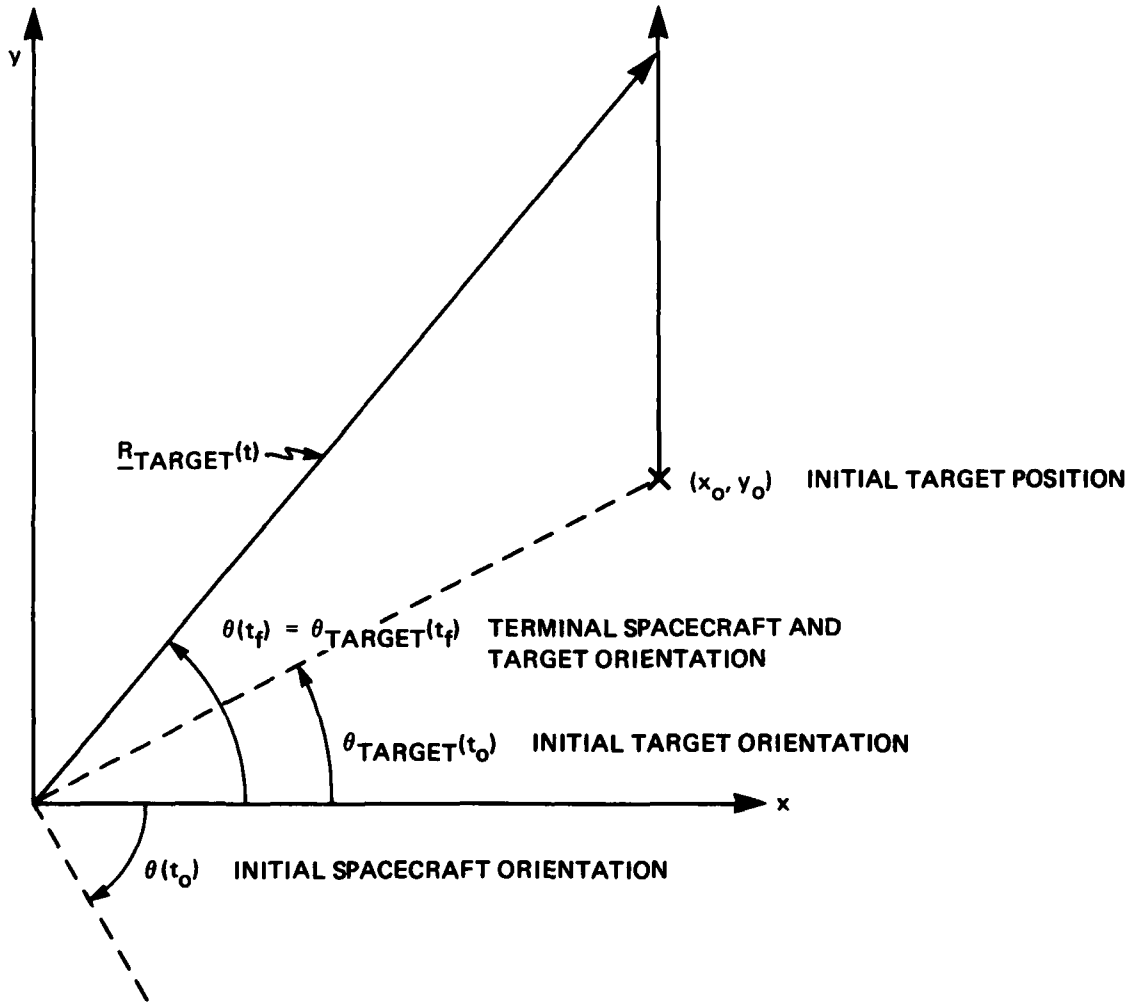

Figure 7-1. Geometry for slewing to engage and track a moving target.

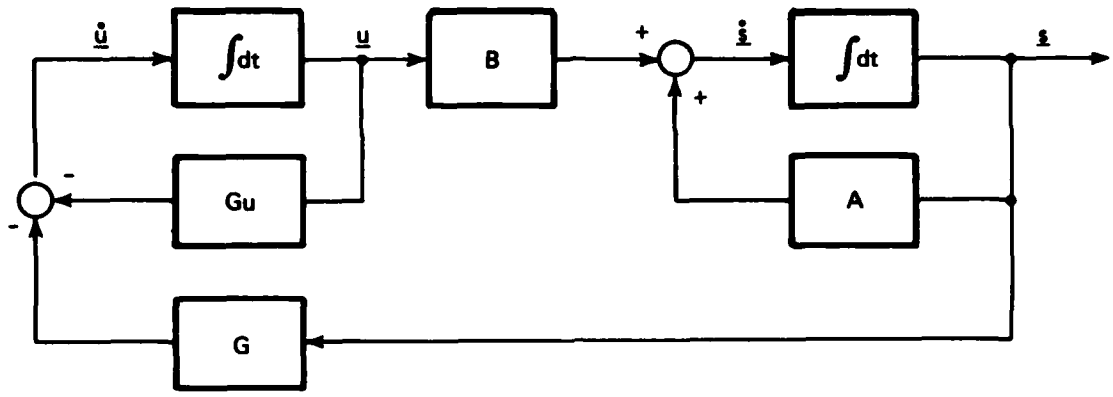

Figure 7-2. Block diagram for the integral precompensation LQ regulator design using full-state and full-control feedback.

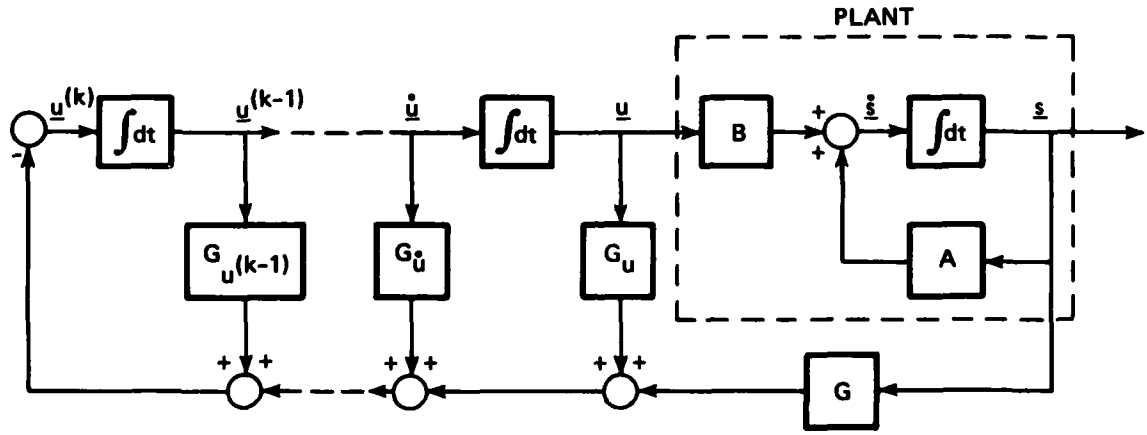

Figure 7-3. Block diagram for the k-th order integral precompensation LQ regulator design using full-state, control, and control-rate feedback.

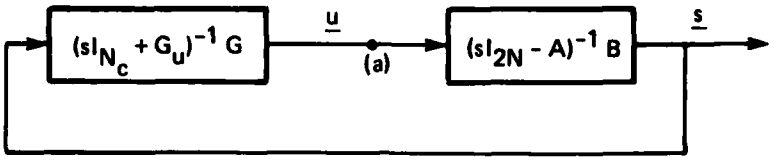

Figure 7-4. Block reduction for the integral precompensation LQ regulator design.

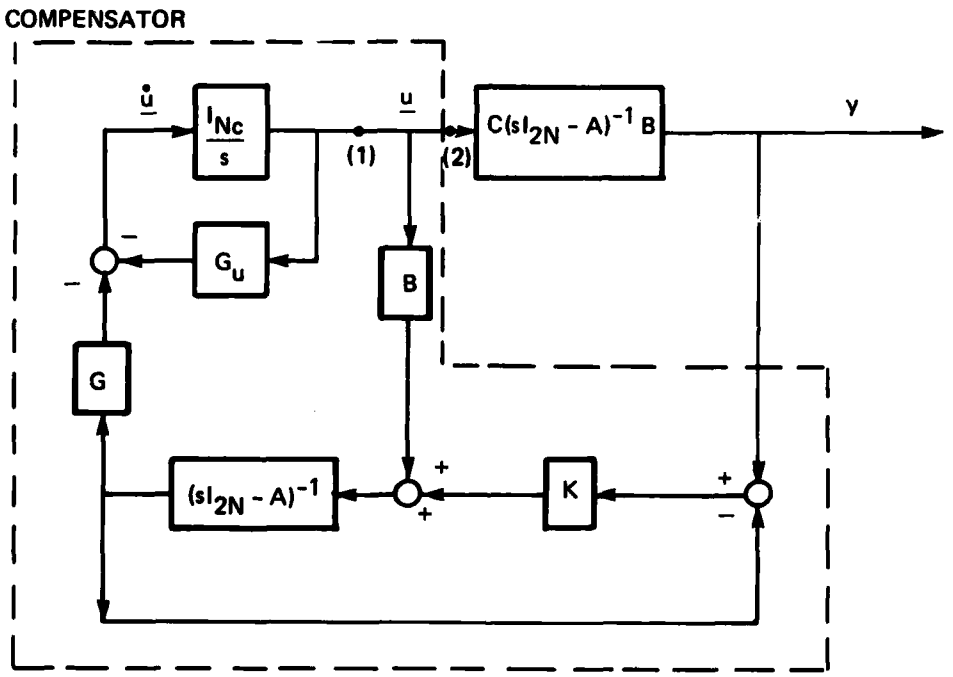

Figure 7-5. Block diagram structure for observer-based integral precompensation control.

MISSION
of
Rome Air Development Center

RADC plans and executes research, development, test and selected acquisition programs in support of Command, Control Communications and Intelligence (C^3I) activities. Technical and engineering support within areas of technical competence is provided to ESD Program Offices (POs) and other ESD elements. The principal technical mission areas are communications, electromagnetic guidance and control, surveillance of ground and aerospace objects, intelligence data collection and handling, information system technology, ionospheric propagation, solid state sciences, microwave physics and electronic reliability, maintainability and compatibility.